Development of a Chemical Gas Sensor System

Entwicklung eines Chemischen Gas Sensor Systems

DISSERTATION

der Fakultät für Chemie und Pharmazie
der Eberhard Karls Universität Tübingen
zur Erlangung des Grades eines Doktors
der Naturwissenschaften

2005

vorgelegt von

Patrick Reichel

Tag der mündlichen Prüfung: 07.10.2005
Dekan: Prof. Dr. Stefan Laufer
1. Berichterstatter: PD Dr. Udo Weimar
2. Berichterstatter: Prof. Dr. Günter Gauglitz

Table of Contents

1 Introduction

1.1 Motivation

The last century has seen increased industrial growth worldwide. A side effect of this development is an exponential increase in pollution of earth, air and water, especially in densely populated areas such as the EU. While land pollution is locally restricted and great efforts have been made during the last decades to improve the quality of rivers and larger bodies of water, air pollution is not so easily reduced. Wind, rain and other meteorological phenomena make the spread of pollutants difficult to predict and impossible to control. The measures taken over the last years are therefore focussing on preventing or reducing the emission at its source, e.g. the use of air filters for industrial combustion. However, complete prevention of pollutant emission is not always viable and much more difficult if applied to mobile (e.g. automotive) or unpredictable (e.g. wood fire) sources. This pollution threatens nature and human health alike. People, especially in urban areas, are exposed to a high quantity of harmful airborne substances at work, in traffic and at home. To be able to devise effective countermeasures and reduce the personal exposure to pollutants, their exact nature and quantity must be known with a high spatial resolution.

Nowadays, the qualitative and quantitative analysis of gaseous compounds is performed almost exclusively by analytical instruments; wet chemistry and one-way tests having a small complementary function. These instruments use a broad range of chemical and physical methods to determine the properties of a given sample [1]. Chromatography, spectroscopy and spectrometry play a prominent role among these systems. These classical analytical instruments are highly accurate and reliable devices, able to detect even traces of pollutants in mixtures and with lifetimes in the range of several years. Their drawbacks are a high initial cost, high maintenance costs, size and weight, high power consumption (no battery operation possible), the need for qualified personnel and a comparably low time-resolution. The high costs often entail a low spatial resolution due to a restricted number of instruments, relevant in applications with a large area to cover.

Figure 1.1: Standard analytical instrument (GCMS) and gas sensor.

Most data on the levels and spread of airborne pollutants is gathered through the environmental monitoring networks present in all large European cities. They are composed of a number of expensive and very accurate analytical instruments and give a measure of hourly to daily concentration levels of known pollutants as well as indicate seasonal trends and long-term developments. However, even large cities such as Madrid (Spain) are covered by only 25 measuring stations [2], limiting the geographical relevance of the gathered

information. At the same time the idea of personal exposure becomes more and more important in our society. From personal gas alarms for pedestrians to medical monitors of patient health and intelligent household instruments (e.g. refrigerator, oven) small and cheap (gas) sensing devices experience an increased consumer attention. One answer to this growing need is the development of smaller, cheaper and autonomous measurement units - sensors.

1.2 Gas Sensors

The main difference between classical analytical instruments and sensors is cost and accuracy. In contrast to classical analytical instruments sensors are small and cheap devices with lower lifetime and accuracy. The one's strengths are the others weaknesses. Attempts to close this gap from both sides are currently made by the industry and researchers alike: increasing the accuracy of sensors and miniaturising classical instruments [3].
But what is a sensor? As sensors are originating from many different disciplines (physics, chemistry, biology) a similarly high number of definitions exist [4]-[6]. The field of chemical gas sensors alone already hosts many sensors based on very different measurement principles.

Measurement parameters	Transducer	Sensor system
Conductance ΔG	2-, 3- or 4-point electrodes	Metal Oxide Semiconductors, Conducting polymers
Current ΔI	2- and 3-point electrodes	Electrochemical cell
Mass Δm	oscillating quartzes	Polymer coated microbalances
Work function $\Delta \Phi$	Kelvin probes	Gas-FETs
Temperature ΔT	Thermopiles, ntc- or ptc-resistors	Calorimetric sensor, Pellistor
Capacitance ΔC	Interdigital capacitors	Humidity sensors
Optical layer thickness Δn	Light	RIFS
Intensity ΔI or Phase $\Delta \varphi$	Fibre optics	Optical sensors

Table 1.1: Chemical gas sensors and their measurement principles [7].

For our purposes, chemical gas sensors will be defined as "a device which provides an electrical output in response to the partial pressure change of a gas". They consist of two parts: the sensing element and the transducer. The sensing element changes its chemical properties in response to changes in the ambient concentration of a gas. The transducer transforms the chemical signal into an easily measurable electrical one.
The most important characteristics of gas sensors are:

- Sensitivity - response to small concentrations or concentration changes of pollutants
- Selectivity - strong response to some pollutants, none to others
- Stability - signal reproducibility over time

A high performance gas sensor has a high sensitivity to very few selected pollutants and provides a stable and reproducible signal over long time periods.

1.2.1 Electrochemical Cells

Electrochemical gas sensors are based on the measurement of a current in an electrochemical cell between a sensing or working electrode and a counter electrode at a certain potential (amperometric sensor). The current is created by the electrochemical oxidation or reduction of the target gas at a catalytic electrode surface that is in contact with an electrolyte. The magnitude of the current is directly proportional to the gas concentration.
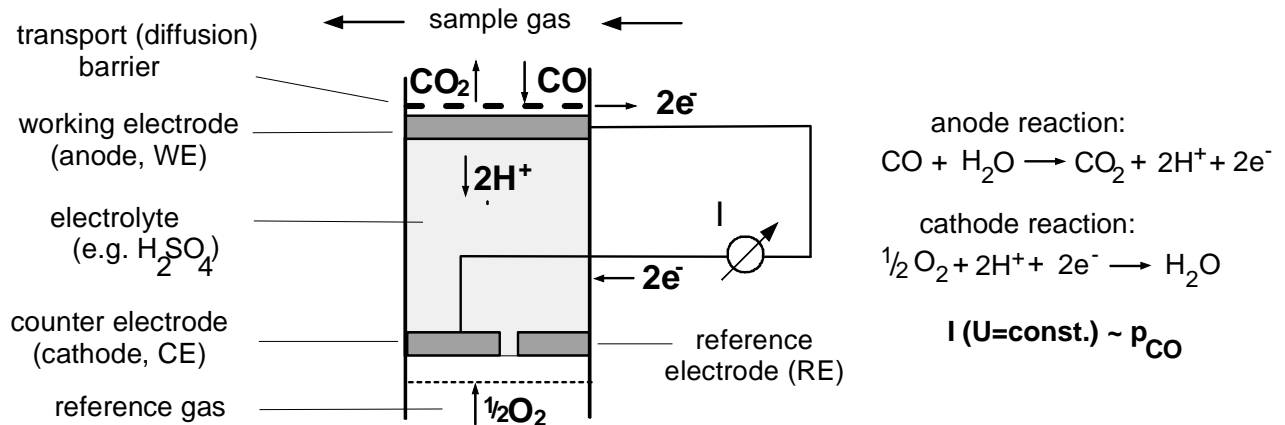
Figure 1.2: Schematic sensor structure of a three electrode amperometric gas sensor with CO as example for a target gas and the oxidation reaction to CO_2 as electrochemical reaction [8].

The advantage of electrochemical sensors is their good selectivity and stability. The linear signal dependency on gas concentrations is an advantage at higher concentrations and for wide concentration ranges. However, it is a disadvantage for the detection of very small concentrations.

1.2.2 Microbalances

Quartz Crystal Microbalances (QMB) [9] are composed of a piezo-electric crystal disc coated with a polymer. The crystal is swinging with a defined excitation frequency. Gaseous molecules interact with the polymer, changing the mass of the sensing element and thereby also the frequency [10]. Different microbalances employed as sensor systems are thickness-shear mode resonator (TSM), surface and bulk acoustic wave devices (SAW, BAW).
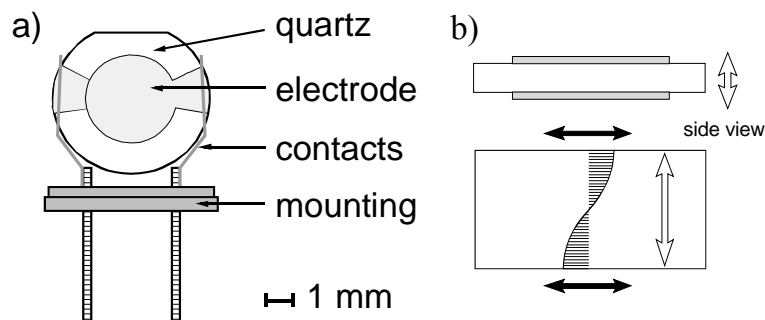
Figure 1.3: a) Set up of a swinging quartz b) TSM resonator; white arrows: wave propagation, black arrows: particle propagation [11].

The advantage of microbalances is their easily variable selectivity (polymer-dependent) and sensitivity to Volatile Organic Compounds (VOCs) [12]. Disadvantageous are the low maximum operation temperature and slow recovery times.

1.2.3 Metal Oxide Semiconductor Gas Sensors

The idea of using semiconductors as gas sensitive devices leads back to 1952 when Brattain and Bardeen first reported gas sensitive effects on Germanium[13]. Later, Seiyama found gas sensing effects on metal oxides [14]. Taguchi finally brought semiconductor sensors based on metal oxides to an industrial product [15]-[17]. Since then, metal oxide semiconductor sensors have attracted a lot of attention due to their cheap and easy-to-use gas monitoring capabilities. They comprise a sensing layer deposited on a substrate provided with electrodes and a heating element (sensor operation temperature between 200 and 400°C). The substrate is usually mounted on a socket, e.g. TO-socket, provided with a cap and sometimes a filter as shown in figure 1.4. Such Taguchi-type sensors are still on the market, but most of the commercially available sensors are nowadays manufactured in screen-printing technology on small and thin ceramic substrates [18]-[20].

Figure 1.4:   Schematics of a Taguchi-type thick film sensor.

The measured parameter is the resistance of the sensing layer which directly correlates to the concentration of the targeted gas. The major advantage of thick film sensors is their good sensitivity, resulting from the exponential signal dependency on gas concentrations. Disadvantageous is their lack of selectivity, resulting in a high number of cross-sensitivities for most applications. Other advantages include good stability, extensive material experience and low manufacturing price.
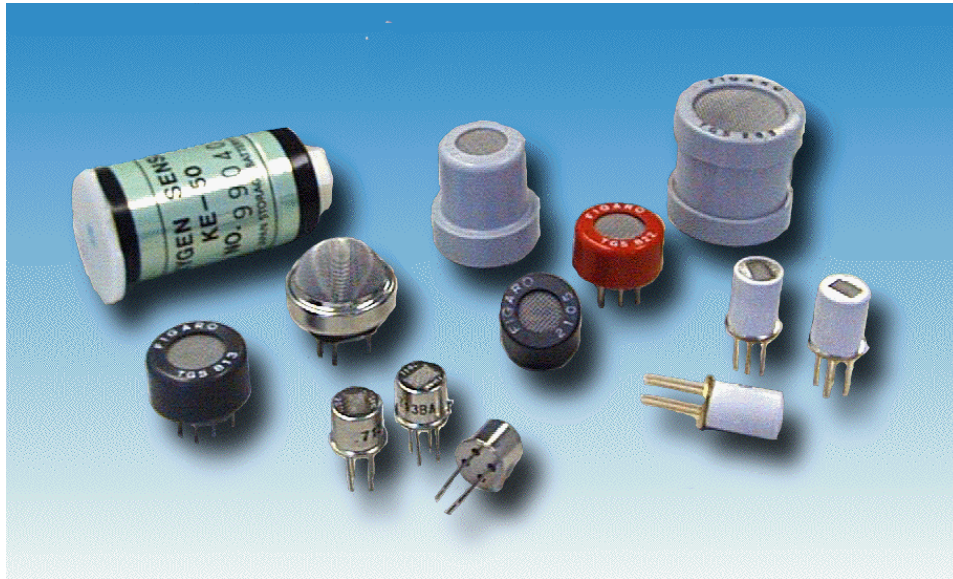
Figure 1.5: Different commercially available single sensors using semiconductor technology, Figaro Engineering.

Since the first commercial semiconductor gas sensors have been offered by the company Figaro in 1968, the sensor market has continued to grow steadily. Nowadays, millions of gas sensors are sold every year in many different applications, as demonstrated in table 1.2. Among them, domestic alarms, automobile air quality control and industrial process control are the most prominent areas of application. Other fields are currently experiencing strong research efforts by public and private societies.

Actual and future areas of application for chemical gas sensors	
Domestic Alarms	fire (CO), natural gas heating
Automobile	driver's cabin air quality, control of ventilation hatches, exhaust
Medical	disease detection through breath analysis
Military	chemical and biological warfare
Ventilation	air quality monitoring in tunnels or underground parking garages
Environment	environmental monitoring systems, personal exposure alarms
Industry	process-control, leakage alarm
Traffic	city traffic control and management
Household Appliances	intelligent refrigerator or oven
Life-Style	bad breath detection, blood alcohol

Table 1.2: Actual and future areas of application for chemical gas sensors.

However, in spite of many efforts by science and the industry to promote gas sensor technology, the market breakthrough has not yet been accomplished. For chemical gas sensors to be accepted two obstacles have to be overcome.

8

The knowledge of the chemical and physical properties fundamental to gas sensing is not satisfactory for all techniques. Mastery can only be achieved by completely understanding the microscopic mechanisms by which sensors interact with ambient gases. To this end, the fundamental research on well established chemical gas sensors has to be intensified and new methods and materials have to be investigated.

The other barrier to the wide-spread use of chemical gas sensors is the gap in performance between sensors offered by the manufacturing companies and the performance requirements demanded by the users. The development of gas sensors has to be focused more towards the needs of its users. Current research efforts focus on reducing size, cost and power consumption, increasing the long-term stability and enabling compatibility with modern telecommunication systems (sensors usable e.g. in mobile phones). However, the price pressure is very high. To be competitive, sensors have to cost 5 to 20 € or, as complete sensor systems (including electronics, calibration…), 100 to 1,000 €. By meeting these criteria and proving themselves in demanding applications the market can be convinced by chemical gas sensors.

1.3   Target and Outline of this Work

The present work contributes towards increasing the acceptance of chemical gas sensors based on metal oxide semiconductors. Its objectives were to develop a smart, mobile gas sensor system with low power consumption. A sensor system consists of the sensing element itself and the supporting system. As sensing element a monolithic micro-machined metal oxide sensor was chosen, the ADA sensor chip, developed by the Physical Electronics Laboratory, University of Zurich [21]. The authors contribution to the sensor chip development was a thorough laboratory assessment of its chemical sensing properties. In parallel to the chip development a supporting sensor system was developed in co-operation with AppliedSensor GmbH [22]. The authors contribution was to test all components and various system prototypes, evaluate different operation modes and improve the sensor selectivity. The latter constitutes the main research focus of this work: investigating possibilities to improve the sensor's selectivity and applying them to the developed sensor and system. Due to the parallel development of sensor chip and supporting system, substitute sensors were employed during the early sensor system tests. Both conventional thick film sensors and micro-machined sensors were used. Several final ADA sensor system prototypes with integrated sensor chip and full packaging were produced, characterised and calibrated. These calibrated sensor systems were submitted to a 3-month field trial, where they were investigated in both outdoor (traffic hot-spot in Madrid, Spain) and indoor (offices and car parking in Turin, Italy) applications.

The developed sensor system constitutes a successful transfer of metal oxide sensor technology to micro system technology with all advantages a monolithic micromachined sensor system offers: reduced size, packaging and power consumption, integration of electronics, sensor array and on-chip data-evaluation. The integration of metal oxide sensor technology into CMOS-compatible structures allows for a sensor mass production with established microelectronic and microtechnological processes and facilitates cost-effective commercialisation.

The thesis is organised as follows:

Chapter 1: gives an introduction to chemical gas sensors and the motivation for this work

Chapter 2: discusses the measurement principle of metal oxide semiconductor gas sensors

Chapter 3: details the sensor system development process from first concept to final prototype and discusses difficulties encountered and strategies employed

Chapter 4: detailed report on laboratory validation of the ADA sensor system prototype (ADA sensor chip with supporting sensor system) and results of the real world applications tested in the field trials

Chapter 5: summarises the presented work, highlighting the main achievements

2 Metal oxide gas sensors

Metal oxide semiconductor gas sensors are, essentially, gas dependent resistors. A broad range of metal oxides are known for their gas sensing properties, each with a unique sensitivity and selectivity, as given in the literature survey in table 2.1. Their detection principle is based on a modulation of their electrical conduction properties by surface adsorbed gas molecules. The sensitive layer is deposited onto a substrate with a set of electrodes for measuring resistance changes and heating the sensitive layer; normally 2-point resistance measurements are accurate enough for gas sensors. The used metal-oxides are n- or p-type semiconductors, due to the presence of oxygen-vacancies in the bulk. In the case of tin dioxide (SnO_2), the resulting surplus valence electrons can be easily energised and elevated to the conduction band. At the usual operation temperatures of 200 to 400°C all surplus valence electrons can be considered energised and available in the conduction band as free charge carriers. These free charge carriers in the conduction band of tin dioxide determine its conductivity. A change in their concentration due to changes in oxygen partial pressure or other ambient atmospheric changes will change the semiconductor resistance, respectively conductance. It is by such chemical reactions at the surface of the semiconductor involving a charge transfer that a gas induces a sensor signal. This mechanism will be discussed in detail in the following sections.

Metal oxide semiconductor gas sensors			
Semiconductor	**Additives**	**Gas**	**Reference**
SnO_2	Pd, Pt	CO, NO_x, H_2, CH_4	[23], [24]
SnO_2		H_2S, NO_x, O_2	[25]
SnO_2	Ag	H_2	[26]
SnO_2	Ru	LPG	[27]
Ba-, Sr-, $CaTiO_3$		O_2	[28]
WO_3	Pt	NH_3	[29]
WO_3	Au	H_2S	[30]
WO_3		NO_x	[31], [32]
ZnO	Er	NO_x	[33]
ZnO	CuO	H_2, O_2	[34], [35]
TiO_2		O_2, H_2, CO, C_2H_5OH	[36]
In_2O_3	MgO, TiO_2	NH_3	[37]
In_2O_3		O_3	[38]
Fe_2O_3	Zn	NO_2	[39]
Ga_2O_3		O_2, H_2, CO, CH_4	[40], [42]

Table 2.1:   Non exhaustive literature survey of semiconductor materials used as gas sensors. For gas specific literature see [43].

2.1 Material Properties of Tin Dioxide

All sensors used in this thesis are based on tin dioxide (SnO_2). The following observations and discussions will therefore focus on SnO_2 and only include references to other materials where appropriate.

2.1.1 Crystalline Structure

SnO_2 is a semiconductor crystallising in the space group $P4_2mnm$[44], [45]. Its tetragonal unit cell is composed of two tin and four oxygen atoms, with each tin atom octaedrically coordinated by six oxygen atoms. The lattice parameters are a=b=4.74nm and c=3.19nm. The tin atoms are arranged on (0/0/0) and (0.5/0.5/0.5) in the unit cell; the oxygen atoms on ±(0.307/0.307/0) and ±(0.807/0.193/0.5). The corresponding structure is shown in figure 2.1.
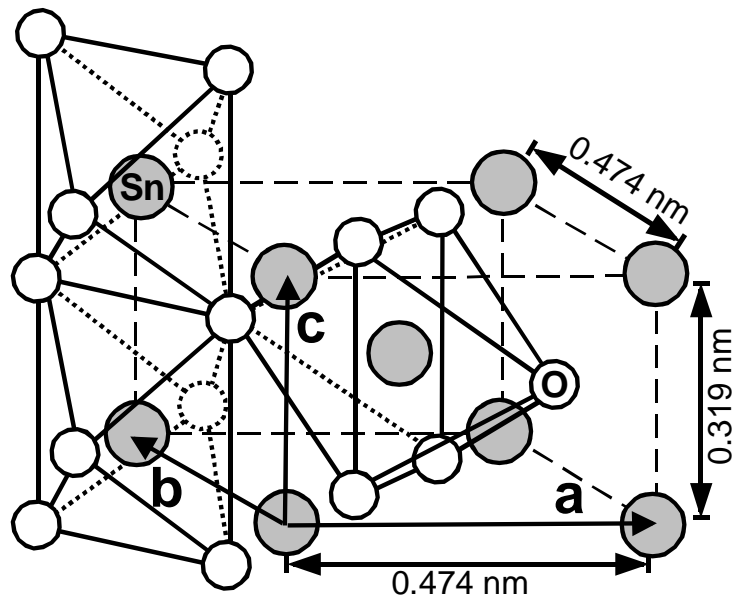
Figure 2.1: SnO$_2$ unit cell with four O^{2-} anions and two Sn^{4+} cations. The crystal structure of SnO$_2$ is rutile crystal, space group 136.

2.1.2 Electronic Properties

SnO_2 is an n-type, wide-bandgap semiconductor [46]. The n-type behaviour of SnO_2 is due to a deficit in oxygen. Donors are simply and doubly ionised oxygen deficiencies with donor states E_{D1} and E_{D2} at 0.03eV respectively 0.15eV below the conduction band [47], [48]. Investigations have proven both donor levels to be completely ionised at the usual operation temperature of 200-400°C (473-673°K) [49], [50]. The conduction band has its minimum at the Γ point in the Brillouin zone and is a 90% tin s-like state. The valence band consists of a set of three bands (2^+, 3^+ and 5^+). The valence band maximum is a Γ_3^+ state. In this way, SnO_2 has a direct bandgap, with energy $E_{cir}(\Gamma_{3v}^+ - \Gamma_{1c}^+) = 3.596$eV for $E_\perp$ and 3.99eV for $E_\parallel$, measured at 4K. Figure 2.2 shows the band diagram for SnO_2 and the projection of the density of states (DOS) for the 1-states of Sn and O. According to results of Barbarat et al. [51] a large contribution of Sn(s)-states is found at the bottom of the valence band between −7 and −5eV. From −5eV to the top of the valence band, Sn(p)-states contribution is decreasing, as the Sn(d)-states are occupying the top of the valence band. A large and extended contribution of the O(p)-states is found in the valence band. Clearly, bonding between Sn and O is dominated by the p-states of the latter. Each anion in the unit cell is found to be bonded to the cations in

a planar-trigonal configuration in such a way that the oxygen p-orbitals contained in the four-atom plane, i.e. p_x and p_y, define the bonding plane. Consequently, the oxygen p orbitals perpendicular to the bonding plane, i.e. p_z orbitals, have a non-bonding character and are expected to form the upper valence levels [51]. The conduction band shows a predominant contribution of Sn(s) states up to 9eV. For energies larger than 9eV an equal contribution of Sn- and O-states is found in the conduction band. More information, mainly about the valence band, can be found in [52]-[54] and references therein.
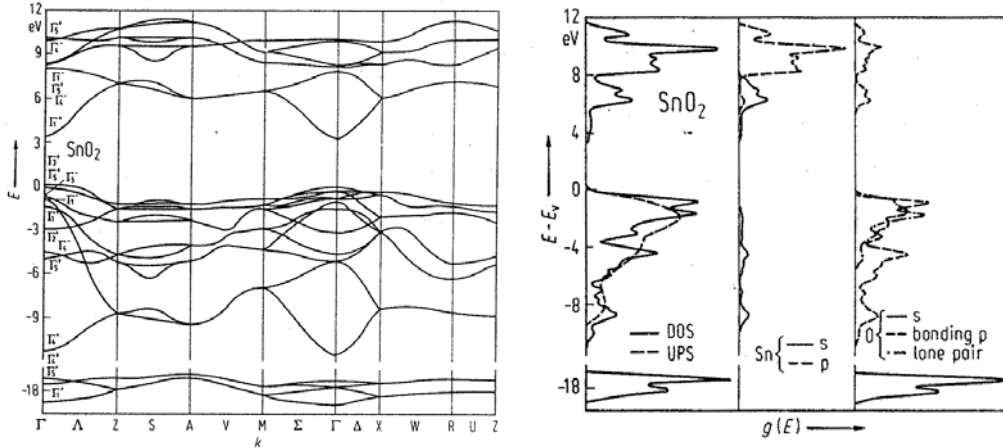
Figure 2.2: Band diagram of SnO₂ (left) and projection of the DOS for the 1-s states of SnO₂, Sn and O (right) [51].

2.1.3 Bulk Conductivity

The conductivity of a semiconductor crystal can be described as the sum of electronic and ionic conductivity if the conduction processes are considered independent. SnO_2 gas sensors are typically operated at temperatures between 200 and 400°C. At these temperatures the ionic contribution can be neglected and the conductivity of SnO_2 be calculated according to:

$$\sigma = \sigma_e + \sigma_p + \Sigma\sigma_{ion,i} \approx \sigma_e + \sigma_p \qquad (2.1)$$

The resistance of homogeneous bulk material with bulk conductivity σ_b, mobility μ, length l and cross section A can be calculated according to:

$$R_b = \sigma_b \cdot l/(b \cdot d) = \sigma_b \cdot l/A, \text{ with } \sigma_b = \sigma_e + \sigma_p = n \cdot \mu_e \cdot e + p \cdot \mu_p \cdot e \qquad (2.2)$$

where the charge carrier concentration n and p for an intrinsic semiconductor can be calculated according to:

$$n = \int_{E_C}^{\infty} D(E)f(E)dE ; \quad p = \int_{\infty}^{E_V} D(E)(1-f(E))dE \qquad (2.3)$$

with the Fermi-Dirac distribution f(E) and the density of states D(E):

13

$$D(E) = \frac{1}{2\pi^2}\left(\frac{2m_e}{h^2}\right)^{\frac{3}{2}}(E-E_C)^{\frac{1}{2}}; \quad f(E) = \frac{1}{1+\exp\left(\dfrac{E-E_F}{kT}\right)} \tag{2.4}$$

For $E_C - E_F \geq 4kT$, the charge carrier concentrations n and p can be approximated by:

$$n = N_C \exp\left(\frac{E_F - E_C}{kT}\right); \quad N_C = 2\left(\frac{2\pi m_e kT}{h^2}\right)^{3/2} \tag{2.5}$$

$$p = N_V \exp\left(\frac{E_V - E_F}{kT}\right); \quad N_V = 2\left(\frac{2\pi m_p kT}{h^2}\right)^{3/2} \tag{2.6}$$

In an extrinsic semiconductor additional donor or acceptor levels appear. Also, in the case of extrinsic semiconductors the equations (2.5) and (2.6) hold and the extrinsic doping shifts the Fermi level towards the conduction band for n-doped semiconductors and towards the valence band for p-doped semiconductors.

For operation at room temperature (300K), literature suggests charge carrier densities in the range of $2\cdot10^{15}$ to $6.8\cdot10^{20}$ / cm^3 [55][57]. The influence of temperature on the charge carrier density can be determined with Hall measurements [48]. From these results it seems that the shallow donor levels (0.03eV) are completely ionised above 100K, the deep donor levels (0.15eV) start to be completely ionised around 500K. Therefore the donors can be considered completely ionised in the typical temperature range for sensor operation (200-400°C, i.e. 473-673K) [47], [48].

To conclude, the conductivity of SnO$_2$ is determined by donor and acceptor energy levels, charge carrier concentration and the operation temperature. So far, only the bulk conductivity has been discussed. In the following sections, the surface of SnO$_2$ crystals will be taken into account. Here, the gas-sensor interaction occurs and thus its contribution determines the influence of the ambient gas atmosphere on conductivity.

2.2   Chemical and Physical Properties of Metal Oxide Surfaces

When discussing the atomistic and electronic behaviour of a surface there are two dominant models in literature: the atomistic model [58]-[60], or surface molecule model, generally preferred by chemists. And the band model [61], [62], generally preferred by physicists. The atomistic model is most appropriate for chemical processes at a solid surface. It describes the solid surface in terms of surface sites or atoms, ignoring the band structure of the solid. The band model is preferable for electron exchanges between (semiconductor) solids and surface groups that include a conductivity change of the solid. It describes the surface in terms of surface states, i.e. localised electronic energy levels available at the surface, ignoring the microscopic details of atom-atom interaction between surface species and its neighbouring atoms.

Both models have their merits, but to understand the surface reactions of semiconductors with gases both chemical and physical view have to be considered [63].

From a chemical point of view a surface can be divided into surface sites of varying reactivity. Usually, more reactive sites can be associated with heterogeneous surface regions or surface imperfections. Examples of reactive sites are surface atoms with unoccupied or

unsaturated orbitals ("dangling bonds"), surface atoms with unsaturated coordination sphere, crystallographic steps, intersections, interstitial defects or superstructures.

From a physical point of view the interruption of the crystal periodicity at the surface results in localised energy levels. These can function as acceptor or donor states, exchanging or sharing electrons with the non-localised energy bands in the bulk of the solid. Those energy levels in the band gap have an effect on the electronic properties of the solid, especially for semiconductors. Surface states can result from non-ideal stoichiometry or bulk defects (intrinsic) or arise from (intentional) impurities, as for doping (extrinsic).

In the following sections, the interaction of gases with surfaces is discussed and how this can lead to a change in the conductivity of a semiconductor and finally, a sensor signal.
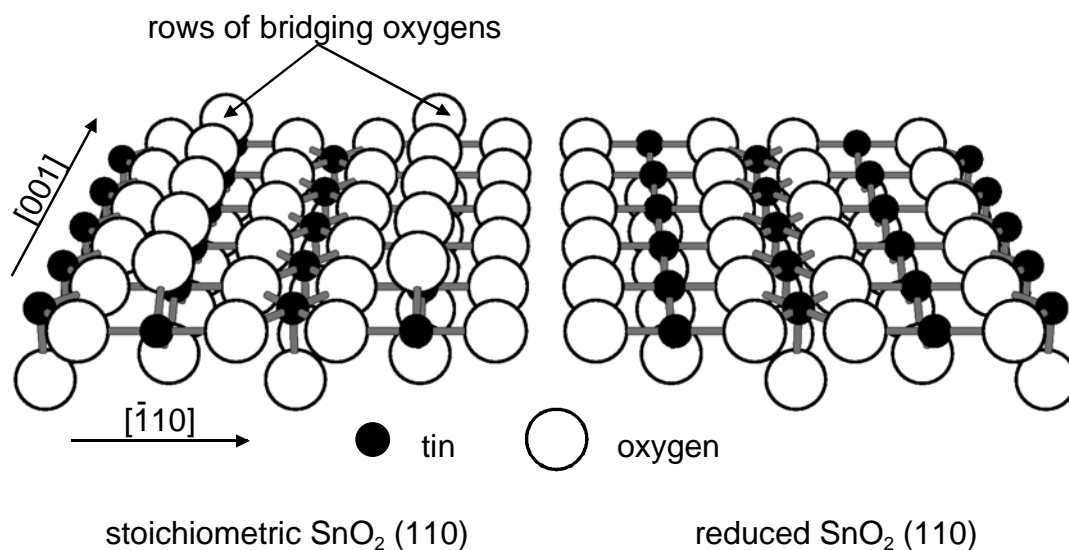
Figure 2.3: Ideal and reduced (compact) SnO2 (110) surfaces; the latter is obtained by removing the bridging oxygen layers.

2.2.1 Physisorption and Chemisorption

The fundamental stage of all surface processes is the adsorption of foreign atoms or molecules that causes essential rearrangements of surface chemical bonds and, consequently, the variation of the surface states density and surface potentials. When discussing the interaction of gaseous molecules with surfaces of solids it is of interest to differentiate between physisorption and chemisorption [64].

Interaction type	Energy [kJ/mol]	Comment
covalent	120 - 800	chemical reaction
ion - ion	250	only between ions
coordination, complexion	8 - 200	weak chemical interaction
ion - dipole	15	between ions and polar molecules
hydrogen bond	20	hydrogen bond $A-H^{\delta+}...B^{\delta-}$
dipole - dipole	0.3 - 30	between polar molecules
London (induced dipole to induced dipole)	0.1 - 2	physical interaction between all molecules

Table 2.2: Bond energies for different types of interaction [65].

Physisorption takes place at a relatively large distance r from the surface (adsorbant). A gaseous molecule (adsorbate) approaching the surface is slightly polarised and induces an equivalent dipole in the adsorbant. This dipole - dipole bond between gas and surface results in an interaction energy $\Delta E = 0\text{-}30kJ/mol$ with $\Delta E \sim r^6$ (see table 2.2).

Physisorption is the first step in the interaction between a gas and the surface of a solid. Physisorbed molecules may thereafter become chemisorbed if they exchange electrons with the surface of the semiconductor. Physisorption is characterised by a high surface coverage with gaseous molecules at low temperatures and a low coverage at high temperatures. For the adsorption of up to one monolayer, this coverage θ is defined as follows:

$$\theta = \frac{N}{N_t} \tag{2.7}$$

with the number of molecules adsorbed per surface unit N and the total number of surface adsorption sites N_t.

Chemisorption introduces higher bonding energies and consequently stronger interactions between adsorbate and adsorbant. It results from a profound modification of the charge distribution of the adsorbed molecule: the bonding energies are of similar strength as for chemical bonds. One can distinguish between neutral chemisorption and ionosorption. Figure 2.4 details the potential energies in case of physisoption (E_{phys}) and chemisorption (E_{chem}) as a function of the distance r from the surface.
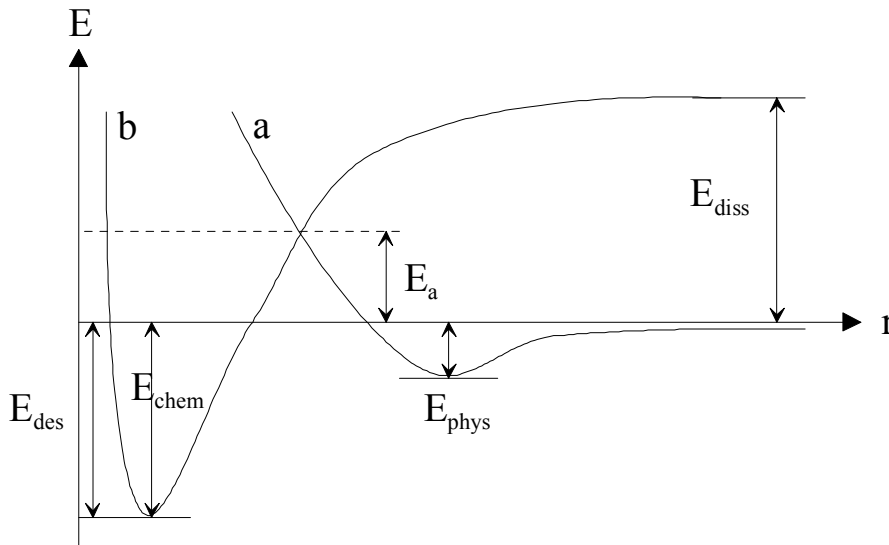
Figure 2.4:   *Lennard-Jones model of physisorption and chemisorption: (a) physisorption of a molecule; (b) chemisorption of a molecule. Activation energy E_a, dissociation energy E_{diss}, desorption energy E_{des}.*

If a gaseous molecule approaches the surface it will first be physisorbed, gaining ΔE equal to E_{phys}. Upon a further approach towards the surface the molecule encounters a growing energy barrier, tending towards an infinite energy for a finite distance r. By spending the activation energy E_a the gaseous molecule can dissociate, thereby allowing a further approach to the surface. This stronger interaction with the surface (chemisorption) results in a higher energy gain ΔE equal to E_{chem} than during physisorption. This energy gain ΔE_{chem} depends strongly on the individual surface sites available and their reactivity. The most reactive sites will

16

therefore be occupied with gaseous molecules during thermodynamic equilibration. However, the chemisorption energy not only depends on the number of reactive sites (high potential gain in ΔE_{chem}) but also on the ambient gas concentration p_{gas} and temperature T (probability of molecules overcoming the energy barrier E_A).

As for chemisorption, desorption also requires the molecule to overcome an energy barrier $E_{des} = E_{chem} + E_a$. Therefore chemisorption and desorption are both activated processes requiring an activation energy supplied either thermally or by photoexcitation, contrary to physisorption which is a slightly exothermic process. The adsorption rate of gaseous molecules is proportional to the gas pressure and to the number of unoccupied adsorption sites according to

$$\frac{d\theta}{dt} = k_{ads}(1-\theta)p_{gas} \qquad (2.8)$$

with the adsorption constant $k_{ads} = A \cdot \exp(-E_A/kT)$.

The desorption rate is proportional to the number of occupied sites according to

$$\frac{d\theta}{dt} = k_{des}\theta \qquad (2.9)$$

with the desorption constant $k_{des} = B \cdot \exp(-E_{Diss}/kT)$.

The net adsorption rate can therefore be described through (2.8) and (2.9) by

$$\frac{d\theta}{dt} = k_{ads}(1-\theta)p_{gas} - k_{des}\theta \qquad (2.10)$$

With a resulting equilibrium coverage θ for $d\theta/dt=0$ of

$$\theta = \frac{p_{gas}}{p_{gas} + \dfrac{k_{des}}{k_{ads}}} ; \qquad \theta = f(p_{gas}, T) \qquad (2.11)$$

Equation (2.12) represents the Langmuir isotherm. It shows that all adsorption and desorption processes not only depend on the nature of the adsorbate and adsorbant but also on the availability of absorbates (partial pressure) and on the temperature. The above observations are correct only for adsorption and desorption of gaseous monolayers on surfaces of solids. Taking also multi-layer adsorption and desorption processes into consideration results in the Brunauer-Emmet-Teller (BET) isotherm with related rate constant equations [66].

2.2.2 Acidic and Basic Properties of Surface Sites

The detection of gases with a semiconductor sensor induces chemical reactions between gas phase and solid. Electrons, and possibly even protons, are transferred between adsorbate and adsorbant; the detection of gases is in many aspects very similar to heterogenous catalysis. The essential step, in most chemical reactions, is the interaction of a non-bonding electron pair (of a molecule or ion) with a centre of electron deficiency (a vacant orbital or partial positive charge) on another species. The electron donating sites, or Lewis basic sites, and the electron accepting sites, or Lewis acid sites, determine the reactivity of the molecules [67]-[69]. The strength of the acido-basic properties of surfaces can be determined by probe molecules [70], [71], such as NH_3, pyridine, CO (for acid sites) and CO_2, SO_2 (for basic sites).

The complex interactions at the interface gas/solid prevent simple models and predictions for the chemical reactions taking place. Gases have differing acido-basic properties and their interaction with solid surfaces depends on the acidic or basic character of these surfaces. Correspondingly, the surface of a solid can be described as an accumulation of acid-base pairs.

Two theories are dominant in describing the acid-base character of a system [72]: the theory of Brønsted [73] and the theory of Lewis [74]. According to the first theory, an acid-base reaction is simply the transfer of a proton from the acid to the base, resulting in a conjugated acid and conjugated base. The strength of acidity is defined as the tendency to impart a proton and the strength of basicity as the tendency to accept a proton. According to Lewis, an acid is a species with a vacant orbital and an acid-base reaction is a reaction where the free electron pair of the base starts a covalent bond with the vacant orbital of the acid. Brønsted sees the proton himself as the acid as it has a vacant orbital. The theory of Lewis is more general as it works with concepts of free and vacant orbitals without relying on protons.

Coming back to semiconductor surfaces, their properties can be described in terms of Lewis' acidity and basicity. The metallic cations, deficient in electrons, are generally Lewis acid sites while the oxygen anions, rich in electrons, are generally Lewis basic sites [75], [76]. The acidic or basic strength of molecules can be characterised by a set of empiric rules. The acidic strength of molecules MX_n

- diminishes with the shell of M (attraction between positive nucleus M and the electron pair diminishes)
- increases with the electronegativity of X
- is maximal for compounds with a minimum value of n

The basic strength of bases OM_2

- grows with the electron donating character of M
- increases with the electropositive character of M and its oxidation state, if M is a metal

As the semiconductor surface is in constant interaction with ambient gases, we have to consider at least a partial hydroxylation of the surface. Such surface hydroxyl-groups are potential acceptors or donors of protons. It is therefore also necessary to consider the Brønsted acid and basic properties of the semiconductor surface. The strength of Brønsted acid sites AH increases with

- the electron affinity of A
- the stability of A^-
- the ability of the conjugated base A^- to delocalise and distribute the negative charge

The presence of surface sites with various properties (acidic, basic or redox) leads to concerted mechanisms and sequential interactions during chemical reactions with gases. Consequently, materials with acid-base pairs on the surface may decrease the activation energy of chemical reactions, stabilise reaction intermediates or offer faster reaction kinetics than surfaces with only acid or basic sites [67]. As discussed, the acido-basic properties of surface sites influence the chemical reactions and in some cases can even determine reaction paths. An example is the oxidation of ethanol, which follows different reactions depending on the acidity or basicity of surface oxygen [77][78]:
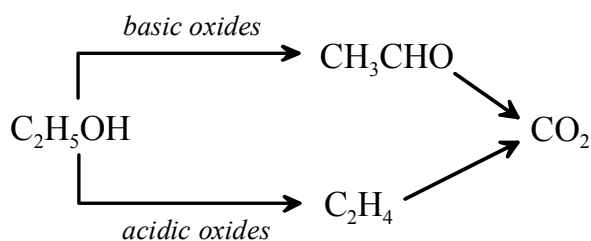
The acido-basic properties control the adsorption and desorption of the reactands, the intermediaries and reaction products [79], [80]. Acidic sites favour the adsorption of basic molecules and increase desorption of acidic products, and vice-versa [81].

2.2.3 Space Charge Effects

If we move from discussing the bulk properties of ideal crystals to surfaces in realistic environments, we have to accept a state of constant adsorption and desorption in a thermodynamic equilibrium situation. It is of interest to analyse the effect the adsorption of oxygen has on the electrical properties of a semiconductor. Due to the high electronegativity of oxygen its adsorption leads to an oxidation of the semiconductor surface and a reduction of the gas, i.e. a transition of electrons from the conduction band E_C to surface acceptor states. A negative charge is created at the surface. This negative surface layer has to be compensated by a positive countercharge in the solid. Would the adsorption take place at the surface of a metal, this would simply result in a planar countercharge: a double layer situation as for a capacitor. However, unlike a metal, a semiconductor does not have a large amount of mobile free charge carriers available at the surface. The countercharge will therefore be formed in the bulk (donor ions), resulting in a space charge region. According to the Schottky approximation [82], this region is characterised by a total exhaustion of mobile charge carriers (all moved to the surface) and therefore called depletion layer. Between these two space charge layers (the planar at the surface and the region in the bulk), an electric field develops. A measure for the reach of this electrical field is the Debye-Length L_D:

$$L_D = \sqrt{\frac{\varepsilon_r \varepsilon_0 kT}{e^2 N_{(V)}}} \qquad (2.12)$$

Equation (2.13) gives a relation between the Debye-Length L_D (the extension of the space charge region into the bulk) and the concentration of free charge carriers $N_{(V)}$: assuming a high enough temperature to allow mobility to all potentially free charge carriers, L_D is high for a low density of free charge carriers in the volume and vice-versa. Hereby, the concentration of free charge carriers $N_{(V)}$ can be set as equivalent to the concentration of free electrons $N_{e(V)}$, as the concentration of other charge carriers is negligible for the usual operation temperatures (200-400°C) of SnO_2.

The space charge region corresponds to a band bending in the band model of the semiconductor: the potential energy of an electron near the surface is increased by the electrostatic repulsion of the negative surface layer; the negative charge at the surface creates a surface barrier qV_S.

These discussed considerations lead to an adaptation of the semiconductor band model for surface situations as detailed in figure 2.5.
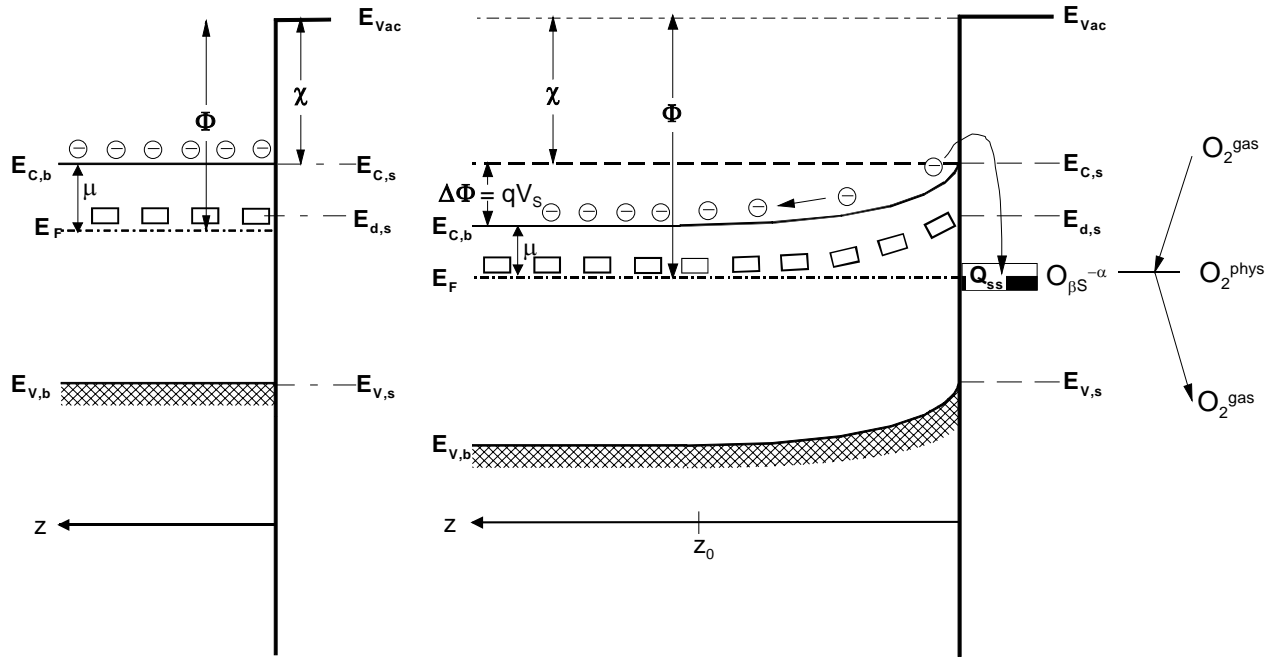
Figure 2.5:   Flat band situation for an n-type semiconductor (SnO₂) in the bulk (left) and at the surface with oxygen adsorption (right). With the axis perpendicular to the surface z, the depletion region z₀, work function Φ, electron affinity χ and electrochemical potential μ.

The behaviour of the semiconductor solid, both its chemical and electrical characteristics, is strongly influenced by the development of double layers at the surface and can even be dominated by them.

From an electrical point of view, the formation of a double layer represents injection or withdrawal of charge to or from the bands of the semiconductor. This represents a change in the density of current carriers. Additionally, through the relocation of the Fermi level E_F in relation to the vacuum energy E_{Vac}, the work function Φ of the solid changes.

The chemical properties of the solid surface are also dominated in many cases by double layers. The newly introduced surface barrier translates to an activation energy increase $\Delta E_A = qV_S$ for an electron transfer between the semiconductor and a gaseous molecule (necessary for a chemical reaction); the availability of electrons and thereby the probability of a reaction is decreased. Or, differently put, the double layer forming will, by electrostatic repulsion, decrease the density of charge carriers near the surface. Which, in turn, will decrease the rate and energy of further adsorptions.

2.2.4 From Charge Transfer to Sensor Signal

The band bending (i.e. surface energy barrier for electrons trying to travel from the bulk to the surface) induced by interaction of the tin dioxide solid with oxygen is the initial electronic situation a gaseous species encounters if converging to the sensor surface. Depending on the reactivity of the remaining surface sites and of the gaseous species adsorption on the metal oxide will result in one of the following [70]:

- Molecular (non-dissociative) adsorption, in which the interaction is mainly by σ-donation and/or π-bonding interaction

20

- Dissociative adsorption, in which a molecule dissociates homolytically or heterolytically upon adsorption. Usually an anion-cation coordinatively unsaturated pair site is required. Dissociation of H_2O into H^+ and OH^- is an example of heterolytic dissociative adsorption into charged species.
- Abstractive adsorption, in which the adsorbate abstracts a species from the surface or a previously adsorbed species from the surface. The former is often a proton and commonly occurs on acidic oxides. The latter could be previously adsorbed oxygen.
- Reductive (oxidative) adsorption, in which an adsorbed molecule is oxidised while the surface is reduced, or vice-versa.
- Catalysis, in which the surface acts as catalyst and lowers the activation energy for a reaction between adsorbed species and a previously adsorbed molecule. The surface remains chemically unchanged by the interaction.

As the sensor measures a change in the surface conductivity of the sensitive material (SnO_2), only a change of its electronic properties, i.e. a free charge transfer from or to an adsorbed species will result in a sensor signal. Other surface reactions may occur that do not influence the surface band bending. Examples include reactions on the surface that do not involve the solid and dipole-dipole-interactions with adsorbed hydroxyl groups. Thereby the electron affinity χ or work function Φ of the sensor surface may be changed without resulting in a sensor signal. Therefore only the reductive/oxidative adsorption and abstractive adsorption will result in a sensor signal as defined in this work, i.e. a change of the metal oxide sensors conductivity. Figure 2.6 gives an overview of the possible effects such an adsorption with charge transfer has on the electronic properties of the semiconductor.

Gases with low electronegativity can act as donors, transferring electrons to the semiconductor. The increase in charge density will reduce the surface potential barrier, depth of the depletion region and work function resulting in an increased conductivity. However, reducing gases utilised in this work, such as carbon monoxide or hydrocarbons, do not choose this direct interaction with the semiconductor. Instead, they react with adsorbed oxygen as mentioned for the abstractive adsorption. The electron previously trapped by the adsorbed oxygen species is released into the conduction band of the metal oxide upon desorption of the reaction product. In this way the electronic properties of the semiconductor are affected indirectly by a surface reaction with the same results as for a donor interaction: increase in charge density and thereby increase of the conductivity.

Oxidising gases utilised in this work, such as nitrogen dioxide or ozone, will act as acceptors, trapping electrons from the semiconductor at surface states. The decrease in charge concentration will increase the surface potential barrier, depth of the depletion region and work function resulting in a decreased conductivity just as for the adsorption of oxygen discussed in *section 2.2.3.*
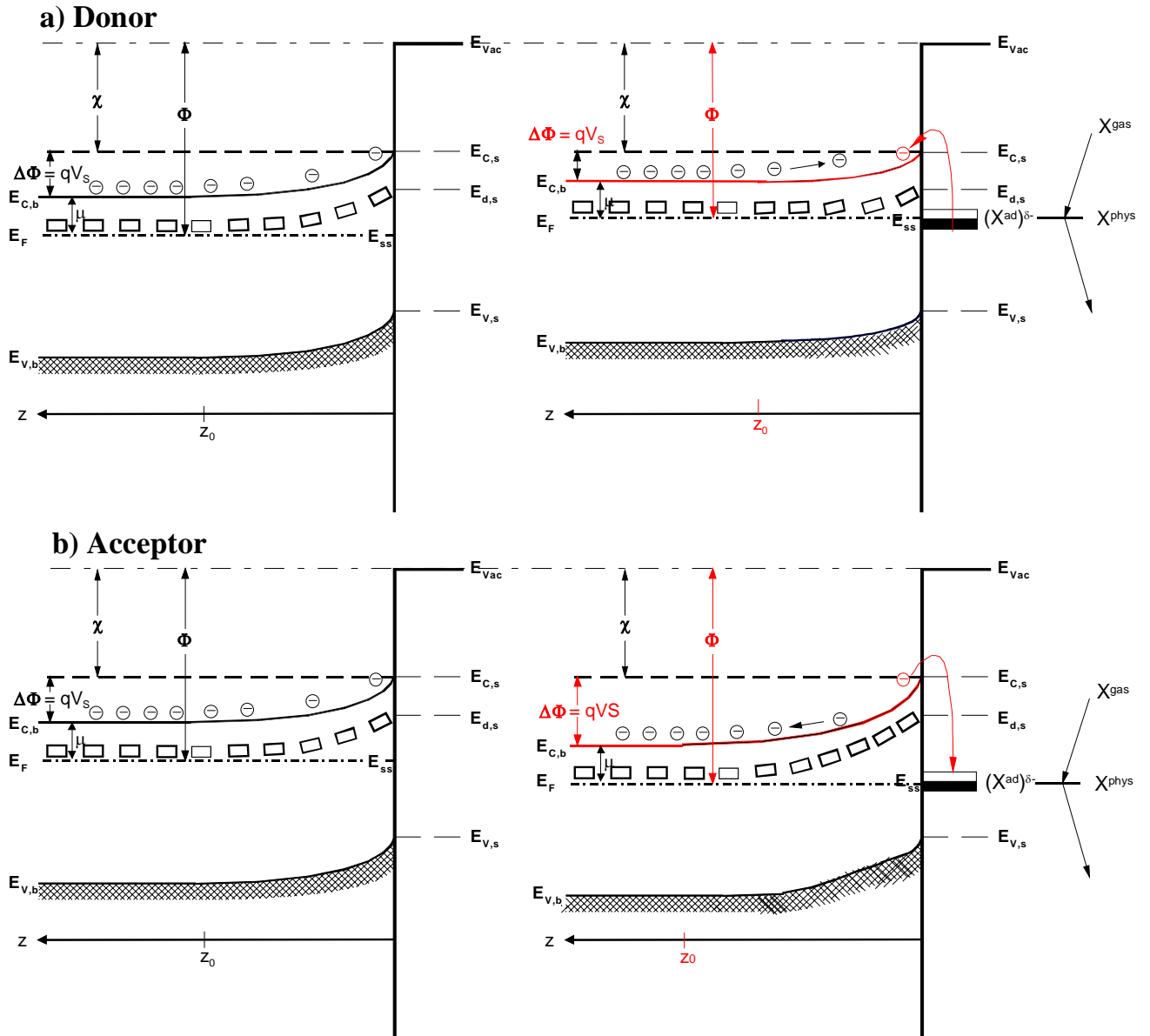
Figure 2.6: *Adsorption of gaseous species and their effect on the electronic properties of an n-type semiconductor (SnO_2). a) Gaseous species acts as donor: (left) surface band model, (right) changes to the electronic properties induced by the charge transfer from the adsorbate to the conduction band E_C: decrease of the surface potential barrier qV_S, depth of the depletion region z_0 and work function Φ and increase of free charge carrier concentration. b) Gaseous species acts as acceptor: (left) surface band model, (right) changes to the electronic properties induced by the charge transfer from the conduction band E_C to the adsorbate: increase of the surface potential barrier qV_S, depth of the depletion region z_0 and work function Φ and decrease of free charge carrier concentration.*

2.2.5 Conduction in the Sensing Layer

We can conclude from the above discussions that the conductivity of poly-crystalline SnO_2 depends not only on the intrinsic and extrinsic (oxygen-)defect concentration in the bulk and the mobility of the charge carriers but also on the partial pressure of ambient gaseous species. While the conductivity of mono-crystalline samples is understood (see *section 2.1.3*), the

matter is more difficult for poly-crystalline samples. It is necessary to differentiate between compact and porous layers. A compact layer situation is encountered nearly exclusively for thin film sensors. The bulk of the sensitive layer is not accessible to the ambient gases and all reactions take place at the continuous surface. For thick film sensors, such as used in this work, porous layers are most commonly encountered. The sensitive layer is composed of a multitude of metal oxide grains of a similar size. Ambient gases have access to the solid of the sensitive layer and chemical reactions can take place at the surface of the grains, resulting in a much higher surface area than for compact layers.

The grain size in relation to the Debye-Length L_D (extension of the depletion region into the grain) is a defining factor for the conductivity. Two different cases can be discriminated: partly depleted grains, i.e. grains with a grain radius $r > L_D$ and fully depleted grains with $r < L_D$. In the first case, electrons have to overcome a surface potential barrier every time they cross from one grain to the next, similar to a Schottky barrier [83] (see figure 2.7). Therefore grain boundaries, the bottlenecks of electronic conduction, play an important role in the conduction and consequently the sensing mechanism. In the second case, the band bending (and thereby change of free charge carrier concentration by adsorption of gases) extends throughout the complete grain. The small size of such nanocrystalline grains limits the strength of the band bending and thereby the potential drop between grain surface and grain centre. This can result in a surface potential barrier $qV_S < kT$. The energy barrier will then be too small to hinder the mobility of free charge carriers, resulting in a flat band situation. The effect of gases can be approximated by a shift in bands on the surface relative to the Fermi level and the related shift in electron concentration. The conduction models and their dependency on geometric effects are discussed in detail by Bârsan and Weimar [84].
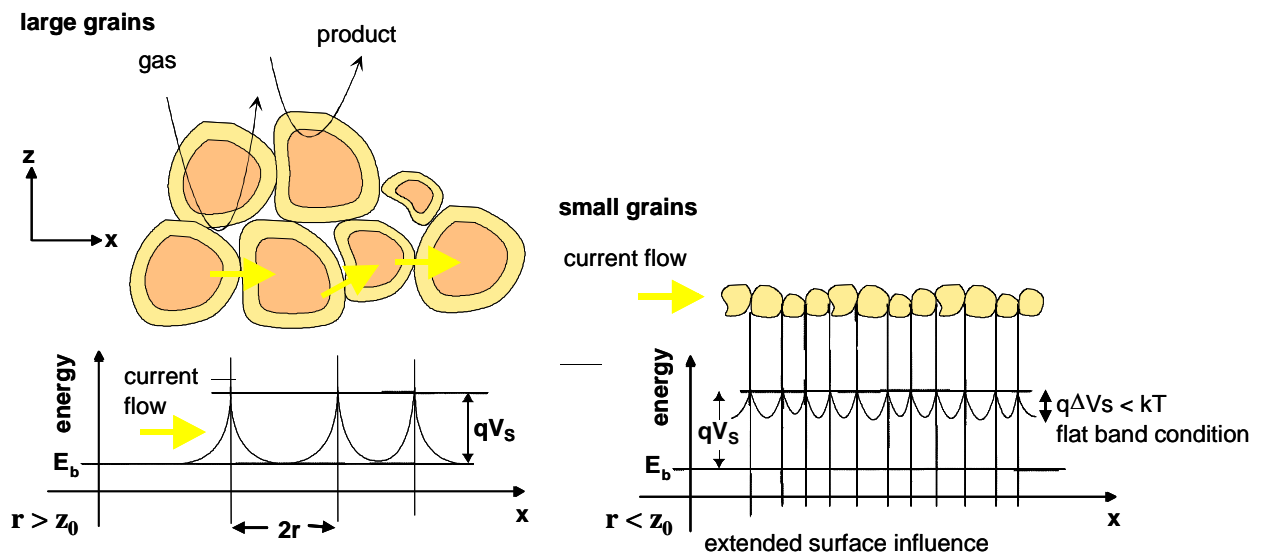
Figure 2.7: *Grain size and gas interaction. Two cases can be discriminated: grains with a radius r larger than the Debye-Length L_D (left) and grains with a radius smaller than the Debye-Length L_D (right). In the first case an energy barrier is built up at the grain boundaries which electrons have to overcome. In the second case, the energy barrier extends throughout the grain. This situation can be approximated by a shift in the Fermi energy in relation to the conduction and valence bands.*

2.3 Interaction of Selected Adsorbants with SnO$_2$ Surface

2.3.1 Adsorption of Oxygen (O$_2$)

Gas sensors are usually operated in an ambient atmosphere containing oxygen. Therefore, the interaction with oxygen is crucial as discussed above. At temperatures between 100 and 500°C oxygen is ionosorbed onto the sensor surface as molecular (O$_2^-$) and atomic (O$^-$, O^{--}) species according to:

$$\frac{\beta}{2}O_2^{Gas} + \alpha \cdot e^- + [S] \longleftrightarrow O_{\beta S}^{-\alpha} \qquad (2.13)$$
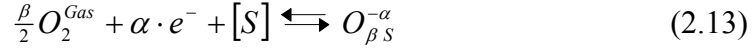
where O$_2^{gas}$ is an oxygen molecule in the ambient atmosphere and e$^-$ is an electron which can reach the surface despite the electric field resulting from the surface double layer. The concentration of free charge carriers (electrons) is n$_S$, S is an unoccupied chemisorption site for oxygen, $O_{\beta S}^{-\alpha}$ is a chemisorbed oxygen species with: α = 1 for singly ionised forms, α = 2 for doubly ionised forms, β = 1 for atomic forms, β = 2 for molecular forms.

The concentration of adsorbed oxygen species, such as O$_2^-$, O$^-$ and O^{2-}, is a key element in the response of semiconductor gas sensors to gases [85]. TPD (*Temperature Programmed Desorption*), FTIR (*Fourier Transform Infrared Analysis*) and EPR (*Electron Paramagnetic Resonance*) have been used to examine the oxygen species present at the surface with results as detailed in figure 2.8. Below 180°C the molecular form dominates and above this temperature the ionic forms dominate.
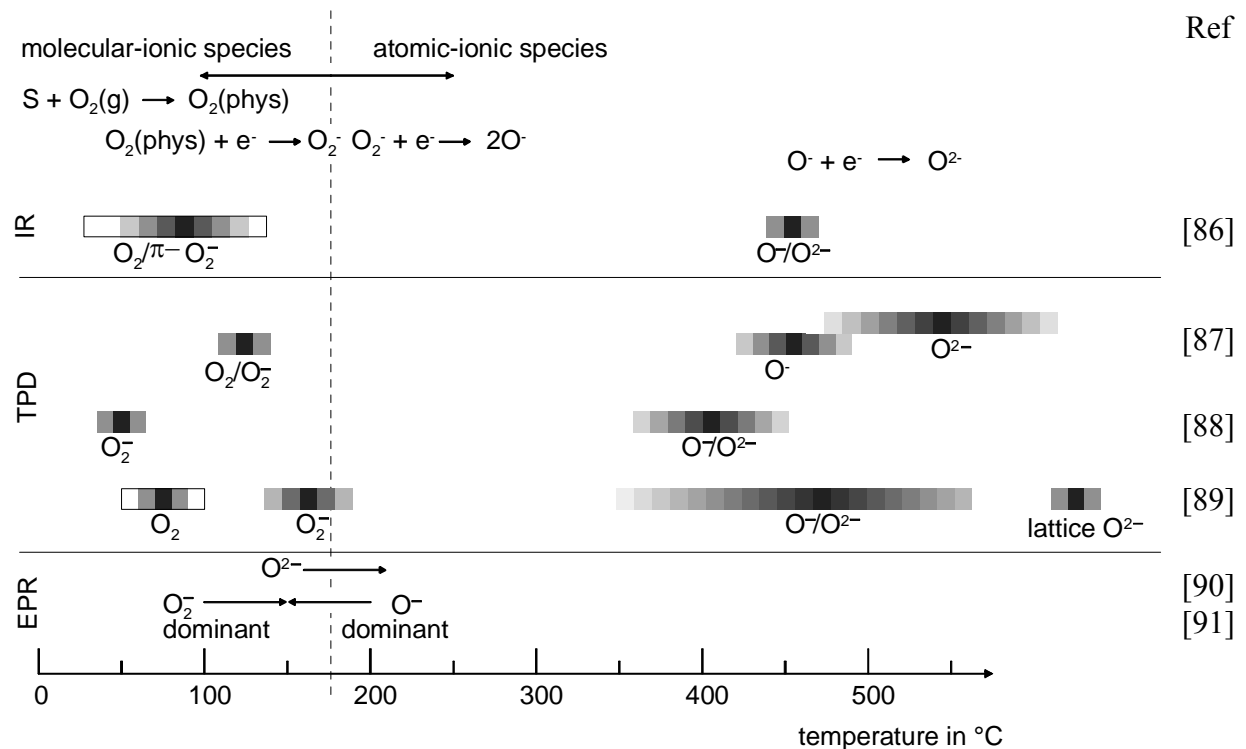
Figure 2.8: Literature survey of oxygen species detected at different temperatures at SnO$_2$ surfaces with TPD, FTIR and EPR [92].

The chemisorption of oxygen is a process that can be divided into two parts: an electronic one and a chemical one. Adsorption is produced by a charge transfer between adsorbate and adsorbant at a surface state, which does not exist previous to adsorption. Therefore, the limiting factor is chemical (activation energy) at the beginning of the adsorption, due to the unlimited availability of free electrons in the absence of band bending. After the building of

the surface charge, a strong limitation is coming from the potential barrier, which has to be overcome by electrons in order to reach the surface. Desorption is controlled from the beginning by both electronic and chemical parts; the activation energy is not changed during the process if the coverage is not high enough to provide interaction between the chemisorbed species [63]. Because of electrostatic repulsion, surface coverage with adsorbed oxygen species is normally limited to 10^{-5} to 10^{-3} of a monolayer. Assuming the Schottky approximation [63] to be valid and a temperature high enough to have all donors ionised the relation between the sensor conductance and the oxygen partial pressure can be described by

$$G \propto p_{O_2}^{-0.5} \qquad\qquad (2.14)$$

The exact relationship is influenced by the sensor material (doping) and geometry (layer thickness, grain size, sintering) [84].

2.3.2 Adsorption of Water (H_2O)

For many applications water will be present as an interfering gas. Therefore, the interaction of water with the semiconductor surface is of great interest. TPD and IR studies have shown that the adsorption of water vapour results in molecular water, adsorbed by either physisorption or hydrogen bonding, and hydroxyl groups formed at the surface as a consequence of the dissociation of water (see figure 2.9).

physisorbed | bonded via hydrogen bridge | chemisorbed hydroxyl groups | Ref

$H_2O(g)+ S \longrightarrow H_2O(phys)$

$H_2O(phys) \longrightarrow H_2O$ (H-H bond)

H_2O (H-H-bond) $+ O_{I,s}^- \longrightarrow 2\ OH + V_{O,s}$ $V_{O,s} \longrightarrow V_{O,I}^{\cdot} + e^-$ [93]

TPD:
- H_2O (phys) | HOH—O (s) | different OH bondings | [94]
- OH on different faces | [95]
- H_2O (phys) | OH | [89]

QMB:
- H_2O (phys) | HOH O (s) | OH on different faces | [96]
- H_2O (phys) | HOH O (s) | (H-bonds), OH | [97]

IR:
- H_2O (cond.) | H_2O (phys) | isolated OH | H...OH | [86]
- H_2O (phys) | OH | [98]

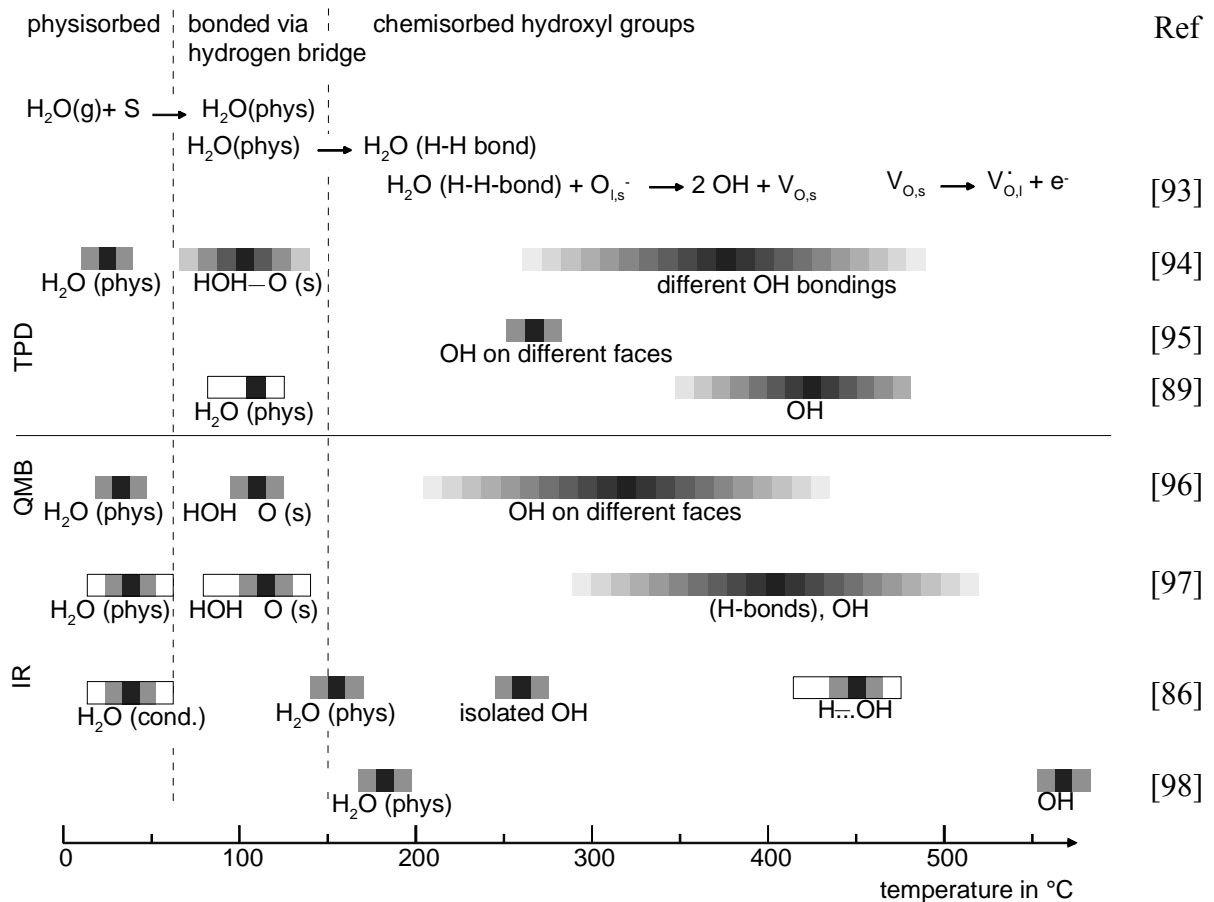temperature in °C: 0, 100, 200, 300, 400, 500

Figure 2.9: Literature survey of water-related species formed at different temperatures at SnO₂ surfaces [92].

Above 200°C molecular water is no longer present, whereas OH groups are still present above 400°C. IR investigations prove the presence of hydroxyl groups. However, the way in which and where the hydroxyl groups are fixed on the tin dioxide is still under discussion. Barteau [99] proposes an acid/base reaction with the hydroxyl OH⁻ sharing its electron pair with the Lewis acid site (Sn) and leaving the weakly bonded proton H⁺ ready for reactions with the Lewis base (lattice oxygen or adsorbed oxygen). Heiland and Kohl [100] assume a homolytic dissociation of water resulting in two hydroxyl groups, an "isolated" hydroxyl bond to lattice tin and a "rooted" hydroxyl group including lattice oxygen.

All experiments reported a reversible increase in the surface conductance in the presence of water. The conductance increase does not vanish with the molecular water but with the disappearance of hydroxyl groups [101]. Several mechanisms have been suggested to explain this finding. Two direct mechanisms have been proposed by Heiland and Kohl [100]. The first attributes the role of electron donors to the rooted OH group, which includes lattice oxygen according to:

$$H_2O^{gas} + Sn_{lat} + O_{lat} \longleftrightarrow \left(Sn_{lat}^+ - OH^-\right) + \left(OH\right)_{lat}^+ + e^- \qquad (2.15)$$
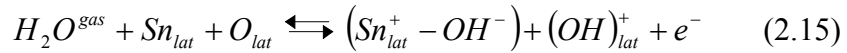
where Sn_{lat} and O_{lat} are tin and oxygen atoms in the lattice.

The reaction would imply the homolytic dissociation of water and the reaction of the neutral H atom with the lattice oxygen:

$$H + O_{lat}^{2-} \longleftrightarrow \left(O_{lat}H\right)^- + e^- \qquad (2.16)$$

The second mechanism takes into account the reaction between the proton and the lattice oxygen and the binding of the resulting hydroxyl group to the tin atom. The resulting oxygen vacancy produces additional electrons by ionisation according to:

$$H_2O^{gas} + 2 \cdot Sn_{lat} + O_{lat} \longleftrightarrow 2 \cdot \left(Sn_{lat}^+ - OH^-\right) + V_O^{++} + 2 \cdot e^- \qquad (2.17)$$
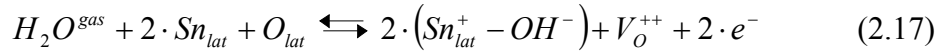
However, Yamazoe [89] found a minimum temperature of 600°C is necessary to extract oxygen from the bulk. Due to the weak abstractive powers of the hydrogen atom it is therefore highly unlikely that equation (2.18) takes place at low to medium temperatures. Others [102], [103] assumed a reaction with chemisorbed oxygen instead of the surface lattice, which would result in two hydroxyl groups linked to tin. Morrison [63], as well as Henrich and Cox [104], consider an indirect effect, i.e. the interaction between either hydroxyl OH⁻ or proton H⁺ with an acidic or basic group, which are also acceptor surface states. The coadsorption of water with another adsorbate, which could be an electron acceptor such as oxygen, may change the electron affinity of the latter. Such an interaction of adsorbed species was recently proven by Koziej et al. [105] for water and oxygen.

Henrich and Cox suggested that preadsorbed oxygen can be displaced by water adsorption. Caldararu and others [106]-[108] assume a blocking of the adsorption sites for oxygen by water. For all these mechanisms the particular state of the surface plays an important role. Egashira et al [94] showed by TPD and isotopic tracer studies that the rearrangement of oxygen adsorbates due to the presence of water vapour depends on the surface doping. Clifford and Tuma [109] approximated the influence of water vapour in synthetic air empirically by:

$$R = R_0 (1 + k_{H_2O} \cdot p_{H_2O})^{-\beta} \qquad (2.18)$$

with the water-independent constants R_0, k_{H_2O} and β and the water concentration in volumetric ppm p_{H_2O}.

2.3.3 Adsorption of Carbon Monoxide (CO)

Carbon monoxide is considered to react with pre-adsorbed or lattice oxygen [104]. IR studies identified CO-related species, i.e. unidentate and bidentate carbonate between 150 and 400°C and carboxylate between 250 and 400°C. A summary of the IR results is presented in figure 2.10. Moreover, the formation of carbon dioxide CO_2 as a reaction product between 200 and 400°C was identified by FTIR. All experimental studies in air at temperatures between 150 and 400°C reported an increase of the surface conduction in the presence of carbon monoxide.
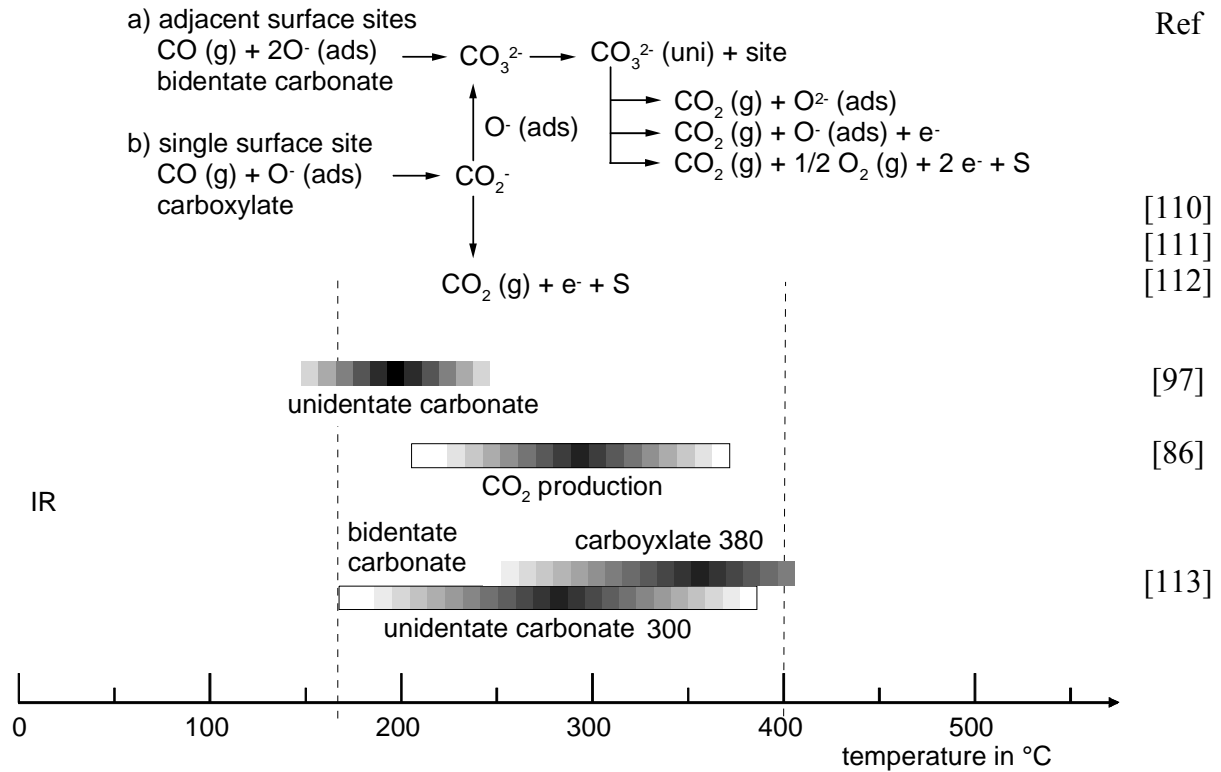
Figure 2.10: Literature survey of CO-related species found by means of IR (infrared analysis) at different temperatures on a (O_2) preconditioned SnO_2 surface [92].

Morrison derived, using a simplified model, the dependence of the resistance on the partial pressure of carbon monoxide. He assumed that oxygen is present as O_2^- and O^- at the sensor surface according to:

$$e^- + O_2 \leftrightarrow O_2^- \ ; \ e^- + O_2^- \rightarrow 2O^- \tag{2.19}$$

Hereby the reverse reaction is neglected due to the small probability of a reaction which is of second order in O^- concentration. The adsorbed carbon monoxide then reacts with the oxygen species to carbon dioxide. In addition, he assumes that due to the high reactivity of O^-, the reaction of O_2^- with carbon monoxide can be neglected.

$$CO + O^- \rightarrow CO_2 + e^- \tag{2.20}$$

Equation (2.14) can therefore be amended to

27

$$\beta \cdot CO^{gas} + O_{\beta S}^{-\alpha} \rightarrow \beta \cdot CO_2^{gas} + \alpha \cdot e^- + [S] \qquad (2.21)$$
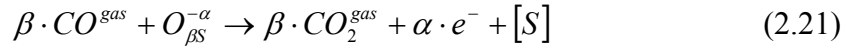
and the rate equation for the oxygen surface coverage will be, by combining equations (2.14) and (2.22):

$$\frac{d[O_{\beta S}^{-\alpha}]}{dt} = \underbrace{k_{ads} \cdot [S] \cdot n_S^\alpha \cdot p_{O_2}^{\beta/2} - k_{des} \cdot [O_{\beta S}^{-\alpha}]}_{related\ to\ ad-and\ desorption\ of\ O_2} - \underbrace{k_{react} \cdot p_{CO}^\beta [O_{\beta S}^{-\alpha}]}_{related\ to\ the\ reaction\ of\ CO} \qquad (2.22)$$

where k_{react} is the reaction constant for carbon dioxide production.
By considering the surface coverage, the Poisson equation and the electro-neutrality condition the relation between conductance and partial pressure of carbon monoxide can be calculated in dependence of the sensor geometry (layer thickness, grain size, sintering) [84].
For thick films and large grains, which is the case for sensors used in this work, the calculations result in a power law dependency according to:

$$G \sim n_S \sim p_{CO}^{\frac{\beta}{\alpha+\delta}} \qquad (2.23)$$

with values of δ typically in the range of 0 to 0.2.

In the previous section the influence of water on the adsorption of oxygen was discussed. It is therefore natural to expect a similar influence on the interaction with carbon monoxide. As anticipated, it has been observed [103], [109] that water enhances the interaction with carbon monoxide, but only for doped metal oxides [114]. Several models have been proposed which may account for this observation. Egashira et al. [115] suggested that water enhances the reaction with oxygen. Harbeck [114] and others propose a reaction of carbon monoxide with pre-adsorbed hydroxyl groups [115], [116]. Koziej [117] observed an indirect effect of water: in concurrence with carbon monoxide, water molecules react with surface adsorbed oxygen resulting in an increase of conductance.
Various equations have been derived for the sensor conductance in the presence of water vapour [109], [118], [119]. In some cases even a correlation between ageing and the irreproducibility of sensors and the presence of water-related species could be found [102], [120].

2.3.4 Adsorption of Methane (CH$_4$)

In heterogeneous catalysis the adsorption and subsequent oxidation of hydrocarbons on metal oxide catalysts has been studied intensively. For saturated hydrocarbons such as methane the activation of the C-H bond is the first crucial step in all oxidation reactions [121]. Once the first bond is broken, sequential reactions to carbon dioxide and water are relatively facile. Methane is more difficult to activate than higher hydrocarbons, partly due to the ease of adsorption of the different hydrocarbons on oxide surfaces [122]. After the initial homolytic activation at a surface oxide site gas phase methyl radicals are formed. Two pathways are considered for the further reaction of methane: oxygenation to carbon dioxide and water and dehydrogenation and subsequent dimerisation to ethane [123]:

$$2CH_3 \bullet \rightarrow C_2H \xrightarrow{\Delta, H_2O} C_2H_4 \qquad (2.24)$$

28

$$CH_3 \bullet + O_2 \rightarrow C_2HO/CH_3OH \rightarrow CO/CO_2 + H_2O \qquad (2.25)$$
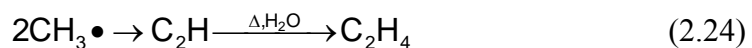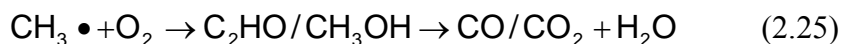
Sokolovskii et al pointed out that the rates as well as the reaction pathways and product distribution of the oxidative transformation of light alkanes depend on the acid-base properties of the solid catalyst [124]. Generally, basicity promotes the dehydrogenation reaction (owing to the basic character of alkenes), while acidity facilitates the formation of oxygenates (being more acidic) [125], [126]. Since the C-H bond in methane is only very weakly acidic (pK_a=4.6), surface sites capable of deprotonation of methane must be very basic. Such sites would be expected to strongly adsorb carbon dioxide, so there might be a rapid self-poisoning by the reaction products. Others [127] have proposed an acid-base pair as active site, arguing that both acidic and basic sites are important. Deprotonation would lead to the formation of an OH(ads) and a CH_3^- ion attached to a metal cation.

Kohl et al [93] assumed, based on TDS and reactive scattering results, two principle oxygenation pathways for methane. The first one involves the reaction with ionosorbed oxygen and the second one the reaction with lattice oxygen. The product fluxes were independent of the primary oxygen flux. Kohl attributed this observation to the surface oxygen density due to Weisz limitation [128]. Tournier et al [129] interpreted similar results as a hint for a methane interaction which does not involve oxygen adsorbed species. The reaction of methane with lattice oxygen leads to the creation of oxygen vacancies which are tin oxide donors and can therefore account for the removal of ionosorbed oxygen and also the conductance increase observed in the presence of methane at higher temperatures.

For the influence of water on methane several models have been proposed. Egashira et al [115] found a decreasing reaction of methane with oxygen in the presence of water. They assumed that water blocks the adsorption sites for methane. Ionescu et al [108] proposed a model which is based on dynamic resistance measurements for the water influence on the methane interaction. They assume that methane reacts with lattice oxygen, thereby competing with water for the same oxygen sites, whereas carbon monoxide and water react with different oxygen types. This competition for adsorption and thereby reaction sites was also observed by Burch et al [121] on Pd catalysts. This could mean the rate determining step for methane combustion could be the release of water from surface-OH groups rather than the initial C-H bond breaking step for some catalysts. Furthermore, water increases the number of Brønsted surface acid sites by dissociative adsorption which, in turn, enhances alkene selectivity at the expense of the CO_x selectivity [130]. Clifford and Tuma [109] offer an empirical formula to describe the influence of methane in the presence of water vapour on the sensor resistance.

2.3.5 Adsorption of Nitrogen Dioxide (NO$_2$)

The main environmentally relevant source of nitrogen dioxide is the combustion process of diesel engines. There, it is formed together with nitrogen oxide (NO). Both are in a delicate equilibrium in air, according to

$$2NO \leftrightarrows (NO)_2; \quad (NO)_2 + O_2 \rightarrow 2NO_2 + 114.2 kJ \qquad (2.26)$$
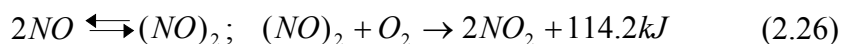
and therefore often referred to collectively as NO$_x$. This reaction is reversible and exothermic. However, it is very slow because NO reacts after a reaction mechanism of second order to the short-lived dimer (NO)$_2$ before a reaction with oxygen leads to NO$_2$. Therefore NO can be considered as the dominant species even for some time and distance away from the exhaust pipe [131]. Eventually, conversion to NO$_2$ will take place.

Nitrogen dioxide is an oxidising gas and a strong acceptor on SnO$_2$, presumably with a surface state energy below the state energy of adsorbed oxygen [132]. Therefore, it leads to an

29

increase of the electron depletion layer and thus to a decrease in surface conductivity as discussed in *section 2.2.4*. The adsorption can be described according to

$$NO_2(g) + e^- + [S] \rightarrow NO_2^-(s) \qquad (2.27)$$

Next to an interaction with the metal oxide surface, an interaction with adsorbed oxygen, i.e. abstractive adsorption, may occur. Sayago et al. [133] proposed the following reactions:

$$NO_2(g) + O_2^-(s) + 2e^- \rightarrow NO_2^-(s) + 2O^-(s) \qquad (2.28)$$

$$NO_2(g) + O^-(s) \rightarrow NO^+(s) + 2O^-(s) \qquad (2.29)$$
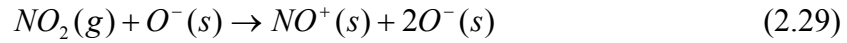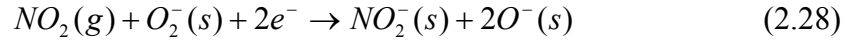
Interaction of NO_2 with adsorbed oxygen is also reported by Leblanc et al. [134]. They examined the adsorption of NO_2 onto dehydroxylated and hydroxylated tin dioxide surface.

For the dry samples three different structures of nitrato groups (NO_3^-) were observed: unidentate, chelating bidentate and bridging bidentate. These groups showed different stabilities. Unidentate species were rather weakly bonded to the tin dioxide surface. They were mainly observed between room temperature and 100°C. At higher temperatures the unidentate species desorbed as NO or NO_2 and or were reorganised to bidentate species. The bidentate nitrato species, especially the bridging nitrato groups, were more stable. Temperatures around 500°C were necessary to decompose them.

For the wet samples, i.e. in the presence of hydroxyl groups, an additional interaction was observed. Hydrogeno nitrate complexes were formed that were more stable than unidentate nitrato species. Furthermore, the presence of hydroxyl groups led to a reduction of NO_2 and NO desorption compared to the dry surface.

These observations demonstrate that the nature and content of species formed by NO_2 adsorption depends strongly on the chemical properties of the SnO_2 surface sites, i.e. the surface coverage with oxygen species (O_2^-, O^- and O^{2-}) and hydroxyl groups, as well as the activation energies for the different surface reactions. Additionally, the adsorption processes depend on temperature. Adsorption processes are generally favoured at low temperatures. However, the adsorption of electron acceptors like NO_2 requires an activation as it leads to an increase of the band bending at the tin dioxide surface. This shifts the optimum value for NO_2 detection to intermediate temperatures, between 150 and 300°C [92], [133], [135], [136]. At such temperatures, adsorption is favoured over desorption. However, the sensor response time to NO_2 exposure is still very high, amounting to several minutes [133], [135], [137] and the sensor behaviour can be irreversible due to the formation of stable surface species (hydrogeno nitrate and bidentate nitrato species are stable up to 500°C). Therefore it is useful to apply operating temperatures above the optimum detection temperature.

2.4 Material Preparation and Sensor Fabrication

The sensor preparation methods can be divided into two classes: preparation by thick film technology or by thin film technology. The first metal oxide sensors were thick film (ceramic) sensors. They were fabricated by pressing powder pellets, to which electrodes and a heater coil were added [138]. Thick film gas sensors can be characterised by being rather thick (a few to several hundred micrometers) and having a very porous sensitive layer. Due to the high porosity of the layer, a high active surface area is exposed to the gas interaction.

Thin film gas sensors on the other hand, are made by established preparation methods from thin film technology (semiconductor technology). The sensitive layers of thin film sensors are

rather compact, with a typical thickness in the range of a few to several hundred nanometres and therefore thin in comparison. In this case, gas interaction is mainly restricted to the surface layer. Typical pictures of thick and thin film layers are shown in figure 2.11.
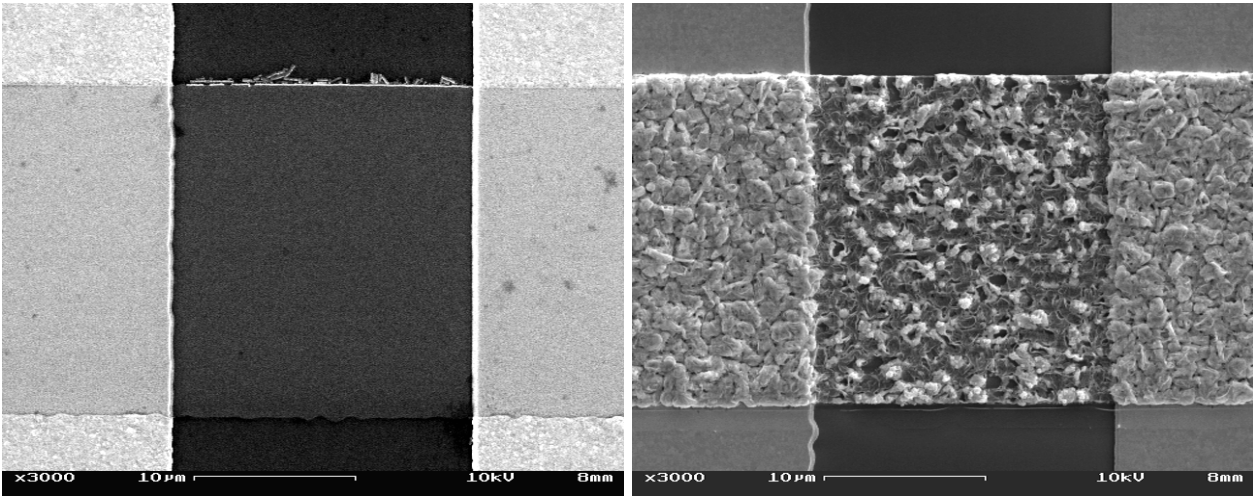
Figure 2.11: SEM pictures of thin and thick film sensor sensitive layers. (Left) thin film sensor, (right) small grain thick film sensor.

Comparisons of thick and thin film layers showed that the resistance changes of metal oxide gas sensors are typically much more significant for thick film sensors than for thin film sensors [7]. It is considered that the different morphology, especially layer porosity, accounts for this fact. Typical preparation methods for thin film sensors are listed in table 2.3.

Chemical vapor deposition (CVD)	Powder preparation	Physical vapor deposition (PVD)	
		Sputtering	**Evaporation**
Thermal CVD	Sol-gel from precursors	Sputtering	Molecular beam epitaxy
Plasma activated CVD		Reactive sputtering	
Laser induced CVD	Precipitation of precursors	Cathode sputtering with bias voltage	Thermal evaporation
Electroless plating			Reactive evaporation
Spray pyrolysis	Laser pyrolysis	Ion beam deposition	Ion plating
Melt dipping		Ionized cluster beam (reactive)	Reactive ion plating
Liquid quenching			Arc evaporation
Deposition of organic polymers		Plasma decomposition	Laser evaporation
Deposition of emulsions			

Table 2.3:   Typical methods for the preparation of SnO_2-based thin film sensors.

In this work thick film sensors based on SnO_2 were used. The reason for this choice is the higher response of thick film sensors to changes in ambient atmosphere, which for comparable noise levels, leads to a higher signal to noise ratio.

Ceramic, i.e. thick film, sensors are usually prepared starting with the base material preparation as detailed in figure 2.12.
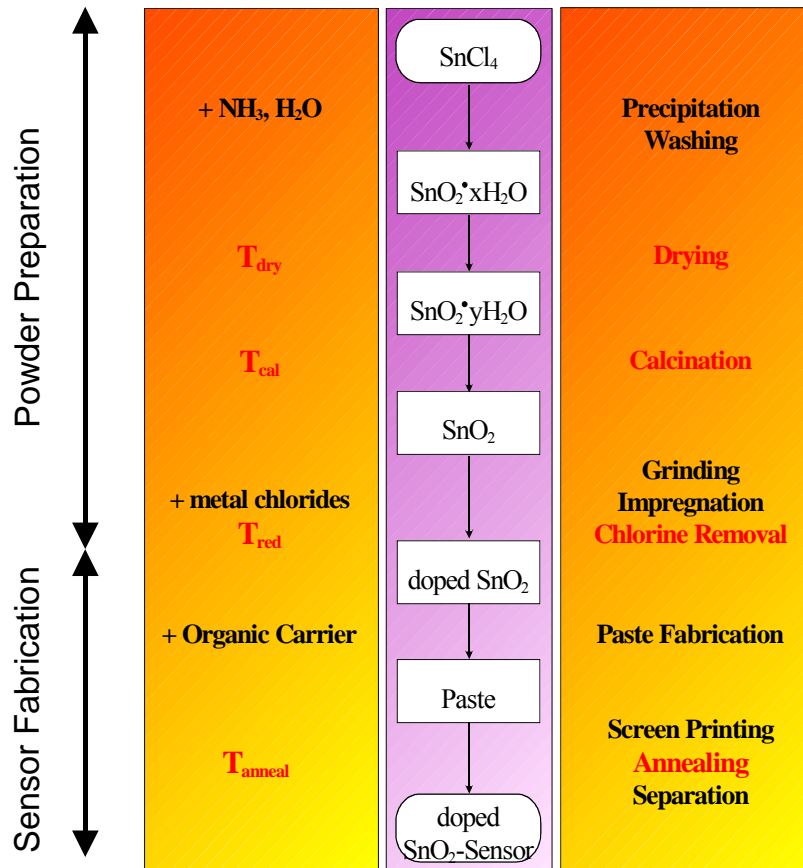
Figure 2.12: Flow chart summarising the preparation of SnO$_2$ thick film sensors based on a modified sol-gel route.

First, the precursor - hydrated tin oxide - is gained by precipitation of ultra-pure, water-free tin chloride. An aqueous, ice-cooled solution of SnCl$_4$ is therefore added at a controlled speed to an ice-cooled, aqueous solution of NH$_3$. The cooling of both aqueous solutions is applied in order to reduce the reaction speed and to ensure a homogeneous precipitate with small grain size. In order to remove the remaining chlorine and ammonia, the precipitate is afterwards washed several times thoroughly with bi-distilled water (Millipore Milli-Q PF Plus; resulting water resistance = 18.2MΩ). Thereafter the suspension is centrifuged and dried at 80°C in a drying oven. Hereby the precursor - hydrated SnO$_2$ - is gained. The next production step is the calcination of the precursor in a furnace at elevated temperatures (250 to 1000°C) for 8h. This removes the remaining water, enables the grain growth and forms the SnO$_2$ powder with a well-defined grain size distribution. Using this method, ultra-pure SnO$_2$ with adjustable grain sizes between 4 and 110nm can be prepared.

The resulting SnO$_2$ powders usually contain large agglomerates that complicate the production of a homogeneous paste. An inhomogeneous paste tends to cause cracks in the final sensitive layer. To eliminate such agglomerates, powders are usually ground before paste fabrication. The final powders are then used to fabricate sensors.

The selection and application of preparation parameters (calcination, grinding, doping, annealing) has a strong influence on the sensor properties. Detailed information is given in literature [139], [140] and references therein.

2.4.1 Effect of Dopants

Metal oxide gas sensors are usually not very selective. To increase their selectivity a catalytically active material, such as Pt, Pd, Au or Ag, is often added in traces (0.1-3wt-%) as dopant. Increased selectivity, sensitivity, signal stability, reaction time and reproducibility of the sensor are among the possible changes [141][143]. From a chemical point of view, newly reactive sites are added to the surface of the semiconductor. Per definition, a catalyst interacts with educts while not changing itself. There are two ways in which a catalyst can influence a reaction. First, it can increase the concentration of reaction partners at the reaction site. Thereby the reaction probability is increased. And second, it can decrease the activation energy of the chemical reaction and thereby open new reaction paths hitherto energetically forbidden.

From a physical point of view, dopants change the amount of free charge carriers in the conduction band by creating new donor (n-doped) or acceptor (p-doped) states. Metals of the oxidation number 3+ are used as acceptor type doping to decrease the conductivity (e.g. Al, B) [144], [145], whereas those with an oxidation number 5+ are used as donor doping to increase the conductivity (e.g. In, Sb) [145][146]. For metals with both oxidation states (3+, 5+) the effect on the conductivity depends on the doping concentration.
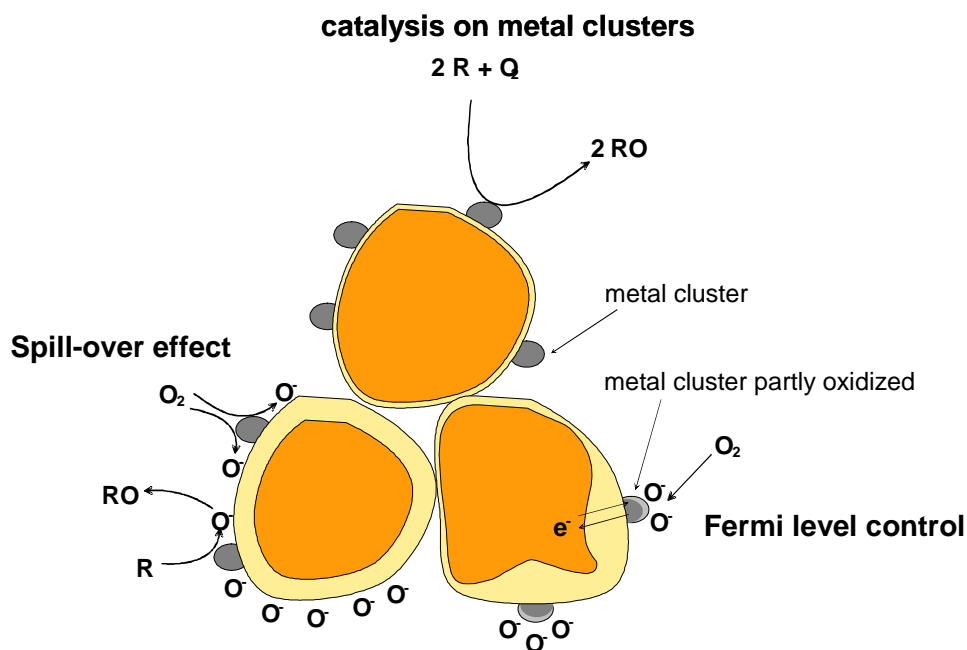
Figure 2.13: Effect of catalysts. Up: catalysis by metal cluster. The reaction takes place exclusively on the cluster; the conductance of the semiconductor remains unchanged. (Left) Spill-over mechanism: dissociation of reactants and higher coverage of the surface with interacting species. (Right) control of the Fermi-level: An adsorption on or a redox-reaction by the metal clusters leads to a shift in the Fermi-level and thus a band bending in the SnO$_2$ [23].

However, unlike in the case of "classical" doping the catalysts are usually added via the impregnation of powders and therefore are mainly located at the surface of the individual SnO$_2$ grains. Therefore the chemical effect has to be considered as dominant. Two theories for the influence of catalysts on sensing properties of semiconductors are discussed in literature [141][147]: the spill-over mechanism and the Fermi level control. Spill-over is attributed to the presence of metallic clusters at the surface of tin oxide grains. The catalyst forces a

dissociation of reactands and thereby increases the concentration of reactive particles at the surface. Fermi level control is related to an electronic interaction in which oxygen adsorption on the catalyst removes electrons from the catalyst. The catalyst, in turn, removes electrons from the supporting semiconductor, thus controlling the energy of the Fermi level and influencing the band bending in the SnO_2 grain.

2.4.2 Sensor Substrates

For sensor operation the sensitive layer has to be heated and its resistance measured. The simplest way of obtaining a sensor is to press powder into a pellet and then add the necessary wiring (see figure 1.4). More sophisticated methods rely on the deposition of a sensitive layer onto heatable substrates provided with electrodes for resistance measurements. The deposition of powders or solutions depends on the substrate. The two most important ones, also used in this work, are conventional alumina substrates and micromachined substrates.

2.4.2.1 Alumina Substrates and Screen Printing

The planar substrates are based on alumina (Al_2O_3, purity 96%). Pt or Au electrodes on the front side measure the sensor resistance and Pt heaters on the back side keep the sensors at operating temperature. The measuring electrodes have the typical shape used for conductivity sensors, the so-called interdigital structure. The width of the fingers of the electrodes is 0.2mm and the gap between the fingers is also 0.2mm. However, different geometries are used depending on the resistance range to be measured.
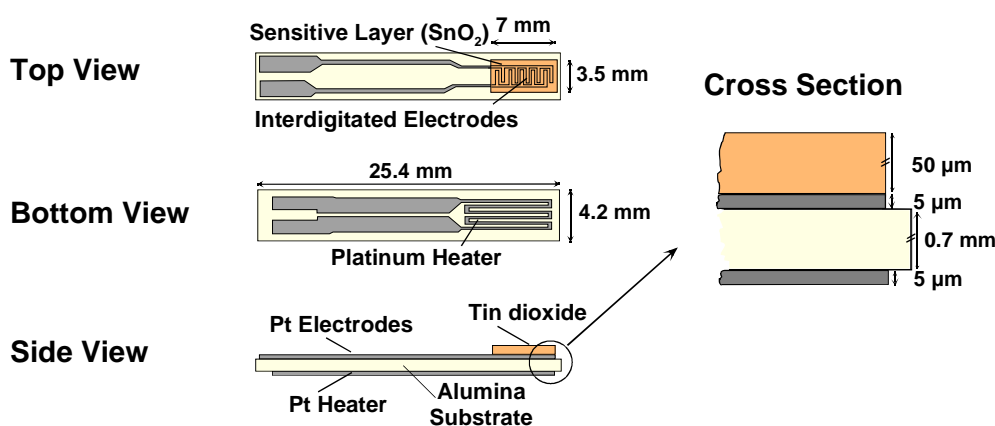
Figure 2.14: Layout of the planar alumina substrate with Pt electrodes and Pt heater. The SnO₂ layer is printed on top of the interdigitated electrodes. The heater on the back keeps the sensor at the operation temperature.

In order to deposit a continuous sensitive layer, the SnO_2 powder is transformed into a homogeneous paste. This is done by adding an organic carrier (1,2-Propanediol) to the powder and mixing by means of a magnetic stirrer until the desired consistency is achieved. After thorough mixing at room temperature (20h) a homogeneous, printable paste is the result. For the transfer of the paste onto ceramic substrates screen printing is used. Hereby, the paste is pressed through the holes in a screen lattice onto the ceramic substrate. By this method the layer thickness can be adjusted with a thickness of a few micrometers to around 100μm.

After screen printing the substrate stays for 1h at room temperature to allow the paste to settle. Subsequently, the substrate is put into a drying oven to dry the paste at 80°C. Finally, the substrate is inserted into a moving belt oven. During the final annealing, the organic binders

of the film are removed, the layer gets mechanically stable and is firmly bonded to the substrate.

2.4.2.2 Micromachined Substrates and Drop Coating

Screen printed ceramic sensors are, with respect to power consumption, mounting technology, selectivity, sensor-to-sensor reproducibility and manufacturing cost, still in need of improvement. To overcome these drawbacks there has been increasing interest and research efforts over the last years in miniaturizing gas sensors and systems [148], [149]. This led to the development of μ-hotplates and micromachined gas sensors. As shown in figure 2.15, μ-hotplates consist of a thermally isolated area with a heater structure, a temperature sensor and contact electrodes for the sensitive layer.
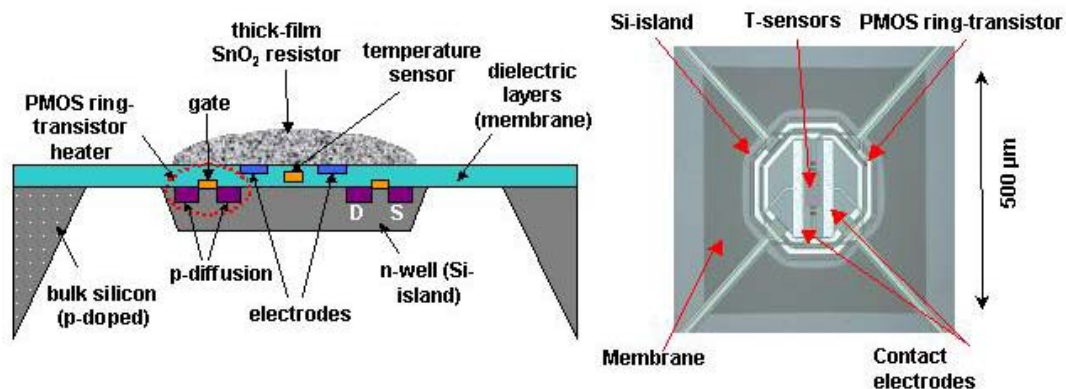
Figure 2.15: Micrograph of a micromachined sensor with μ-hotplate.

Micromachining offers a number of advantages over conventional screen-printed ceramic sensors [150]. The sensitive layer of micromachined metal oxide gas sensors is deposited onto a thin dielectric membrane of low thermal conductivity which provides good thermal insulation between the substrate and the gas-sensitive heated area on the membrane. In this way the power consumption can be kept very low (typical values obtained lie in the range of 30 to 150mW [151]-[153]) and the substrate itself stays nearly at ambient temperature. The mounting of the sensor element becomes therefore much easier than for an overall hot ceramic sensor element, and control and signal-processing electronics can be integrated on the same substrate if desired. Using microtechnological processes to pattern electrode structures results in a further advantage. The minimal structure sizes get much smaller, a minimal width between electrodes lying in the μm range can be achieved [154]. The gas sensitive area can in this way be tremendously reduced and the use of interdigitated electrodes with a high length-to-width ratio allows even the evaluation of sensing films with a high sheet resistivity. Sensor arrays which are often needed to overcome the problematic selectivity of single sensor elements can be implemented in this technology. Beyond that, the small thermal mass of each micromachined element allows rapid thermal programming which can be used to study the kinetics of surface processes and to achieve kinetically controlled selectivity [155].

Most micromachined gas sensors published so far still retain the separation of sensing element (μ-hotplate with sensitive material, electrodes, temperature sensor and heater) and sensor electronics (temperature controller, sensor read-outs, data processing and interface). The next development step, a monolithic system with both parts integrated on one chip, has been reported recently [156]. The co-integration of transducers and circuits provides on-chip amplification and conditioning of sensor signals, enables on-chip analog-digital conversion,

and allows for using on-chip standard interfaces, which alleviates the packaging problem (less pins and connectors).

The currently dominant and dwell-established technology for integrated circuits is CMOS (Complementary Metal Oxide Semiconductor). Consequently, there are ongoing efforts in using CMOS technology for fabricating chemical sensors, and several CMOS- based monolithic systems have been successfully realised [157]. CMOS-based systems do not only feature small size and low power consumption, but also offer batch fabrication at industrial standards and low costs. Drawbacks of using CMOS technology include a limited selection of materials and a predefined fabrication process for the CMOS part. The integration of µ-hotplates using CMOS technology is particularly challenging, since metal-oxide operation temperatures are usually in the range of 200 to 400°C, much higher than the temperature specifications of common integrated circuits (between -20 and 150°C).

To fabricate micromachined gas sensors, appropriate sensor substrate materials have to be chosen and functional elements have to be designed. Well-controlled temperature distributions over the sensing layer are desired as the sensing properties of semiconductor sensors are strongly temperature dependent. Generally the goal is a uniform temperature distribution. High mechanical strength is needed for all processing steps used to form the micromachined substrate. Beyond that, the micromachined substrate should be stable during the deposition of the sensing film and subsequent processing.

The microhotplate becomes a chemical gas sensor by deposition of a sensitive layer. In this work, only micromachined metal oxide gas sensors based on thick film technology were used. Through micromachining new sensor production steps are introduced [158]. The deposition of the sensitive layer is challenging. Screen-printing is difficult, as micromachined substrates are often too fragile to survive the involved material stress. By using a special drop deposition technique [159] thick films can also be deposited on micromachined substrates [149], [160]. The deposition of the sensitive layer is the most crucial part in the preparation of gas sensors. Normally the deposition is carried out as the last step in the fabrication of a micromachined gas sensor. This way poisoning of standard equipment with tin oxide can be avoided and the gas sensing film can be protected from uncontrollable modifications during later manufacturing steps.

3 Sensor System Development

The aim of the present work was the development of a chemical gas sensor system. Although past research and publications have shown gas sensors to be promising for commercial use, the nature of chemical sensors inhibits a "one-size-fits-all" solution for a broad range of applications. The first step in any development process is a clear definition of the application and its boundaries. Then, sensor and system architecture around it have to be carefully selected and developed to enable a success. The targeted applications were defined as:

Outdoor
Qualitative and quantitative detection of carbon monoxide (CO) and nitrogen dioxide (NO_2). Both are relevant toxic gases and are considered as indicators for automotive pollution levels [161]. The sensor system would be installed in areas with high traffic volume and industrial activity, complementary to existing environmental monitoring stations. Apart from this stationary use an operation on a mobile platform (such as a public transport unit) and as a hand-held device (to find a local "hot-spot") is envisioned.

Indoor
Qualitative and quantitative detection of carbon monoxide (CO) and methane (CH_4). They are indicators for smoke (fire alarms) and gas leaks (relevant for households with gas heating), respectively. The sensor system would be installed in kitchens, residential buildings and offices, essentially stationary with constant power supply.

3.1 Concept

As we have seen, the sensor system has to function in two different environments with varying target gases and boundary conditions. The heart of any sensing system is the sensing element. In this case it was decided to base the system on an array of metal oxide sensors, more precisely tin dioxide (SnO_2). The advantages of metal oxide sensors are their easily adjustable sensitivity and selectivity, low production costs and a long history of use as gas sensors.
The next important factors are size and power consumption. The outdoor application requires the system to be also operable as a hand-held device, i.e. it has to be portable and battery-operated. The resulting requirements are small size and low power consumption, possibly with sleep/wake modes. These two factors are also of great interest if we consider the market which the sensor system has to convince. To be accepted as a complementary system at the side of classical analytical instruments, it has to offered clear advantages next to the expected lower performance in accuracy and reliability. Size, power consumption and cost are therefore defining factors.
The last consideration concerns the integration of the different subsystems and packaging of the whole. An intelligent gas flow architecture, which makes optimal use of the little space available, a pump to supply fresh air samples and small electronics managing the system are needed. A filtering system, possibly with heating for purging, and a pre-concentrator are optional components. They would increase the systems selectivity and sensitivity, respectively. The pre-concentrator is not essential as metal oxide sensors generally show a good sensitivity. The filtering system is more important. As the sensor system will have to perform in changing environments with background concentrations of other pollutants, there is a strong risk of signal interferences or false alarm. Especially the indoor application is delicate in this aspect, as short-term exposure to high concentrations of solvents, smoke or

37

cooking related gases are to be expected. A data transmission interface, wired and wireless, completes the system. However, not only the proper design and selection of the sensor system elements but also the proper choice of packaging solutions for the sensor chip and sensor system prototype is absolutely necessary to obtain finally a gas sensor system which can withstand the harsh environment of practical applications, e.g. shock, vibration, ambient temperature changes and so on.

The considerations on the sensor system performance requirements can be summarised as follows:

- Measurement range of 0-50ppm CO, 0-2ppm NO_2, 0-8000ppm CH_4
- Lower Detection Limit (LDL) of 0.5ppm CO, 20ppb NO_2, 100ppm CH_4
- Cross-sensitivity to VOCs and ozone < 10%
- Operation parameters 0 to 40°C, 10-90% relative humidity (r.h.)
- Sensor system size < 1l, weight < 1kg
- Energy consumption < 500mW for 1 analysis/min

These requirements were defined in accordance with IAQ guidelines [162] and international standards for gas detection devices [163], [169].

In the following the development process as well as the experimental set-ups used to validate the various prototypes will be discussed in detail.

3.2 Experimental

The experimental set-up, which has been used to evaluate the performance of the developed sensor system and its various prototypes in laboratory is discussed in the following. It can be divided into the gas mixing bench, which provides the desired gas atmosphere, the sensor heating, the data acquisition, the reference instruments and the different test chambers for filter and temperature modulation research.

3.2.1 Gas Mixing Bench

In order to test and calibrate gas sensors, they are exposed to gas mixtures, which mimic the actual ambient gas atmospheres of the specific application. To ensure accurate gas mixtures, gas mixing benches are employed. These gas mixing benches consist of computer controlled mass flow controllers (MFCs) and valves, as depicted in figure 3.1. By means of the illustrated multi-channel gas mixing station, several test gases can be supplied with a mixture of dry and water vapour saturated synthetic air, which is usually used as the carrier gas. During the laboratory evaluation of the sensor system prototypes several different gas mixing stations have been in use, as some experiments (e.g. with highly reactive gases such as NO_2) could only be performed at dedicated stations. The gas mixing station attributes discussed hereafter cover all specific modifications of the stations employed.
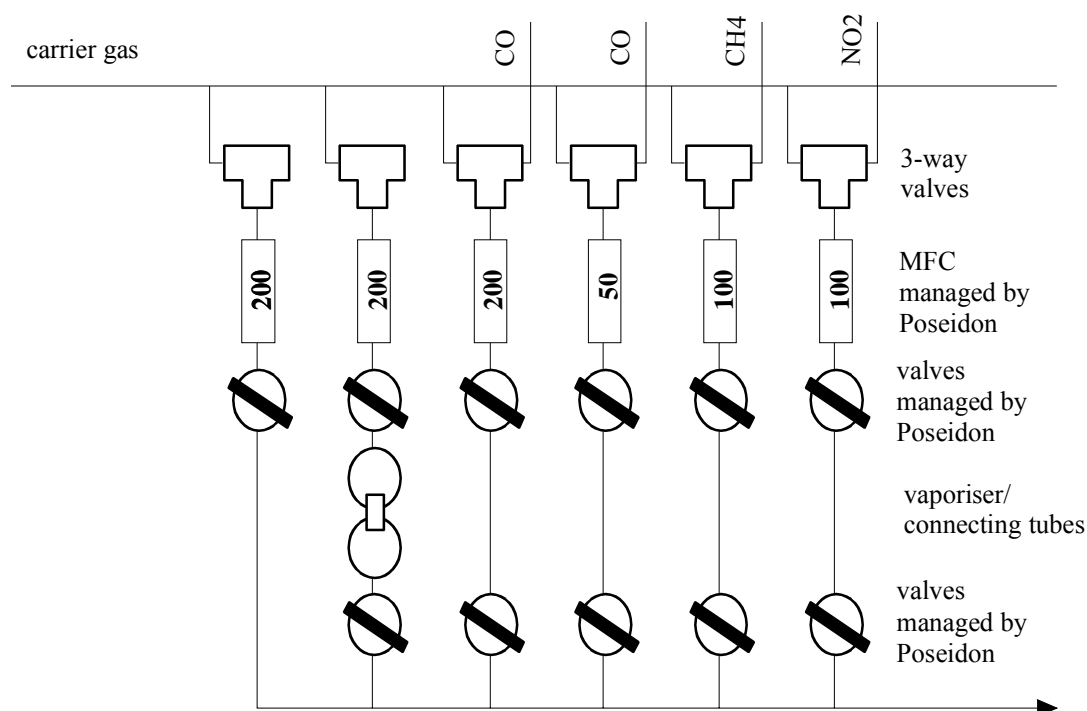
Figure 3.1: Schematic picture of a six-channel gas mixing station. Test gases are introduced from gas cylinders. Synthetic air (carrier gas) is introduced by gas cylinders or a zero-air generator and humidified as desired through a vaporiser. Two rows of electromagnetic valves prevent unintended diffusion of test gases.

The gas mixing bench is operated by a home-made software programme called POSEIDON. The mass flow controllers and the electromagnetic valves are controlled via D/A card. An A/D card is used to check the performance of the gas mixing bench by recording the actual gas flows through the mass flow controllers. The tubing of the gas channels consists mainly of electrically polished stainless steel pipes; the tubings of the channels which are dedicated to highly reactive gases (e.g. nitrogen dioxide NO_2) are made from teflone (PTFA).

The gas flows through individual channels are adjusted by means of computer controlled mass flow controllers. The pairs of electromagnetic valves are interconnected via either stainless steel tubes, glass tubes or U-shaped glass vessels, the so-called vaporisers. The vaporisers are filled with an adsorbent with a highly specific surface (Chromosorb P-NAW, Macherey-Nagel). It is filled with water to provide carrier gas saturated with water vapour (100% r.h.).

By means of pairs of computer controlled valves unintended diffusion of test gases is prevented. The row of valves which is further away from the MFCs prevents the diffusion of test gases into the gas flow and the back diffusion of gases from the gas flow into the vaporisers; the other row of valves ensures that no pressure is built up in the liquid-filled vaporiser due to an unintended gas flow through the MFCs.

The test gas concentrations are adjusted by controlling the ratio of test gas flow to total gas flow. Certified gravimetrically produced gas mixtures are used as test gases (Praxair, Messer-Griesheim). The carrier gas is synthetic air, either provided together with the test gases or synthesised in the laboratory by means of a zero-air generator (TG 8000, TOC-Gas Generator, WGA). The total accuracy of the system is in the range of 2%.

3.2.2 Sensor Heating

Tin dioxide sensors are operated at elevated temperatures between 200 and 400°C. To keep the sensor at the operation temperature a power supply is used to ensure a constant voltage drop over the platinum electrodes. In order to calibrate the platinum heater, i.e to obtain the relationship between the applied voltage and the thereby adjusted temperature, an infrared pyrometer (Maurer KTR 2300-1) was used. The pyrometer detects the infrared emission from a measurement spot of $3mm^2$ and calculates, using the specific emission coefficient ε of the material ($ε_{SnO2} = 0.75$), the temperature of the sensitive layer. The pyrometer is kept at room temperature and can be used for detecting temperatures from 200 to 500°C.

The final ADA chip uses a different heating element than standard thick film sensors. As a chip with sensitive elements on μ-hotplates, it provides the necessary heating by a transistor heater (*see section 3.4*). Three digital PID controllers provide independent closed-loop temperature regulation for each of the hotplates. The PID parameters and the target temperatures for each hotplate, as well as the system timing, can all be programmed by the user by means of the standard serial interface (I^2C). To calibrate the heater temperatures the software LABVIEW [170] was used.

3.2.3 Data Acquisition

The typical measurement technique for metal oxide sensors is the measurement of resistance. As several different semi-conducting sensors were used in this work, the different measurement techniques and associated instruments will be discussed shortly.

The classical alumina-based thick film gas sensor (*see section 3.1)* was measured with a digital multimeter (DMM; Keithley DMM 196, 199 and 2000). It allows measuring several resistances simultaneously and over a broad range. The measurement principle is the following: a reference voltage drops over a reference resistance and the sensor resistance. The voltage drops over the two resistances are measured and based on the voltage ratio the sensor resistance is determined. Due to limited resolution of the A/D converters, different reference resistances are used for different measurement ranges. A computer was used to control the gas composition and to record the resistance and humidity data via the DMM and IEEE card.

The AS-sensors *(see section 3.3.2)* were installed on the development platforms and read out with a VOCVario (AppliedSensor GmbH). The instrument defines the sensor resistance as frequency determining element in a digital RC-oscillator. Therefore the signal is supplied in form of a frequency change.

The final ADA sensor chip signals are read out by the programme LABVIEW [170]. Part of the innovative concept of the ADA sensor chip is a transfer of hardware and software from normally external instruments to the on-chip electronics. This allows a digital read out of the μ-hotplates resistances through the standard I^2C interface. The ADA sensor chip is therefore also operable as a stand-alone unit, requiring only a standard computer equipped with LABVIEW software and an USB port.
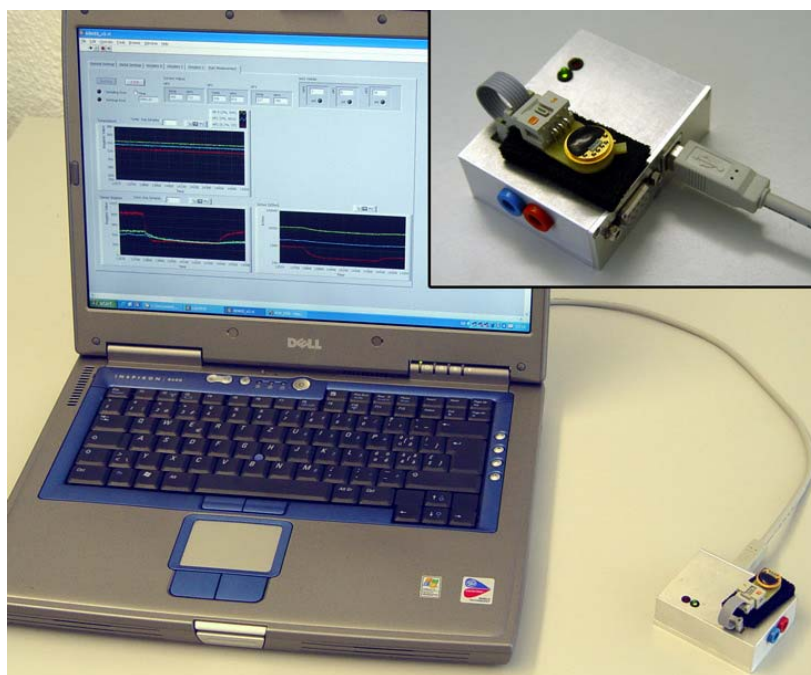
Figure 3.2:   ADA sensor chip. Optional operation as a standalone sensor unit. All references onboard. External connections: 5V power supply and I^2C interface. Usable on an USB port via a microcontroller [21].

3.2.4 Reference Instruments

To verify the exact concentrations of the test gases in mixtures and the ambient parameters (temperature and humidity) reference instruments were installed downstream of the measurement set-ups. These were:

The **Testo hygrotest 625** was used to reference the temperature and humidity. It employs a capacitive humidity sensor and a Pt100/NTC temperature sensor.

The **Innova multi-gas monitor PC1312** was used to reference carbon monoxide and methane. In Photoacoustic Spectroscopy (PAS) the gas to be measured is irradiated by modulated light of a pre-selected wavelength. The gas molecules absorb some of the light energy and convert it into an acoustic signal which is detected by a microphone. An advantage of PAS compared to conventional IR-based gas analyzers is the direct measurement of the adsorption - not relative to a background - for an increased accuracy and stability.

The **Monitor Labs ML 9841A NO$_x$ Analyzer** was used to reference nitrogen dioxide. It is a chemiluminescence based nitrogen oxides analyzer designed to measure ambient levels of NO, NO$_2$, and NO$_x$. The principle of measurement is based upon the reaction of the NO molecule with an internal source of ozone in an evacuated reaction cell which results in the emission of light. The ML®9841A is a single channel instrument that measures the NO in a sample gas which is alternately passed through or around a catalytic converter to convert the NO$_2$ to NO. The measurement of the untreated sample provides a NO value and the measurement of the converted sample provides the NO$_x$ measurement with NO$_2$ calculated as the difference between the two measurements.

The **Alltech Digital Flow Check** was used to reference the gas flow and calibrate the MFCs. It relies on solid-state sensors that measure the mass flow independent of ambient temperature, humidity and pressure changes.

3.3 Development Stages and System Prototypes

During the system development, several experiments were performed with conventional thick film sensors, AS sensors (provided by *AppliedSensor*) and the ADA sensor chip to evaluate the different system approaches. Two sensor system prototypes were developed and tested in cooperation with *AppliedSensor* [22]: the ADA toolbox and the ADA prototype. The ADA sensor chip was developed and manufactured by *ETH Zurich* [21] and the sensor system prototypes were manufactured by *AppliedSensor*. The sensors and system prototypes employed will be detailed in the following. The final sensor system, consisting of the ADA prototype equipped with an ADA sensor chip was thoroughly investigated as will be discussed in *section 4*.

3.3.1 Conventional Thick Film Sensor

These thick film sensors are the basic sensor units developed at the Institute of Physical and Theoretical Chemistry, University of Tübingen, and were used for preliminary research until the availability of the first ADA sensor prototype. The sensor is based on a planar alumina substrate with Pt electrodes on the front side for measuring the sensor resistance and Pt heaters on the back for keeping the sensors at the operating temperature. The sensitive layer was SnO_2 with and without dopants. It was synthesised according to a sol-gel route and deposited through screen printing, as discussed in detail in *section 2.4.2.1*.
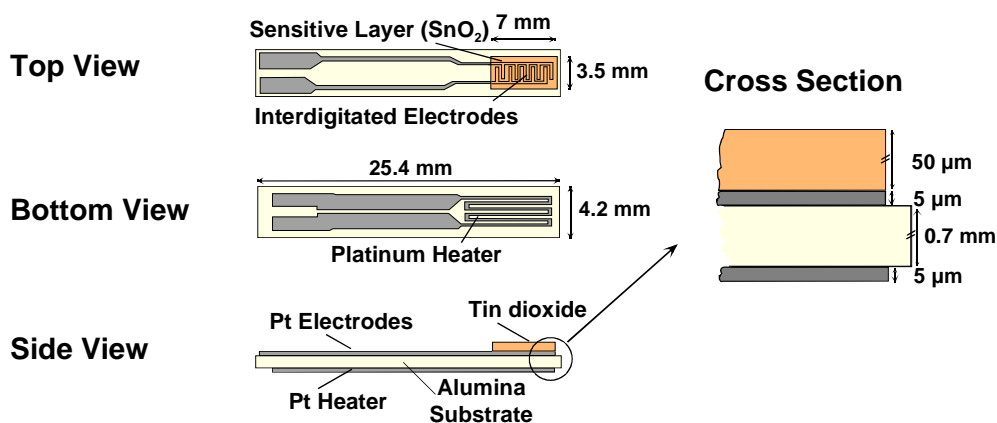
Figure 3.3: Layout of the planar alumina substrate with Pt electrodes and Pt heater. The SnO_2 layer is printed on top of the interdigitated electrodes. The heater on the back keeps the sensor at the operation temperature.

3.3.2 AS-Sensor

The AS-sensor is based on an interdigitated structure with 20μm finger width and finger distance on an area of $320x300\mu m^2$. A $1x1mm^2$ SiO_2 / Si_3N_4 membrane supports the Platinum electrodes. The temperature of the sensitive layer was adjusted through a meander-type heater.
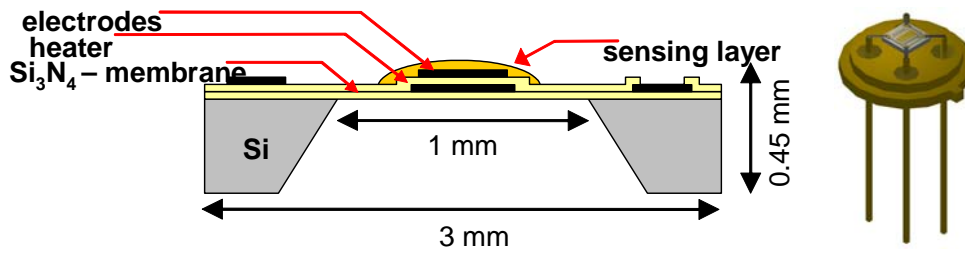
Figure 3.4: Cross-section of the hotplate used during the development process and for test measurements.

These hotplate structures from AppliedSensor were introduced during the first phase of the sensor system development. Unlike the later ADA sensor chip, they did not integrate electronics on the silicon die and the manufacturing process included non-standard CMOS processes (LPCVD, etc.). Those substrates enabled tests on and improvements of the sensitive layers on a stable reference hotplate, which allowed temperature ramping and pulsing without the limitations of the first ADA sensor chip prototypes and test structures made in CMOS. The development of the coating material for a micromachined and temperature-ramped substrate could thereby be decoupled from the development of the ADA sensor chip substrate.

The AS-sensors required a data read-out through a digital RC-oscillator; supplying the sensor signal in form of a frequency. Therefore several results discussed in this work are based on a frequency signal and not the usual conductance (resistance) signal.

3.3.3 ADA Sensor Chip

The ADA sensor chip was developed and manufactured by ETH Zurich [21]. It is a monolithic gas sensor array fabricated in industrial 0.8μm CMOS-technology combined with post-CMOS micromachining. The CMOS microsystem comprised an array of three metal-oxide-coated micro-hotplates with integrated MOS-transistor heaters and the needed driving and signal-conditioning circuitry. First versions of such monolithic micro-hotplate-based gas sensor systems were demonstrated recently [171]-[174]. As presented in figure 3.5, the ADA chip [156] features three micro-hotplates monolithically integrated with digital PID temperature controllers, digital readout, and a serial I^2C interface. The membranes were covered with tin dioxide (SnO_2) as sensitive layer. The SnO_2 sensing layers were doped with different concentrations of palladium (Pd) and thus rendered sensitive and selective to the gases of interest:

- Methane: 3wt%-Pd doped SnO_2
- Carbon monoxide: 0.2wt%-Pd doped SnO_2
- Nitrogen dioxide: undoped SnO_2

The resistance of the SnO_2 material, that varies over a wide range from a few 100Ω to 10MΩ, can be measured with sufficient accuracy of about ±0.05% (>10Ω) of the actual resistance. All sensor values can be set and read via the digital interface.
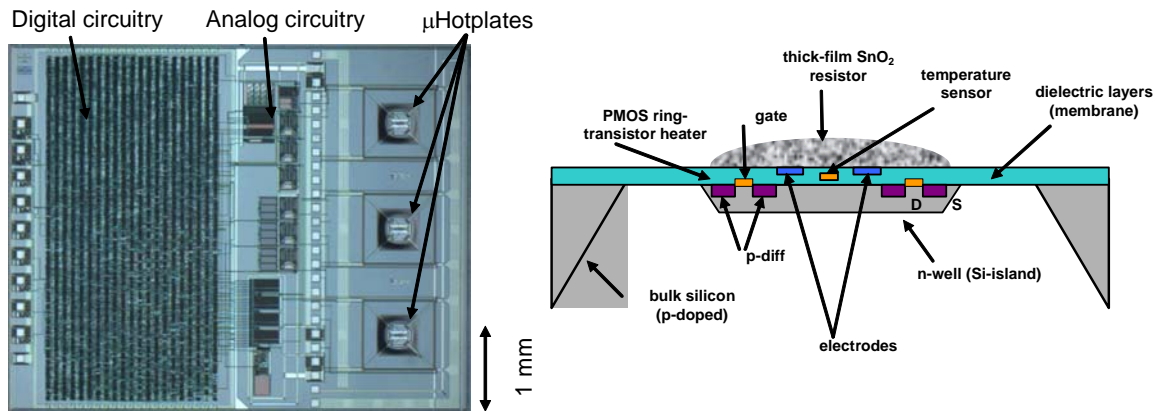
Figure 3.5: Micrograph of the ADA chip and schematic of the transistor based µ-hotplates [156].

The µ-hotplates feature operation temperatures of up to 350°C. Three digital PID controllers provide independent temperature regulation for each hotplate. In contrast to most existing devices, which are based on resistive heating elements, a transistor heater is used [175], [176]. A key advantage of transistor-based heaters is the reduction of the overall power consumption, since no additional transistor is needed on chip for driving the heating current. Moreover, new temperature control modes are feasible, because the micro-hotplate temperature is directly adjustable through the gate voltage of the transistor heater, the correlation between temperature and gate voltage being almost linear.

The PID parameters and the target temperatures for each hotplate, as well as the system timing, can all be programmed by the user by means of the standard serial interface (I^2C), which also enables digital readout of the sensor values.

The two plots below show that the temperature control works in dynamic mode (e.g., a sinusoidal) or static mode (e.g. ramp) without interference from one hotplate to the others. The chip provides all means to apply any arbitrary temperature modulation to the heater.
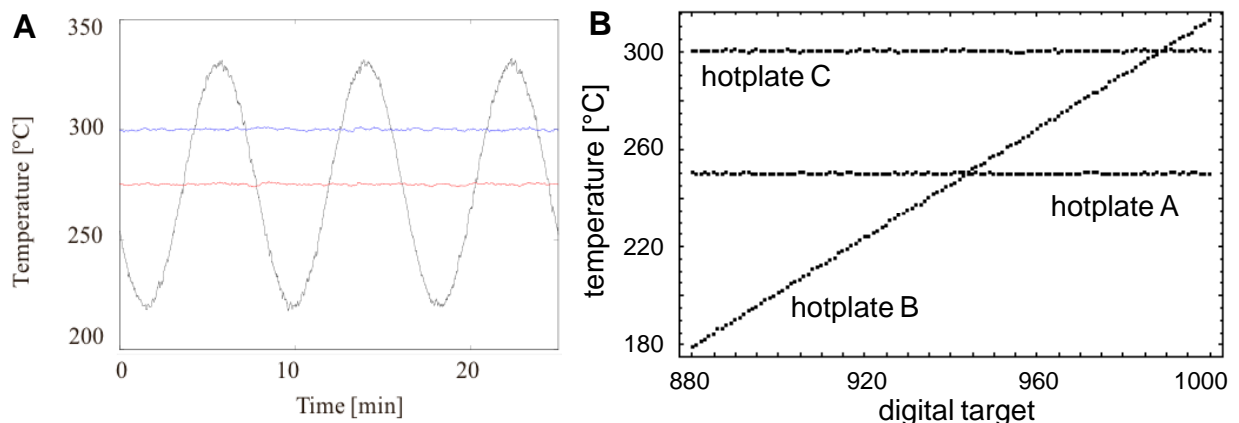
Figure 3.6: Temperature modulation and control examples for the ADA sensor chip: (A) two hotplates at constant temperatures and one sinusoidally modulated, (B) two hotplates at constant temperatures and one linearly modulated (ramp).

44

3.3.4 First Steps: the Development Platform

In order to have a versatile platform during all stages of the system development, a modular toolbox set-up was developed. This toolbox consisted of all components the final sensor system was planned to have installed. All system components were tested separately and as part of the toolbox system towards their performance and reliability. Figure 3.7 gives an overview of the test set-up. System control and data collection was performed by a Personal Computer at this early stage; in the final system an on-board microcontroller performed this task. All gas flow components (chambers, flow restrictors, tubing, etc.) are easily accessible and interchangeable. The selected modular approach allowed to freely change parameters and components during the development.
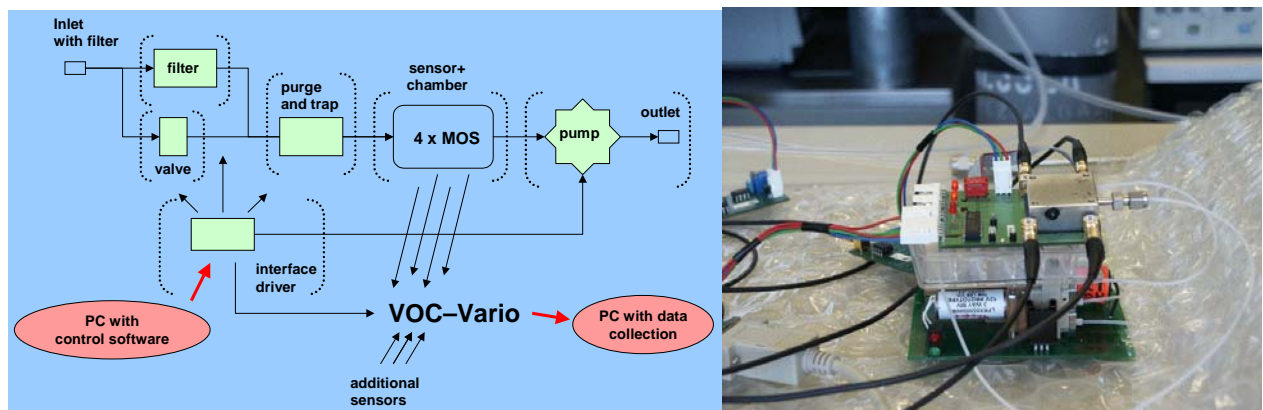
Figure 3.7: Schematic and picture of the toolbox platform manufactured by AppliedSensor. All components are integrated in a modular set-up. Up to four metal oxide sensors included.

In this first approach, the sensor system consisted of the following components:

- Air intake unit (particle filter membrane)
- Metal housing with cavities and connectors for filter material, pump, valve, sensor and pre-concentrator unit electronics
- Purge-and-trap-unit (pre-concentrator)
- Miniaturised pump
- Miniaturised switching valve
- Sensor (sockets for up to 4 AS sensor)
- Electronic platform (sensor system controller)
- Data transmission controller

The single components of the miniaturized sensor system underwent tests according to the overall specifications in terms of low power consumptions, small size, low gas adsorption (to reach low detection levels), high reliability and commercial availability.

3.3.4.1 Valves

Micro machined valves and miniaturized conventional valves were compared. Important specific parameters are the flow resistance, the kind of wetted materials, switching speed and the need for driver electronics. As the micro machined valves were unable to match the desired flow rates (10-50ml/min) and had a low commercial availability paired with high

pricing, miniaturised valves in conventional solenoid technology were employed. The selected valves performed perfectly during the integrated system testing.

3.3.4.2 Pump

The ADA sensor system requires high efficiency and low power consumption of the pump. Different pump principles were tested: conventional membrane pumps, rotary pumps and advanced microsystem pumps. The best performance in power consumption and efficiency was provided by the rotary pump. Early tests revealed some problems due to the small diameter of the tubings (d = 0.2mm).However, the final ADA prototype forewent the tubing system in favour of premilled channels in the plastic housing, solving the problem.

3.3.4.3 Purge-and-Trap-Unit

This pre-concentrator unit was planned as an indicator for the amount of organic material present during the measurements. In regular time intervals, the adsorber phase would be heated shortly, forcing the adsorbed organic materials into the gas phase and towards the measurement chamber. This would allow to measure the concentration of Volatile Organic Compounds (VOCs) and compensate for their interference during the detection of the target pollutants. It was decided during the development phase to drop the pre-concentrator approach, as discussed in *section 4.6.*

3.3.4.4 Sensor System Controller

The sensor system controller manages all system components and provides the driver electronics for pump, valve, sensor, pre-concentrator and microprocessor. Its initial functions were:
- control of valves and pump
- system timing and cycling
- temperature control of purge and trap system
- interface to sensor for control and data transmission
- calculation of concentration information and reliabilities for the different target gases
- buffering the data of the actual measurement and several previous measurements
- control of power-down modes and battery management
- store information about the system (status bits, calibration data, serial number etc...)

The timing protocol allowed adjusting the measurement protocol as desired.

3.3.4.5 Data Transmission Controller

The sensor data stored by the sensor system controller is transmitted to external systems via wired (RS232) connections. Wireless (Bluetooth) data transmission was planned for the later ADA prototype system. All communication follows principal terms and structures as defined by the IEEE standard 1451 [177].

3.3.5 ADA Prototype

After a thorough laboratory investigation of all system components the ADA prototype was constructed. The components with the best performance were selected as detailed above and unsuccessful strategies discarded. The ADA prototype is able to support either the final ADA sensor chip or three separate individual AS sensors. Figure 3.8 presents the ADA prototype

separated into electronic board (microcontroller) and gas flow architecture. This system configuration was used during the development phase (with AS sensors) and the final laboratory characterisation and field trials (with the ADA sensor chip).
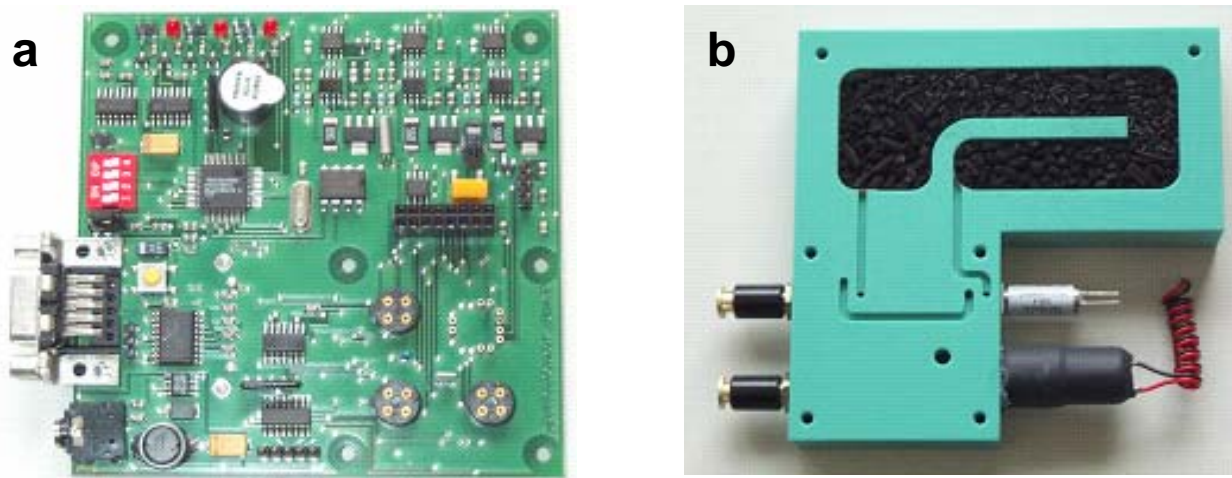
Figure 3.8: ADA prototype: a) microcontroller, sensor interface and data transmission interface b) gas flow architecture, measurement chamber, valve, pump and filtering system. 100mm x 100mm x 80mm, RS232 / Bluetooth plug-n-play, power consumption 240mW for one measurement per minute [22].

The gas filter unit can be switched on and off as part of the measurement program. The microcontroller allows for operating all three micro-hotplates of the ADA sensor chip individually at fixed or modulated temperatures. A separate humidity and temperature sensor is installed next to the ADA sensor chip inside the measurement chamber.

3.3.5.1 Sensor System Controller

The experience gained during development led to the design of the final electronic platform handling the following tasks:

- Generation of supply voltages from battery pack or from external power supply
- Hardware communication interface via Bluetooth adapter or serial interface line
- Optional direct display of measurement results
- System control: Management of valve, pump and the respective time sequences
- Interface to the ADA sensor chip (I^2C interface, clock generation, reset)
- Sensor temperature adjustment
- Sensor data read-out (raw data): analog for AS sensors, digital for ADA sensor chip
- Interface to optional sensors (humidity, gas temperature)
- Generation of system time
- Storage of measurement data and system parameters
- Data evaluation: calculation of qualitative (pollutant identity) and quantitative (concentration) data out of the sensor raw data
- Provision of stored sensor measurement results to accessing external systems (via RS232 or Bluetooth)

The input voltage range is from 6 to 18V. The battery pack for the prototype (array of standard NiMH AA cells, rechargeable) feeds the system for several days.

3.3.6   Sensor chip packaging

The limited number of pins renders the mounting on TO8 packages a good solution for the first-level packaging of the sensor chip (see figure 3.9). The array of membranes is lined up in a row at the upper end of the chip. The readout and control circuitry is integrated on the same chip in some distance from the hot plates (> 500µm) to enable reliable packaging. The bonding pads are placed on the opposite end with regard to the hotplates, and are connected to the socket pins via wire bonds. The chip is attached to a metal TO-socket using a die-attach with a high thermal conductivity. This combination keeps the temperature of the chip low as compared to the operating temperature of the hotplates. The glob top (epoxy) encapsulant covers the bond wires and the chip except the membrane area. This ensures free access of the gas phase to the sensitive area. The chip passivation and the epoxy encapsulant together represent a good protection against humidity.
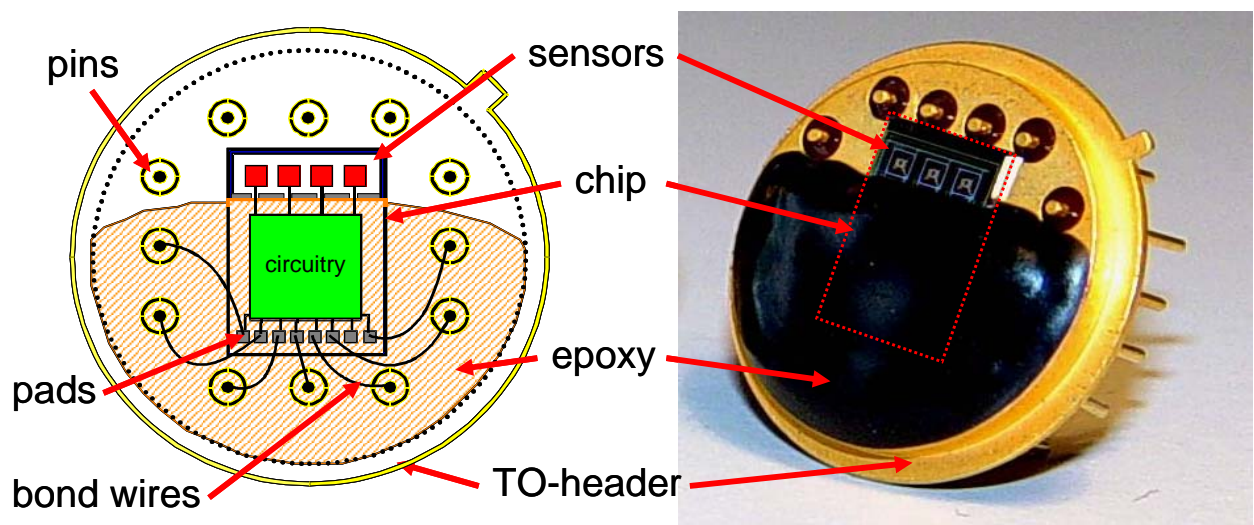
Figure 3.9:   Epoxy-based TO8-socket packaging of the sensor chip [21].

3.3.7   Sensor System Packaging

The layout of the sensor system as conceived for the field trial in Madrid is presented in figure 3.10. A powerful pump and a protective casing have been added to the core system. The pump is continuously pumping air and generating a constant air flow through its tube system. In periodic intervals (20s) the pump of the core ADA sensor system is activated and pumps air from the tube system into the measurement chamber. This configuration is required by the outdoor field trial situation in Spain, where a long tube is necessary to get air from the air inlet of the reference analytic systems in the air pollution measurement stations. The small pump integrated into the ADA prototype cannot provide the necessary pressure difference.

The plastic housing of the field tests set-up allows the use of a Bluetooth data transmission system and can be hermetically sealed. This is especially of use in a configuration without additional pump and with battery supply for the ADA prototype.

48
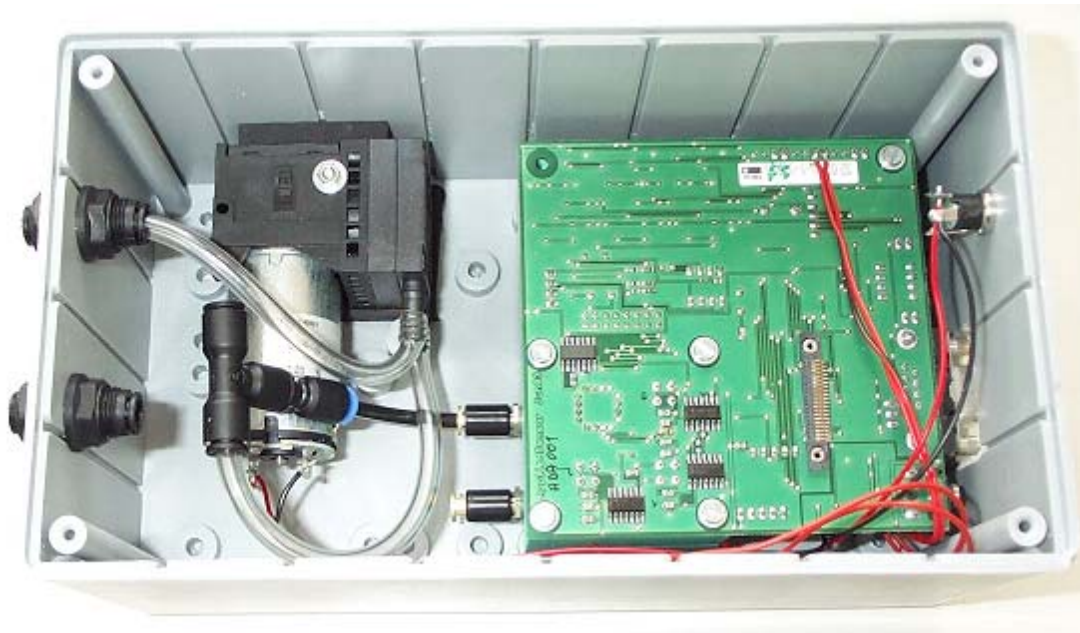
Figure 3.10: ADA sensor system packaging as configured for field trials.

3.4 Solving the Selectivity Problem

The developed sensor system has to be able to qualitatively and quantitatively detect carbon monoxide, methane and nitrogen dioxide. As all gas sensors, tin dioxide sensors face the problem of sensor selectivity: the sensitive material recognises not only the targeted gases but also, to some degree, other volatiles and changes in ambient parameters. This can lead to false negative or false positive alarms. In the following the selectivity problems encountered are shortly discussed.

- **Simultaneous detection of two target gases**, CO/NO_2 outdoor and CO/CH_4 indoor are the targeted applications for the developed sensor system. In the first case, a gas which decreases sensor resistance (CO) and one that increases the resistance (NO_2) have to be quantitatively detected. This can lead to false negative alarms if both are present at the same time. In the second case, both gases decrease sensor resistance, possibly resulting in false positive alarms if both are present at the same time.

- **Presence of interfering gases**, such as VOCs, alcohols, sulfoxides, particles and others are a major problem. All these substances influence the sensor signal to some degree, some even irreversibly (poisoning). Their concentration is strongly fluctuating depending on time and location. Their influence on the validation of a given sensor result is partly unpredictable as not all possible interfering substances are known to date.

- **The drastic variations in ambient humidity** a sensor system is exposed to in real world conditions (e.g. rain) have to be taken into consideration. Sensors signals are, to differing degrees, dependant on the ambient humidity. A strong change in humidity can devaluate previous calibrations and result in false negative or false positive alarms.

49

- **The concentration of NO$_2$** is in a delicate equilibrium with NO (see *section 2.3.5*). Depending on ambient conditions this equilibrium can shift to one side or the other, thereby increasing or decreasing the concentration of the targeted gas.

- **The air flow** generated by the gas flow system (pump, valves) influences the local pressure and temperature above the sensing layer, thereby changing its resistance and corresponding signal.

To solve the problem of selectivity one can target several points in the process of sensor signal generation [139]. Starting with the ambient gas composition itself, gas filters can be used to eliminate unwanted compounds from the atmosphere surrounding the sensor. By changing the gas composition between ambient air and sensor surface the signal to a desired compound will be strengthened compared to an untreated mixture.

Another possibility is to change the sensor, adjusting its performance attributes as needed. This can be achieved by varying the sensitive material, doping or sensor operation temperature among others. These measures increase the sensors sensitivity to certain wanted gases and reduce it to others, thereby improving its selectivity.

Finally, sophisticated data filtering tools are available to use characteristic traits of a sensor signal to identify a specific gas. Pattern recognition algorithms, such as PCA, PCR, MLR and others allow combining all the information provided by a sensor array such as the one developed in this work. Thereby it is possible to qualitatively and quantitatively measure the gases the system was calibrated to detect.

In the following the various approaches to solve the selectivity problems are discussed in detail and a measure of their success is given.

3.4.1 Sensitive Materials and Dopants

As discussed in detail in *section 2* the signal created by a gas interacting with the surface of a semiconductor depends strongly on the chemical, physical and electronic properties of this semiconductor. A change in surface atom distribution, dipoles, occupied or unoccupied atomic orbitals, rifts and ridges and the fullness of the conduction band determine the availability and character of surface states offered to gaseous molecules. Changing these characteristics changes the attractivity of adsorption sites to the molecules: another gas will be preferred in place of the previous favourite. Thereby the selectivity and sensitivity of the sensor is changed. But how to tailor the sensing properties of a sensor to a specific application?

The simplest sensor variation is a change of the sensing material itself [178]. A host of different semiconductors with selectivity to one or more gases are available nowadays (see table 2.1). However, it is not necessary to change the whole sensing material. Dopants have a strong influence on the sensing properties of semiconductors [179]. By adding small quantities of noble metals the electrical and especially chemical properties of the semiconductor are changed (see *section 2.4.1*).

During development of the present sensor system it has been decided to use only one metal oxide, changing its properties by doping. This approach carries a clear advantage for future efforts to produce the sensor system: instead of optimising the powder synthesis and sensitive layer deposition for several different materials it is possible to focus on just one, tin dioxide. The small variations introduced by doping are trivial compared to the difficult task of optimising the synthesis of one or more additional base metal oxide powders.

As detailed earlier the final ADA sensor chip will consist of three separate, but integrated, sensors on one chip, forming a sensor array. Each of them has a different sensitive layer which favours one of the targeted gases carbon monoxide, nitrogen dioxide or methane:

- Nitrogen dioxide: undoped SnO_2
- Carbon monoxide: 0.2wt%-Pd doped SnO_2
- Methane: 3wt%-Pd doped SnO_2

In the next figure, the performance of these three materials is presented. The measurements were conducted with conventional gas sensors to test the performance of the selected materials before implementing them into the final ADA sensor chip. All the sensors were operated at 300°C in order to evaluate the selectivity of the materials only. A change of the temperature, as shown in the following section, would also influence the selectivity. The humidity of the test gas mixture was 50% r.h. and the temperature was 25°C.
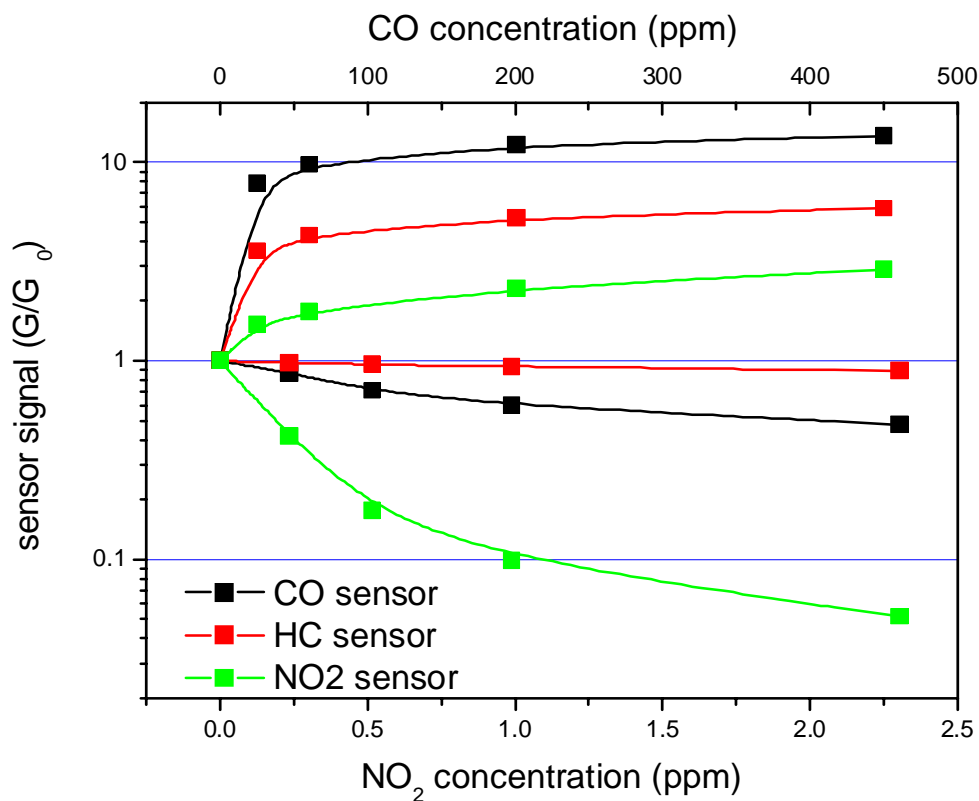
Figure 3.11: The sensor signal of various conventional thick film sensors to the separate exposure to carbon monoxide and nitrogen dioxide. The sensor signal is defined as the ratio between the sensor conductance in air and in the presence of the target gas. For carbon monoxide the conductance increases so the results are all exceeding 1; the opposite happens for nitrogen dioxide.

The CO sensor is tuned towards the detection of very low concentrations of carbon monoxide; it responds also to nitrogen dioxide but in mixtures follows the carbon monoxide concentration. The HC sensor is using a sensing material that allows detection of hydrocarbons (such as methane) at concentrations lower than 5% of the Lower Explosion Limit (LEL); it is, even at a relatively low temperature un-sensitive to nitrogen dioxide. The NO_2 sensor is very sensitive to its target gas and shows little cross-sensitivity to carbon monoxide in the investigated concentration range; it practically shows no sensitivity to

saturated hydrocarbons and in mixtures between nitrogen dioxide and reducing gases it follows the concentration of NO_2.

3.4.2 Sensor Operation Temperatures

A possible additional way for improving the sensors selectivity is a variation of the sensor operation temperature [180]. This is especially interesting as the final ADA chip allows operating three sensors with independent settings, i.e. individual temperature programmes.

The gas sensing mechanism of semiconductors makes their performance susceptible to temperature changes. Different pollutants have characteristic optimum oxidation and reduction temperatures and therefore give rise to characteristic resistance-temperature profiles. By varying the operation temperature of the sensor it is possible to increase or decrease its sensitivity and selectivity towards specific gases. This special attribute of semiconductor gas sensors was exploited to maximise the sensor signal to each target gas, (i.e. increase the sensors sensitivity) and discern between two targeted gases (i.e. increase the selectivity) [181]. The adsorption, reaction and desorption of gases on the sensor surface depend on the temperature. Therefore also the sensor signal kinetics are influenced; in this case the response time t_{90} and the recovery time of the sensor. A higher temperature will improve both [182], and is therefore preferable.

The targeted applications for the sensor system require a selective detection of one pollutant in a binary mixture. As demonstrated in figure 3.12, it is possible to detect carbon monoxide and methane qualitatively and quantitatively in a mixture of both gases. Two conventional thick film sensors with the same sensitive material operated at different temperatures show a completely different reaction to carbon monoxide and methane. This behaviour allows establishing a calibration for the complete sensor system that discriminates between these two gases in mixtures.
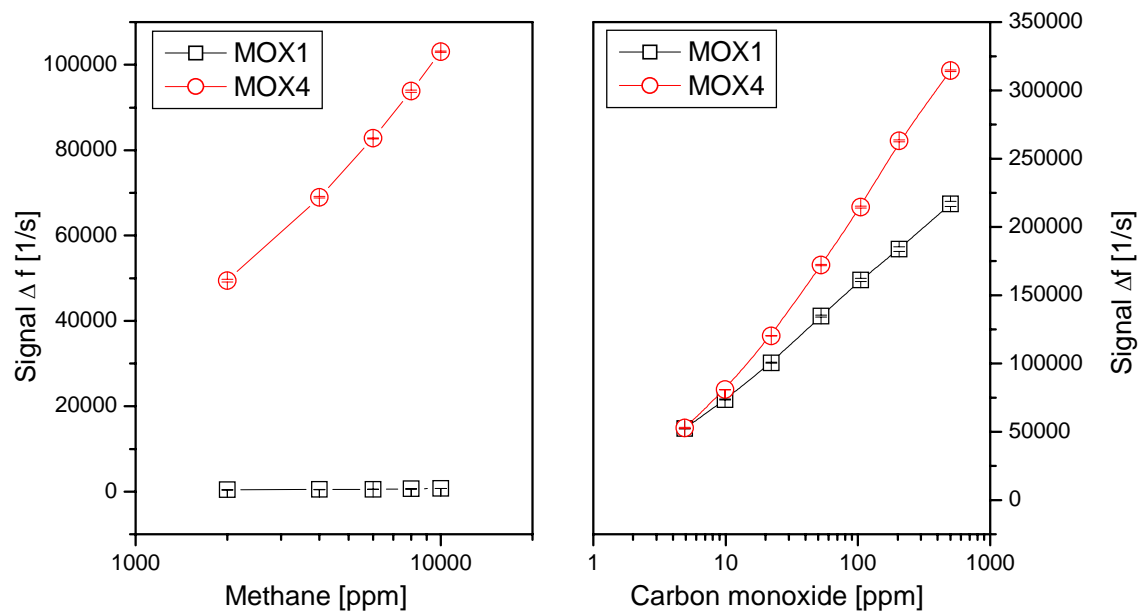
Figure 3.12: Exposure of two AS sensors coated with the same sensitive material and heated at 250°C (MOX1) and 350°C (MOX4) to 0.2-1% methane respectively 5-500ppm carbon monoxide. Measurements at 50% r.h. and RT.

To determine the optimal operation temperatures for the μ-hotplates the ADA sensor chip was exposed to low concentrations of carbon monoxide, methane and nitrogen dioxide at different temperatures. Thereby the sensor signal strength towards each pollutant could be established

as a function of its operation temperature at constant concentration. The conditions tested were:

- 250, 275, 300, 325, 350°C
- CO 1ppm, CH4 500ppm

The μ-hotplates temperatures were controlled individually and each of them was coated with a gas-specific sensitive layer. The aim was to find the maximum in the above function, i.e. the operation temperature with the highest sensitivity and selectivity for the targeted gas for each hotplate. The resulting values were:

- 350°C for the detection of **methane CH$_4$**
- 275°C for the detection of **carbon monoxide CO**
- 275°C for the detection of **nitrogen dioxide NO$_2$**

3.4.3 Temperature Modulation

As we have seen, operating sensors at different constant temperatures already improves their selectivity considerably. The next step for increasing the sensor selectivity is naturally to move from constant to dynamically modulate temperatures [160], [181], [183]. The simplest way to observe a temperature dependent dynamic sensor response is literally to switch the sensor power supply on or off, with and without analyte gas being present. The transient response of the sensor is characteristic of the gas to which the sensor was exposed. This behaviour indicates the potential for qualitative and quantitative analysis of gaseous mixtures [184]. More promising seems the application of a periodic heating voltage to the semiconductor gas sensor [160]. Several advantages can arise from an oscillating heater voltage [185], [186]. Firstly, because of the different reaction rates of various analyte gases at different temperatures, a cyclic temperature variation can give a unique signature for each gas. These "fingerprints" allow for detecting the presence of a specific gas in a mixture of gases and to some degree reveal quantitative information. Furthermore, if the response of one sensor is measured at n temperatures, the sensor becomes analogous to an array of *n* "sensors". Thus if *m* different actual sensors are used, *m*n* dimensional information is available for analysis [187] (assuming all n "sensors" are linearly independent). Secondly, because low temperature operation can lead to the accumulation of incompletely oxidised contaminants, periodic shifts to higher temperatures may help to clean the sensor surface, increasing the desorption rate and reducing the sensor recovery time. Thirdly, thermal cycling leads to improvements in sensitivity, as discussed earlier.

3.4.3.1 Pattern Recognition Methods

As we introduce more sophisticated temperature modulation modes, the increased number of virtual sensors create a huge data output. To analyse the complex sensor signal matrix generated, pattern recognition methods are usually utilised [188], [189]. They allow establishing calibrations based on recurring signal patterns and identify the important linear independent sensors for each application.

The **Principal Component Analysis (PCA)** is widely used in signal processing, statistics, and neural computing [190], [191]. It is a method to reduce a high-dimensional data-space while minimising the loss of information. To enable a graphical presentation, the data-space is projected onto a two-dimensional coordinate system. The axes of this new data-space are the

principal components; the first principal component is the projection of the original data-space on the direction in which the variance of the projection is maximized, the second principal component is established accordingly. Each subsequent principal component describes the maximum of variance that was not included in its predecessor. Apart from allowing to visualise the data in a low-dimensional space, irrelevant information such as noise is reduced and signals from linearly inter-dependent sensors is eliminated.

The **Principal Component Regression (PCR)** [192][193] is a simple extension of multiple linear regression (MLR) and PCA. In the first step, the principal components are calculated. The scores of the most important principal components are used as the basis for the multiple linear regression with the target data. Thereby a common problem in conventional multiple regression (correlations between the predictor variables) is avoided, as the principal components are not correlated. An important point during PCR is the proper selection of the eigenvectors to be included. They are normally selected from the first few principal components. The eigenvectors of a PCA decomposition represent the variations that are common to all of the sensor calibration data. Therefore, using that information to calculate a regression equation (in place of the straight sensor responses) will produce a robust model for predicting concentrations of the desired constituents even in very complex samples.

Artificial Neural Networks (ANN) [194][195] attempt to imitate the operation of neurons in the brain. Such networks have a number of linked layers of artificial neurons, including an input and output layer. The network is trained by various methods using a large training set. Through the training it learns to recognise hidden patterns in the calibration data set, weighting the input data accordingly. The advantage of neural networks lies in their ability to represent both linear and non-linear relationships and in their ability to learn these relationships directly from the data being modelled.

3.4.3.2 Selectivity Improvements

The target of the first experiment with temperature modulation was to eliminate humidity influences during a carbon monoxide measurement using just one single sensor. In constant operation mode there is just one measurement result, which is the resistance of the sensitive layer at the given temperature. Here it is impossible to determine if a change of the signal originates from a concentration change of the target pollutants or of other pollutants.

Figure 3.13 shows a measurement on a single temperature cycled sensor in humid air. The X-axis shows the time in ticks of each around 200ms, depicted are 10s. The red dotted curve represents the temperature of the sensor heater, the blue curve gives the respective resistance of the sensitive layer. In this measurement the temperature of the heater was changed between 180 to 400°C, according to typical operating conditions. The sensor was measured five times at each temperature.

The depicted overshooting in the resistance (typically within the first measurement after adjusting a new temperature) is caused by chemical reactions and desorption / adsorption processes which are partly pollutant-specific. Thus the information content of a measurement with one single sensor can be dramatically increased, in the given case there are up to 50 "virtual" sensors (which means one sensor at different operating temperature each) with a partially different behaviour.
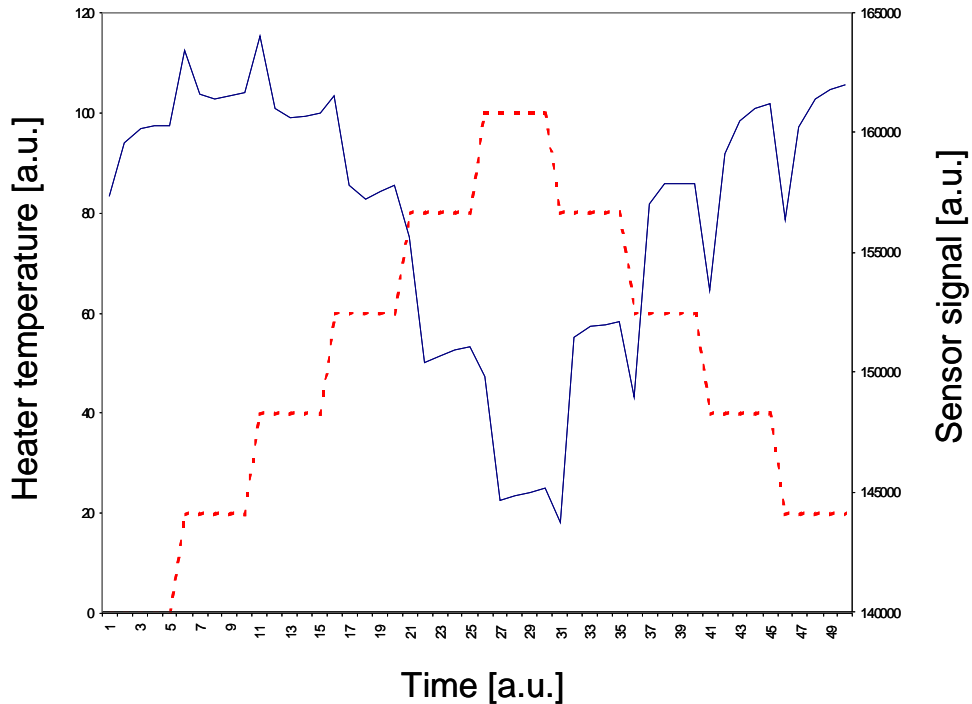
Figure 3.13: Temperature profile and response of the AS sensor. Exposure to 20-80% r.h. and 100-300ppm carbon monoxide at RT. Sensor operation temperature cycled from 180-400°C.

In the following measurement this temperature modulated sensor was exposed to different concentrations of carbon monoxide (100, 200 and 300ppm) in different humidities (20-80% r.h.). The 50 measurements performed within the measurement cycle of 10s (with one single sensor, as described above) were taken as individual sensors and the data was processed using a pattern recognition method (PCR). The following graphic shows the result of the predicted concentrations for 0, 100, 200 and 300ppm carbon monoxide in different humidities (20-80% r.h.) (X-axis: true CO concentration, Y-axis: predicted concentration).
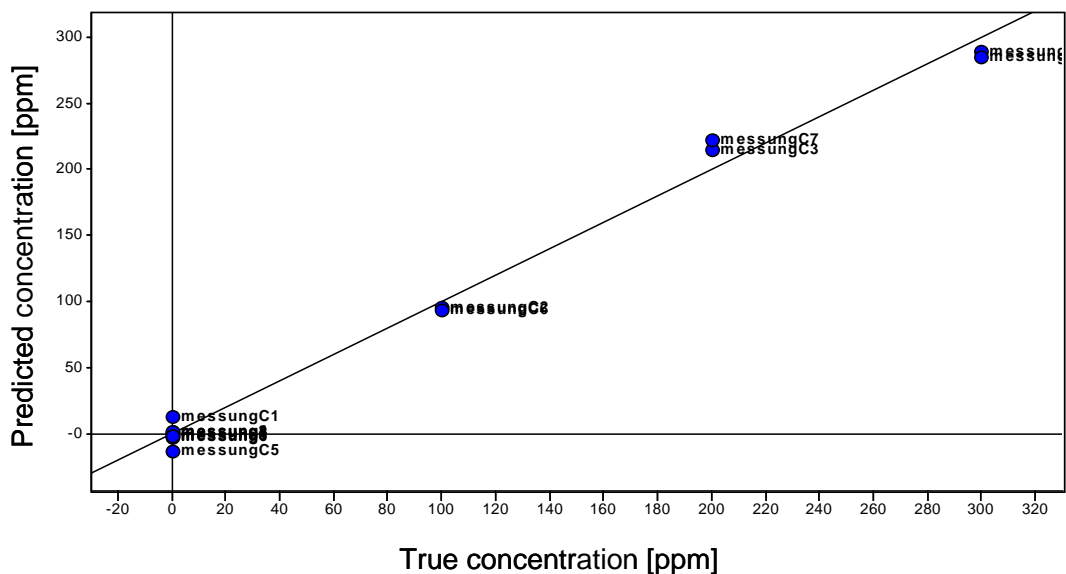
Figure 3.14: PCR-plot, predicted vs. true concentrations for a binary mixture of 100-300ppm carbon monoxide and 20-80% r.h.

Thus it was possible to separate the contribution of carbon monoxide and humidity to the sensor signal and to almost completely suppress the signal from the change of humidity in the concentration prediction.

The next experiment used another temperature profiling to distinguish between different pollutant gases. The temperature modulation was done with very slow temperature changes over a very broad temperature range (RT-450°C), the gas concentration was kept constant. The X-axis in the figure 3.15 gives the time in units of 200ms, the Y-axis shows the resistance in arbitrary units (proportional to 1/R). The overall depicted scan time was 70s, the temperature was increased in 50 steps within 35s, and decreased within another 35s.
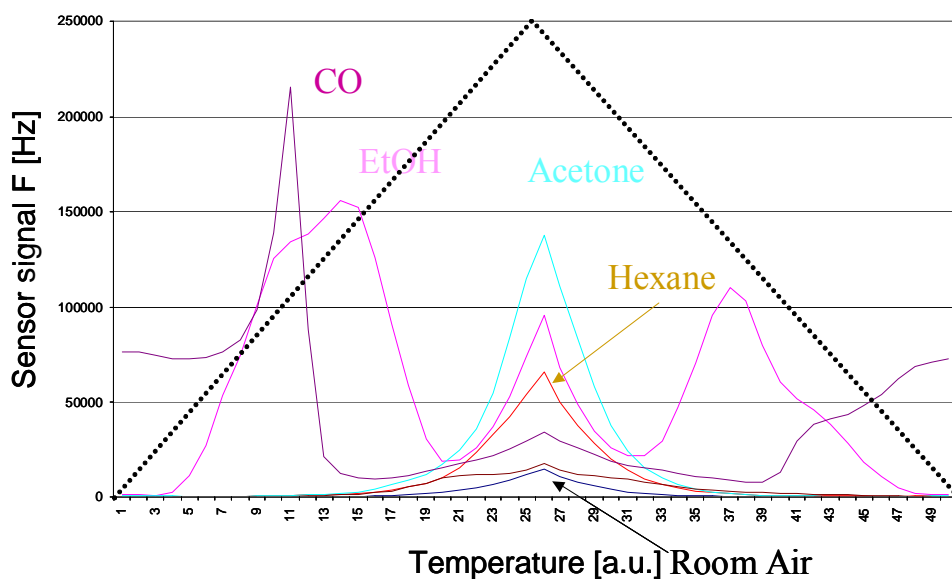
Figure 3.15: Slow temperature ramping measurement. Modulation from RT to 450°C to RT (black dotted line).

It is clearly visible that specific patterns for the different pollutants appear. This holds especially true for carbon monoxide, which showed a large response already in quite small concentrations.

Several temperature modulation experiments have also been performed with the final ADA sensor chip to prove we can transfer the results gained from the experiments discussed above. Different temperature modulations were tested as demonstrated in figure 3.16; in dynamic (sinusoidal) as well as static mode (steps and ramps).
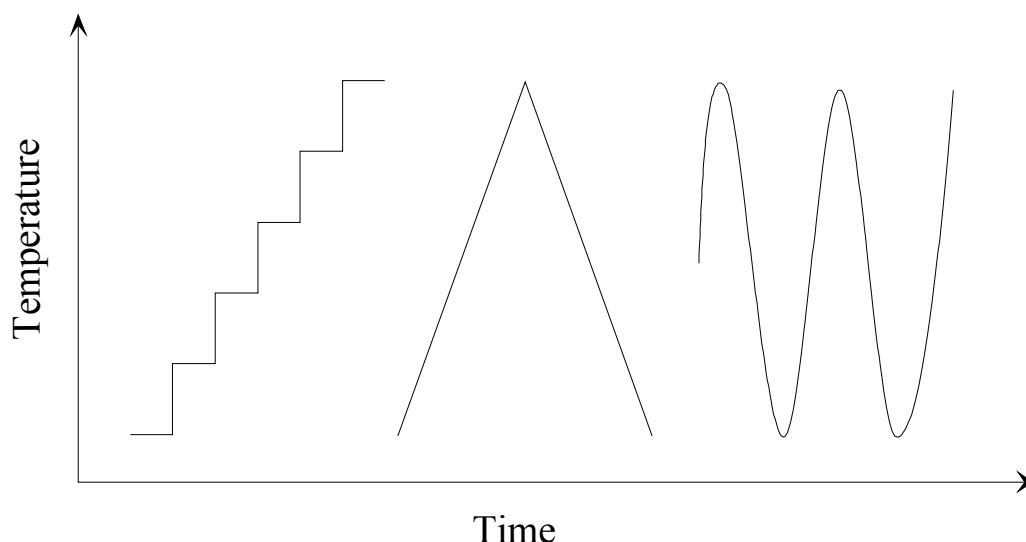
Figure 3.16: Temperature modulation modes investigated with and w/o gases. Each mode was tested in various lengths between 50s and 20min.

An example of the sensors behaviour during these tests is given in figure 3.17. As can be seen, the three hotplates each react differently: HP1 (CH_4-sensitive) and HP3 (CO-sensitive) both show a strong resistance change while HP2 (NO_2-sensitive) shows only a short signal overshooting without any visible reaction to the changed temperature itself. These results prove the temperature modulation is working for the ADA sensor chip.
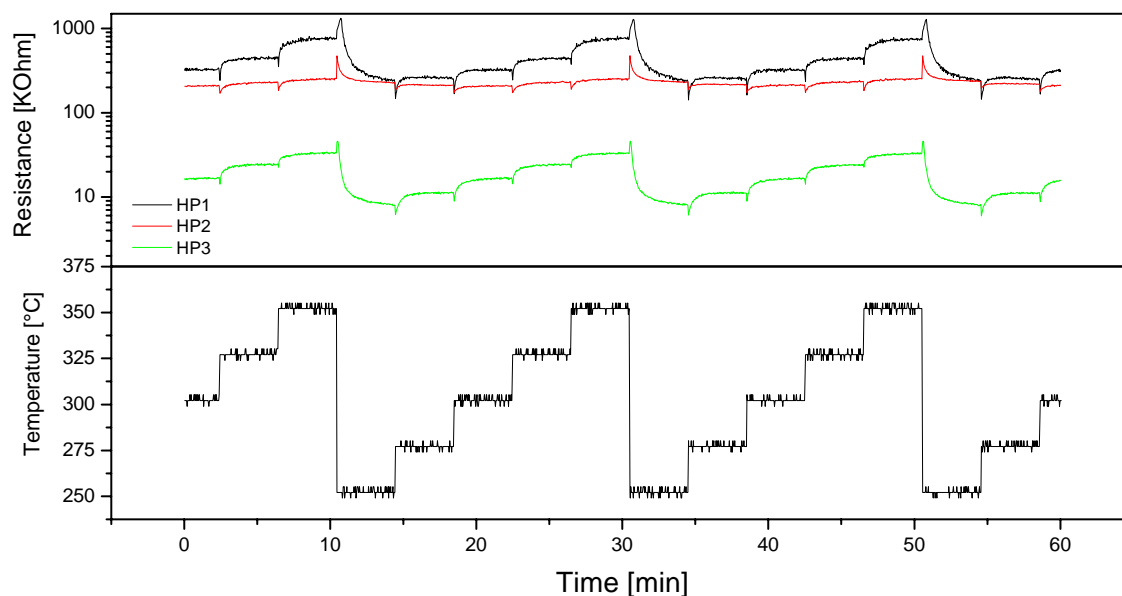
Figure 3.17: ADA sensor chip signals during temperature modulation. All three µ-hotplates active at 250-350°C and 50% r.h.. Long temperature cycle length of 20min.

3.4.4 Gas Filters

The methods discussed so far influence the sensor selectivity by directly changing an integral part of the sensor itself, such as the sensitive material or the operation temperature. Gas filters, on the other hand, offer a solution to cross-sensitivity problems without requiring any change of the sensor itself. By forcing the gas samples to pass a filter, the composition of the gaseous mixture is altered, either by adsorption or catalytic burning of gases. Instead of

changing the sensor reaction to certain gases, the relative concentration of unwanted interfering gases in the gas sample is decreased until their contribution to the sensor signal is reduced to insignificance. By allowing only selected gases to reach the sensor, possible false positive signals and thereby false alarms are eliminated. As most gas filters affect a range of pollutants, they eliminate also unknown interfering gases as a positive side effect. An ideal gas filter is characterised by

- a high selectivity to interfering pollutants
- no influence on the target gas concentration
- a high permeability for humidity
- a weak pollutant desorption
- a high breakthrough threshold

To find the best gas filter a range of materials was investigated, all of them using different filtration techniques. They can be classified according to their filtering technique: adsorbants, catalysts and molecular sieves. Another important issue for the design of the sensor system is the filter operation mode and integration into the gas flow architecture. So far, two different strategies have been pursued by previous authors [196]-[198].

In the diffusion mode a small filter volume is placed above the sensor, forcing potential analytes to reach the sensor surface through diffusion only. The filter material is located either in a separate segment above the sensor or deposited directly on the sensor surface, with and without additional heating. In the direct flow mode the filter is located upstream of the sensor. Here, the complete gas sample has to pass the filter and is subject to its effects, contrary to the diffusion mode.

Volatile organic components (VOCs) are a common nuisance for gas sensor systems in real world applications. Differing vastly in size and polarity, they are a heterogeneous class of gases and a source of cross-sensitivity problems. They have therefore been selected as main targets of the filter system. To facilitate the evaluation of potential filter materials two VOCs have been selected in accordance with international standards [163][169] as representative interferents: ethanol and heptane. The first is a short-chain and highly polar alcohol while the latter is a much longer and non-polar alkane. Together they cover the chemical characteristics of the most frequently encountered VOCs and offer a good representation of the high number of different hydrocarbons present in ambient air. Figure 3.18 illustrates the strong cross-sensitivity of the sensor towards both ethanol and heptane.
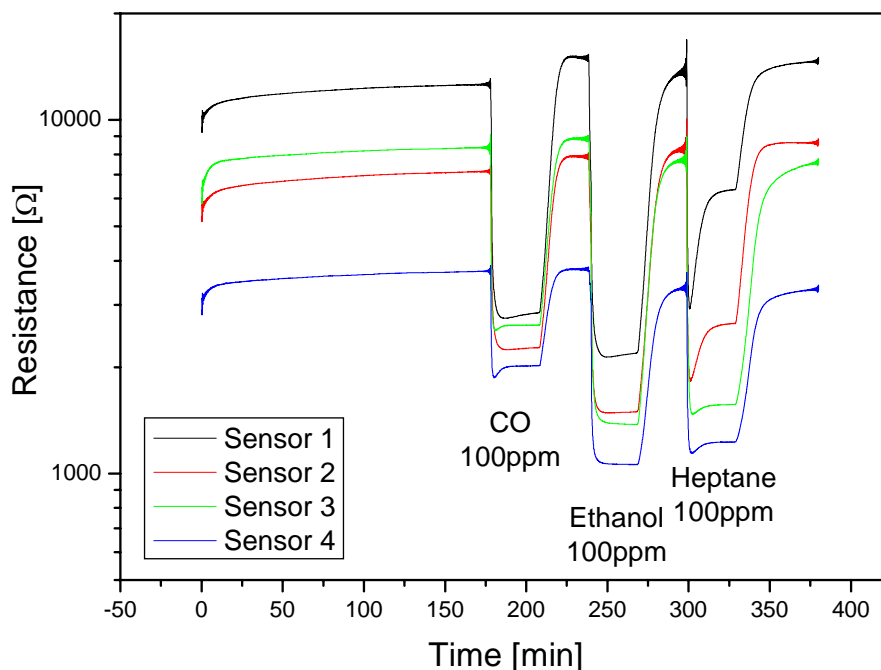
Figure 3.18: Four different conventional thick film sensors exposed to 5ppm carbon monoxide and 500ppm heptane at 50% r.h. and RT.

In the following, the different filter materials investigated will be shortly presented and their performance, according to the criteria defined above, discussed.

3.4.4.1 Adsorbants

By definition, adsorption is the process by which one substance is attracted to and held on the surface of another. The removal capacity of an adsorbant is directly related to its total surface area, and in a porous solid adsorbent, the surface extends well into the interior of the solid. Because of the relatively weak forces involved, adsorption is essentially reversible. Adsorbants are effective versus non-polar organic molecules with a high boiling point while ignoring smaller ones such as methane [199]. The materials investigated were commercially available activated charcoals [200], [201]. They differ in their absolute surface area, grain size and form as well as preparation procedures.

3.4.4.2 Catalysts

Catalysts are materials inducing a chemical reaction on their surface while suffering no chemical property change themselves. The gases arriving are adsorbed at the surface and react to form stable chemical compounds. These are bound to the media as organic or inorganic salts or released into the air as carbon dioxide CO_2 and water vapour. The nature of these reactions makes the process irreversible, contrary to simple physical adsorption. By impregnating catalysts on adsorbants, weakly adsorbed gaseous contaminants can therefore be eliminated from the atmosphere. Similar to adsorbants, impregnated catalysts are more or less specific for a certain contaminant or group of contaminants. The materials investigated were $KMnO_4$ impregnated activated alumina [201] and perfluorinated sulfonic acid (Nafion) [202].

3.4.4.3 Molecular sieves

Molecular sieves are synthetic or natural zeolites with strong adsorption capacities for gases vapours and solved substances [203]. They are aluminasilicates containing alkaline and alkaline earth metals and often employed for ion exchange, catalysis and separation of different solvents or gases [204]. Their anions form a grid-like structure on a molecular level with channels and pores of a defined size. Different molecules will be allowed through these channels or retained depending on their chemical and physical attributes, e.g. straight chain alkanes can enter the pores and will be adsorbed in contrast to cyclic and branched alkanes. This adsorption is reversible given time, temperature or a cleansing gas flow [205]. The material investigated was a commercial molecular sieve (pore size 4Å).

3.4.4.4 Filter performance

Conventional thick film sensors and AS sensors protected by various filter materials were exposed to up to 500ppm ethanol and heptane. The investigated concentration range is at the upper limit of legal requirements [163], [169]. The filter materials were processed to offer a wide range in grain size and morphology, from fine powder to rods and spheres of up to several millimetre diameter. One of the first observations was the high similarity of results between exposures to ethanol and heptane. The strong difference in polarity did not affect their interaction with the selected filter materials: filters were either effective versus both pollutants or versus none. This allows focusing on the results for heptane in the following discussion; the results for ethanol are accordingly, with the sensor signal being approximately 20% stronger during all measurements. Table 3.1 illustrates the elimination strength of the tested materials if exposed to typical concentrations encountered in real world applications.

Filter Evaluation: Sensor Signal [R_0/R]		
Filter material	**Heptane [100ppm]**	**Carbon monoxide [5ppm]**
Ideal	*1.00*	*high*
Active charcoal[a] I	4.29	3.45
CPBlend[a,b] I	17.4	3.43
Active charcoal[a] II	1.16	2.87
Active charcoal[a] III	1.18	3.34
CPSelect[b] II	62.7	3.91
Molecular sieve[c] II	73.2	4.22
Active charcoal[a] V	1.41	3.29
Active charcoal[a] VI	1.12	3.17
Molecular sieve[c] III	65.6	3.54
Active charcoal[a] VII	1.77	3.02
Nafion[b] I	65.3	3.64
Active charcoal[a] VIII	1.04	2.87

Table 3.1: Sensor signal to 100ppm Heptane and 5ppm carbon monoxide. Measurements in diffusion mode. Filter category a=adsorbant, b=catalyst, c=molecular sieve. Measurements at 50% r.h. and RT.

The results clearly point to activated charcoal as the best filter material. Independent of grain size, morphology and manufacturer all active charcoal samples tested were very effective at filtering heptane and ethanol. The low filtering effect of the $KMnO_4$ impregnated activated alumina pure (CPSelect) and mixed with activated charcoal (CPBlend) is as expected from literature [206]. It is more effective at removing nitric oxides NO_x than VOCs. Contrary to literature [202], Nafion did eliminate neither ethanol nor heptane. The catalyst filters can therefore be considered as unsuited to the task of eliminating VOCs from a contaminated atmosphere. The molecular sieves tested not only failed at filtering the pollutants but also disrupted the sensor signal for several hours. The low pore size of the tested zeolites (around 4Å) resulted in a humidity filtration. As the sensors are susceptible to ambient humidity no measurements were possible until complete filter saturation. Of course, this prevented also any filtration effect of the pollutants. The selected zeolites were inadequate for the task of filtering VOCs. However, literature suggests more promising results if the right pore size for the selection process can be determined [207].

Another important aspect is the filter selectivity. In our case, an ideal filter material will not affect the signal to carbon monoxide or methane significantly. The results presented in table 3.1 suggest a very small interaction between pollutant and filter. For molecular sieves this can be explained by lingering effects of the ambient humidity filtration. For catalysts and adsorbants the reduction in signal strength for different filter materials is up to 20%. The effect is strongest for materials processed to fine powder, suggesting diffusion problems between gas stream and filter as the source. A similar problem occurred during measurements in direct flow mode: fine powder filters reduced the gas flow significantly (down to 10% in one case). Therefore, larger grains should be preferred over fine powders to assure a constant flow or diffusion through the filter.

Earlier misgivings on the filter affecting the sensor signal response and recovery time were not confirmed. All measurements with filters displayed response and recovery times equal to measurements without filter. However the filter operation mode did affect the response and recovery times. In diffusion mode, t_{90} was significantly increased compared to direct flow mode.

The last aspect to be considered is the filter breakthrough capacity. Naturally, the filter volume in direct flow mode needs to be much larger than in diffusion mode, where an increase in volume directly affects the sensor response and recovery time. The filter volumes tested range from 0.1 to 6ml. For low volumes (0.1-0.2ml, diffusion mode) a breakthrough appeared after exposure to 500ppm heptane with a flow of 500ml/min for 3-6h (depending on the material). Larger filter volumes (5-6ml, direct flow mode) survived exposure to heptane without breakthrough. The test conditions were 100ppm heptane with a flow of 400ml/min for 30h. The system was also exposed to very high concentrations of > 1% ethanol, resulting in an immediate breakthrough and recovery after 1 day. Without purging of the filter at higher temperatures, small residues of ethanol could still be found downstream of the filter after several days. It can therefore be concluded that the operation in diffusion mode did neither extend the filter lifetime nor improve the response and recovery times significantly. It was therefore decided to install an active charcoal filter (small grains, no powder) in direct flow mode with a filter module size of 20ml in the final sensor system. This equals to a proven filter lifetime of 10days at continuous operation and exposure to 100ppm heptane, a high pollutant concentration not encountered for more than a few minutes at a time. The filter lifetime is even extended if the sensor system measures with a frequency < 1/30s (laboratory standard), but more in the direction of 1/min to 1/5min (envisioned for real world application).

61

3.4.5 Air Flow and Pressure Fluctuations

The gas flow system of the ADA sensor unit prototype depends on active pumping. However, the constant activation and deactivation of the pump and corresponding change in pressure and flow rate in the system has an undesired effect on the sensor signal. An oscillation is superimposed over the signal itself with a phase identical to a complete pumping cycle. This oscillation has an amplitude of 2-10% of the signal strength (depending on pollutant concentration and signal calculation). This effect lowers the sensor resolution and increases the limit of detection; both are worsening the sensor overall performance.
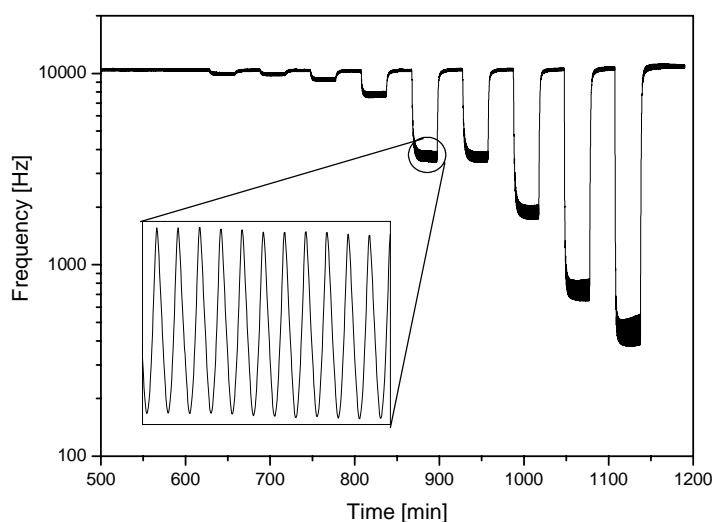
Figure 3.19: Sensor signal oscillation. Exposure to 50-5000ppb NO$_2$ at 50% r.h. and RT.

Two answers to this problem have been tried: filter membrane and data treatment. To prevent the sensors from experiencing a variation in the gas flow rate, thin particle filter membranes were fixed to the sensor casing, sealing its air inlet off. However, this did not help reducing the oscillation. As no further interference with the sensor itself was desired, data treatment was tried. Fast Fourier Transformation (high-pass and low-pass), Savitzky-Golay and averaging filters were applied to the oscillating signal. The averaging signal proved to be most successful, reducing the oscillation to negligible levels. As trade-off, the time resolution was decreased to several seconds. Another option to reduce the sensor signal oscillation is offered by the system operation mode, as discussed in *section 3.6.*

3.4.6 Strategies Discarded

During the development process, a few strategies that initially seemed promising were revealed to be impractical and were disregarded for the final sensor system.

3.4.6.1 Pre-concentrator

The pre-concentrator unit was to be used as an indicator for the amount of organic material present during the measurements. It consists of a small chamber filled with adsorber material and equipped with heating structures. At regular time intervals the gas flow would be redirected to the pre-concentrator unit where VOCs would be adsorbed over 1-2min and subsequently desorbed by a controlled heating of the adsorber phase (150-200°C). The resulting gas sample could then be measured by the sensor and indicate the level of VOCs in the ambient atmosphere. The components were tested in respect of gas adsorption,

performance and life-time. However, it became evident that the pre-concentrator would require a significant increase in system volume and power consumption. Due to the restrictions in size and targeted battery operability of the system it was decided to incorporate only a passive gas filter and no pre-concentrator.

3.4.6.2 Controlled Humidification

The cross-sensitivity of tin dioxide sensors to humidity fluctuations is a known problem. It therefore seemed a plausible strategy to incorporate a humidity reservoir to allow a controlled humidification. This should fix the relative humidity at a constant level and thereby eliminate an important cross-sensitivity source, easing future calibration efforts. The gas flow would be redirected through the humidity reservoir prior to the measurement chamber. Tubings with high humidity permeability are commercially available as are liquid or solid humidity sources. However, the implementation of the humidity reservoir proved problematic. First, a drying phase would be required to reduce even gas samples saturated with humidity (e.g. sampling during rain) to a basic level. Then the humidity reservoir would raise the humidity level to standard. A valve would be necessary to separate these two phases and prevent unintended diffusion. Due to the significant increase in system complexity and size it was decided to rely on calibration algorithms to compensate the sensors cross-sensitivity to humidity.

3.5 Calibration Strategies

So far, the development of sensor hardware and different strategies pursued to increase the system performance has been discussed in detail. Yet, the ADA prototype needs further laboratory activities to be able to operate as a gas detection device: the calibration. The calibration converts the raw sensor data into intelligible qualitative (pollutant) and quantitative (concentration) information. The calibration algorithm has to be selected for a maximum of simplicity and accuracy. The simplicity determines the effort in time and personnel to establish an initial calibration, implement it into the system firmware and adjust it in regular intervals (re-calibration). The accuracy is a measure of how close the algorithm fits the experimental sensor values. Each pollutant gas to be detected needs its own, individual calibration. For semiconductor sensors, a range of algorithms has been proposed in literature derived from theoretical calculations and empirical validations [7], [139].

A simple calibration algorithm has been selected for the sensor system. Two ADA prototype systems equipped with AS sensors were calibrated for two test gases each, carbon monoxide and methane. The process of calibration, prediction and evaluation is discussed in the following example through the calibration of carbon monoxide. No pattern recognition methods were used at this stage.

3.5.1 First Calibration

The first calibration algorithm tested was based on the approximation of the resistance-concentration relationship through a set of three linear functions, each one valid in a defined concentration range. This procedure would be easily implemented into the sensor system controller; it had the advantage of high simplicity, while lacking somewhat in accuracy. The following figure 3.20 gives an overview of the laboratory measurement protocol used for calibration. These measurements were repeated several times to have a calibration data set based on at least three measurements.
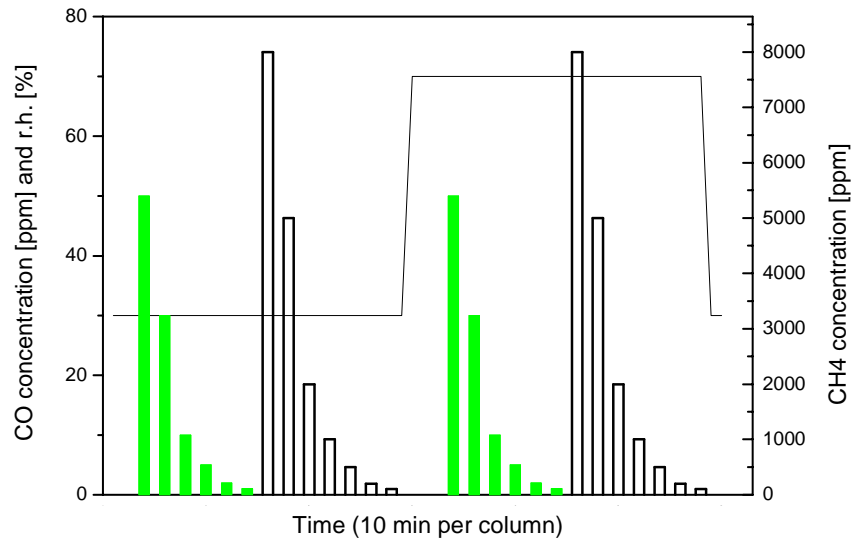
Figure 3.20: Concentrations of 1-50ppm carbon monoxide (filled columns) and 200-8000ppm methane (empty columns) used for generation of the data sets for calibration and prediction in the case of single pollutants.

Previous measurements at different ambient humidities suggested a small cross-sensitivity to humidity variations in the range between 10 to 90% r.h. This led to ignore the humidity influence on the sensor signals for the first calibration. The measured sensor resistance values at 30 and 70% r.h. were averaged for a single calibration data set. Besides the small initial cross-sensitivity of the sensors, the filter material is reducing humidity variations in the measurement chamber to an average value with small deviations even for extended time periods. The parameters tested for calibration and prediction measurements were:

- 1, 2.1, 5.3, 10.9, 30.9, 50.3ppm CO
- 175, 476, 971, 1945, 4801, 7597ppm CH_4
- binary mixtures of CO and CH_4
- all at 30% and 70% relative humidity and at room temperature

3.5.2 Single Pollutant Prediction

After establishing the calibration as detailed above, it was tested with independent prediction data sets. The prediction measurements were conducted at the same gas mixing station and with the same measurement parameters as the calibration measurements. The concentration values predicted by the calibration algorithm were compared with the true values supplied by reference instruments. Results of the prediction of single pollutants are given in figure 3.21 and table 3.2.
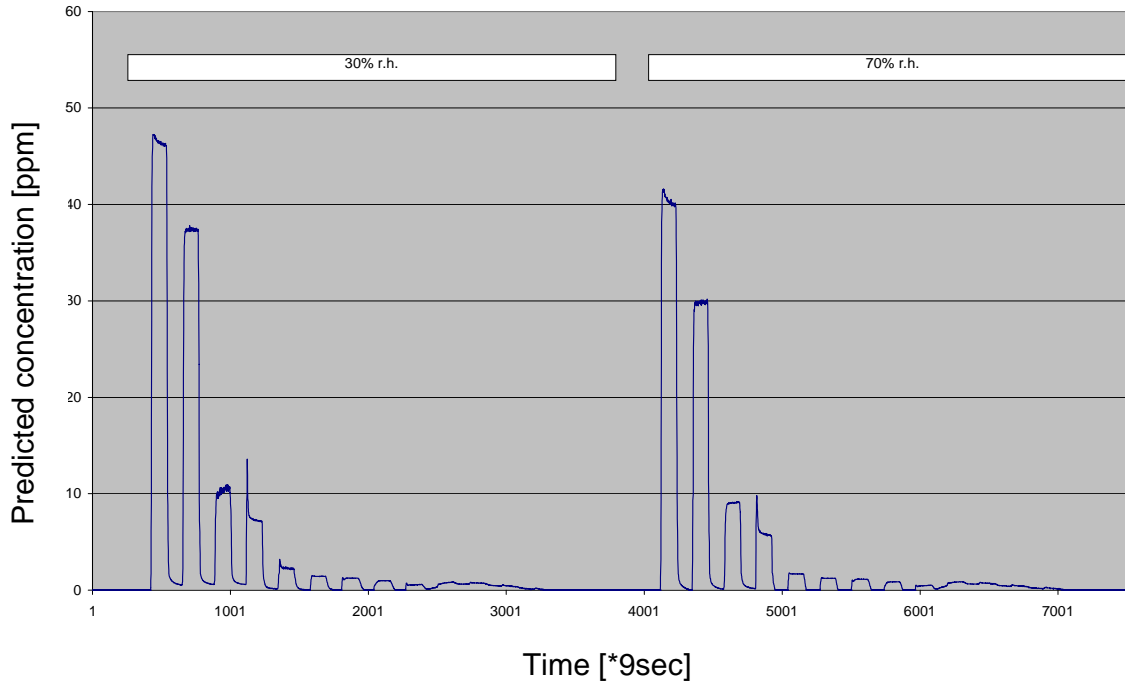
Figure 3.21: Typical prediction measurement. Predicted concentration of carbon monoxide during exposure to 50.3 to 1ppm carbon monoxide and then 7597 to 175ppm methane; measurement conducted 30% and 70% r.h. and RT. Independent data sets for calibration and prediction.

Carbon monoxide - True vs. Predicted Concentration				
True [ppmCO]	**Predicted [30%r.h.]**	**Error, rel. [%]**	**Predicted [70%r.h.]**	**Error, rel. [%]**
50.3	47.1	6.36	41.1	18.3
30.9	37.4	21.0	39.9	29.1
10.9	10.5	3.67	9.0	17.4
5.3	7.2	35.8	5.7	7.55
2.1	2.3	9.52	1.7	19.0
1.0	1.4	40.0	1.2	20.0

Table 3.2:   True and predicted concentrations of carbon monoxide and respective relative deviation values for 30% and 70% r.h.

The average relative error between real concentration and predicted concentration is approximately 20%, with strong variations over the measured concentration range. However, the absolute deviation for low concentrations is good. The cross sensitivity of the calibration of the carbon monoxide signal towards methane is very small. The signal towards methane concentrations of up to 8000ppm is in the range of 1ppm carbon monoxide. The difference between predicted concentrations for 30% and 70% r.h. is much stronger than expected.

3.5.3 Binary Mixture Prediction

In a next step the calibration model, which was established using just single gas pollutants, was tested for the prediction of concentrations in binary gas mixtures at different levels of relative humidity. This was done to test the robustness of the calibration model for the single

gases for real life situations, where several pollutants will be present simultaneously. Figure 3.22 details the measurement protocol used to establish a prediction data set for binary mixtures of carbon monoxide and methane.
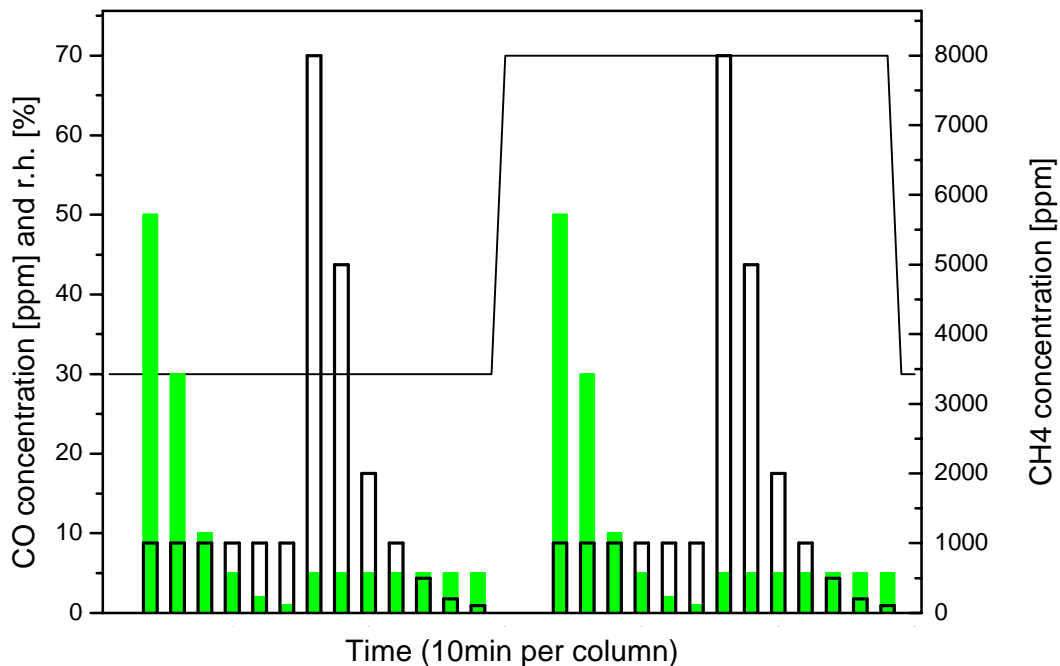
Figure 3.22: Concentrations of carbon monoxide, methane and humidity during prediction measurements. Exposure to variable concentrations of one gas with a constant background level of another. Measurements at 30% and 70% r.h. and RT.

The following figure 3.23 and table 3.3 show the results of the prediction of carbon monoxide in the presence of methane with a calibration established on single pollutant measurements. Despite of a background of 971ppm methane the average prediction error for carbon monoxide is unchanged in the case of 70% r.h.; however, it is doubled in the case of 30% r.h.. The signal of the carbon monoxide sensor to a constant concentration of 5.3ppm carbon monoxide with a background variation of methane is stable (methane variation over two orders of magnitude). Even low concentrations of carbon monoxide are identified with only a small increase in prediction error compared to single gas measurements, proving the selectivity of the calibration to be acceptable.
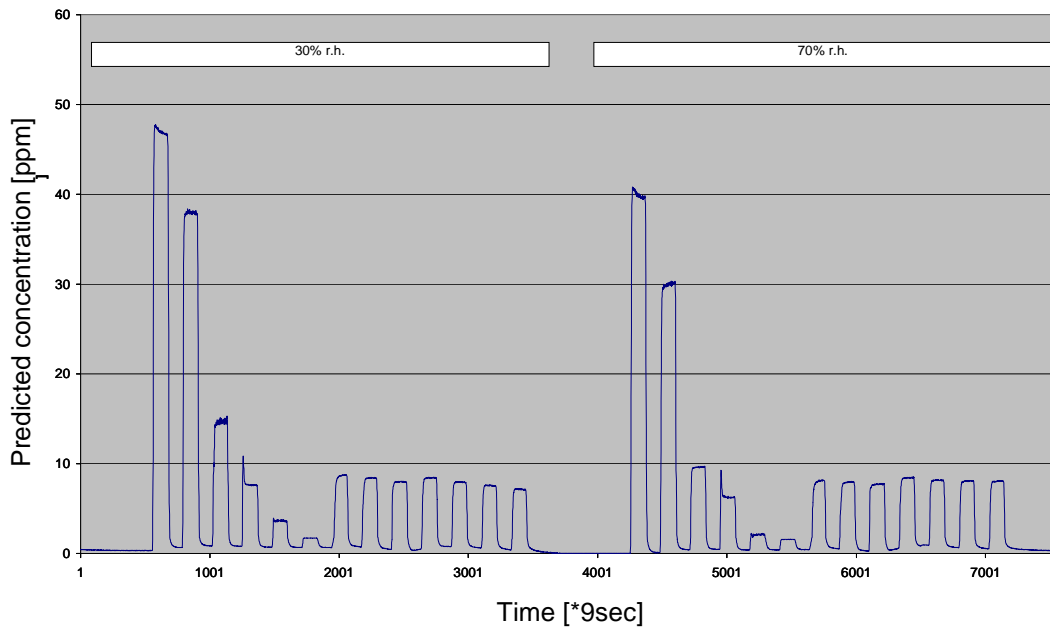
Figure 3.23: Results of the prediction of carbon monoxide in binary mixtures. Variation of carbon monoxide concentration with a background of 971ppm methane and variation of methane concentration with a constant background of 5.3ppm carbon monoxide. Measurement at 30% and 70% r.h. and RT.

Carbon monoxide – True vs. Predicted Concentration				
True [ppmCO]	Predicted [30%r.h.]	Error, rel. [%]	Predicted [70%r.h.]	Error, rel. [%]
50.3	47.4	5.77	40.6	19.3
30.9	37.9	22.7	30	2.91
10.9	14.6	33.9	9.6	11.9
5.3	7.6	43.4	6.2	17.0
2.1	3.6	71.4	2.0	4.76
1.0	1.7	70.0	1.6	60.0

Table 3.3:   True and predicted concentrations of carbon monoxide with a background concentration of 971ppm methane. Measurement as detailed in table 3.3 and figure 3.25.

3.5.4 Evaluation

The prediction experiments have revealed a high relative error of up to 40% for single gases and 70% for binary mixtures. Also, the cross-sensitivity to humidity has been underestimated. To analyse the situation, it is necessary to take a look at the raw sensor values: the resistance change upon exposure to pollutants. The calculated values are detailed in table 3.5.

The value "relative deviation" (standard deviation divided by mean value) gives the deviation of the resistance of the relevant sensor from the mean value of its signals during four independent measurement runs. A small signal deviation means a small difference between sensor responses under the same conditions and therefore a high repeatability. The deviation error is introduced into the final prediction through error propagation. However, it is in the low percentage range for the raw sensor data and therefore much smaller than the prediction errors after calibration. This indicates that the potential of the sensors is better than the results

67

of the prediction would suggest, i.e. the calibration is the error source. Another possibility is a systematic error introduced between measurements used for the calibration and measurements used for prediction. As both calibration and prediction data sets were drawn from the same pool of measurements without discriminating between the timepoint of the actual experiment this possibility can be discarded. Also, a comparison of the sensor values of the data sets did not reveal such a systematic error. It can therefore be concluded that the reason for the low accuracy of the calibration is the algorithm used.

Gas	Humidity [% r.h.]	Concentration [ppm]	Deviation, rel. [%]
Synthetic air	30	0	1.61
CO	30	50.3	1.17
CO	30	30.9	1.34
CO	30	10.9	1.40
CO	30	5.3	0.84
CO	30	2.1	1.23
CO	30	1	1.08
Synthetic air	70	0	1.10
CO	70	50.3	2.15
CO	70	30.9	1.33
CO	70	10.9	2.10
CO	70	5.3	2.09
CO	70	2.1	2.34
CO	70	1	2.80

Table 3.5: Individual sensors reproducibility and protocol of laboratory measurements used for single gas calibration; the relative deviation of relevant individual sensors was calculated on the basis of four independent measurements runs.

Concerning the cross-sensitivity to humidity, it is clear this has to be taken into consideration for an improved calibration. Possibilities include the introduction of a weighted humidity factor into the algorithm and several humidity dependent calibrations valid for defined humidity ranges. All approaches require the knowledge of the exact humidity, i.e. necessitate a separate humidity sensor installed in the sensor system.

3.5.5 Improved Calibration

After analysing the failure of the first calibration, several different calibration models were investigated, all depending on a power law function based on the change in conductance. Among them the following algorithm proved to be most successful in terms of accuracy for single gas measurements.

$$p_{CO} = a \cdot \Delta G^b \tag{3.1}$$

with p_{CO} as partial pressure of carbon monoxide, $\Delta G = G - G_0$ (conductance) and a, b as variables.

Figure 3.24 shows the established improved calibration based on the above algorithm. As can be seen, the calibration gives a good representation of the measurement results for both humidities.
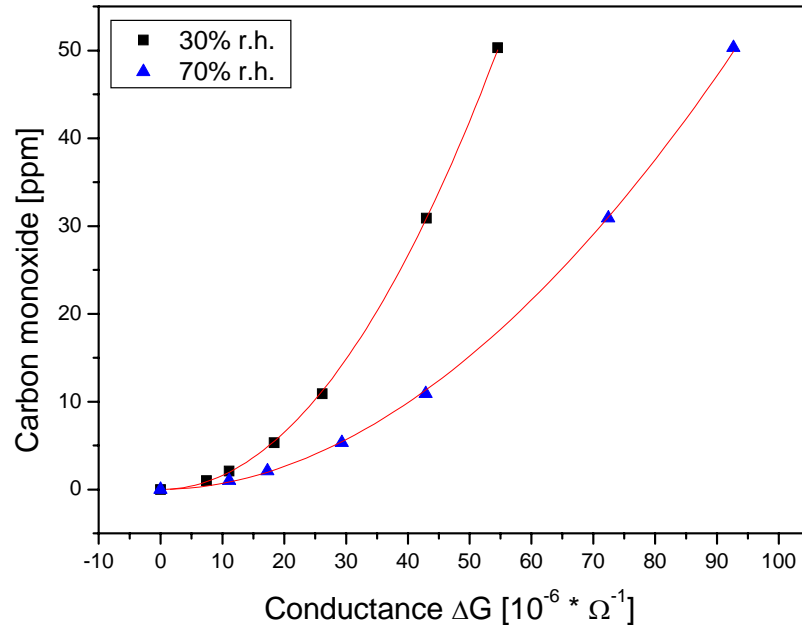
Figure 3.24: Calibration for carbon monoxide at 30% and 70% r.h. with improved calibration algorithm.

The calibration was validated with five independent sets of prediction measurements for 30% and 70% r.h. each. Typical results are presented in table 3.6.

Carbon monoxide - True vs. Predicted concentrations				
True [ppm]	Predicted – 30% r.h. [ppm]	Error, rel. [%]	Predicted – 70% r.h. [ppm]	Error, rel. [%]
50.3	50.4	0.24	50.5	0.38
30.9	31.8	2.80	31.5	1.81
10.9	11.3	3.64	11.5	5.47
5.3	5.53	4.40	5.36	1.13
2.1	1.99	5.30	1.94	7.67
1	0.88	11.9	0.86	14.0

Table 3.6:   Prediction of carbon monoxide based on the improved calibration for 30% and 70% r.h.. Measurements conducted as detailed in figure 3.23. Independent data sets for calibration and prediction.

The average relative error of the prediction is below 5% with a maximum of 6% among the other prediction data sets. As for the first calibration, there is a strong variation of the prediction quality. Lower concentrations tend to produce higher errors with the improved calibration. As this appeared for all prediction measurements with this calibration, it can be assumed to be a systematic deviation between the algorithm and the sensor signal evolution. The good prediction results with an absolute error always lower than 1ppm proves the high quality of the improved calibration algorithm.

As the calibration includes no humidity compensation, it is only valid in a narrow humidity range. Efforts have been made to include a humidity factor into the calibration algorithm, to no avail. The tested algorithm modifications are based on (1) and include

$$y = (a + c) \cdot x^b, \ y = a \cdot x^{(b+c)}, \ y = a \cdot x^b + c \cdot x, \ y = a \cdot x^b + x^c \qquad (3.2)$$

with c = constant and c = f(p_{H2O}).

None of these algorithms was suited to compensate the sensors cross-sensitivity to humidity.

The final ADA sensor system will utilise the improved calibration algorithm. Its establishment and validation for the gases of interest is discussed in *section 4*.

3.6 System Operation

After selecting the components of the sensor system and investigating the various operation strategies destined to increase the selectivity a final issue remained: the system operation mode. The sensor system controller allowed to address all active components (valves and pump) individually, to apply a sophisticated temperature program to the sensor heater and to customise the measurement program. The important system functions to be managed are:

- **Sensor measurement:** to avoid signal oscillations as discussed in *section 3.4.5* the sensor resistance has to be measured under constant atmospheric conditions (pressure, flow), i.e. while the pump is inactive.
- **Sensor heater:** to reduce the power consumption, the sensor heater has to be activated only shortly before an actual measurement. A constant temperature modulation also decreases the required heater power.
- **Pump:** to reduce power consumption and avoid sensor signal oscillations it will be activated only shortly between long inactive phases. However, a complete exchange of the gas volume in the measurement chamber has to be ensured.
- **Filter:** the gas filter has to be active to allow a quantitative measurement of the target pollutants carbon monoxide and methane under real world conditions. The filter has to be deactivated regularly to allow to measure nitrogen dioxide, as it also eliminates this target pollutant next to VOCs.

Examples of system operation modi are detailed in figures 3.25 and 3.26. The timing protocol can be varied from a "standard" measurement cycle of around 5 to 10s time (no temperature modulation) up to an extended cycle of 60 to 120s (with temperature modulation). A stand-by mode to reduce the power consumption especially for applications requiring battery operation is available as well.
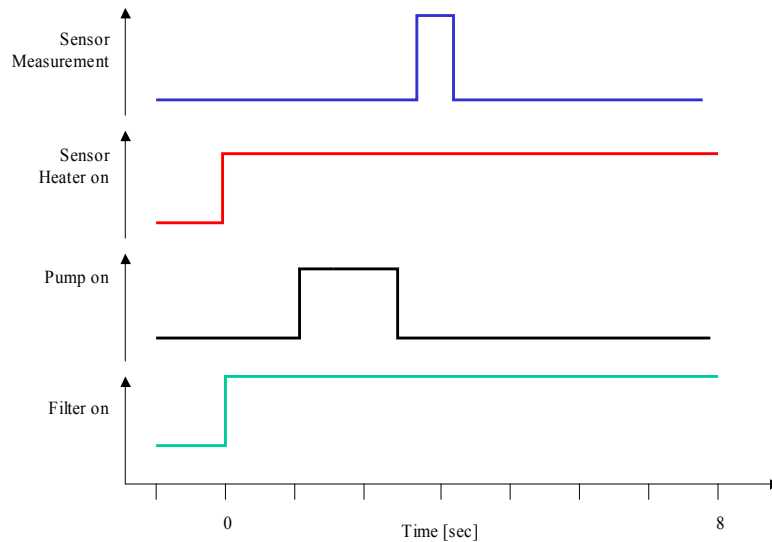
Figure 3.25: System operation mode for indoor applications. The filter is permanently active to eliminate VOCs and nitrogen dioxide. Sensor measurement directly after the active pump phase. No temperature modulation applied.
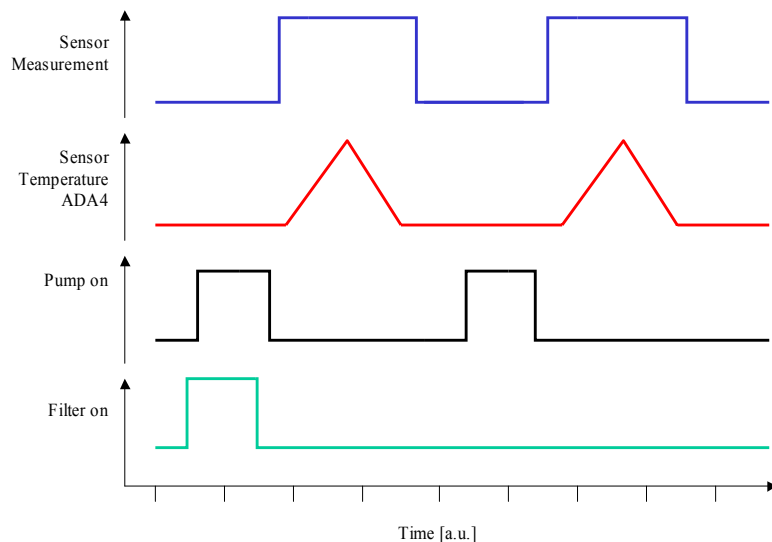
Figure 3.26: System operation mode for outdoor applications. Two measurement cycles are programmed in a loop. First a measurement of carbon monoxide (with filter active) and then of nitrogen dioxide (without filter active). Temperature modulation active to compensate the filter loss with increased input variables. Extended sensor measurement directly after the active pump phase.

3.7 Summary

A smart gas sensor system with high versatility has been developed. The development process started with a concept, a clear definition of the targeted applications and resulting system requirements, and went to a series of prototypes, tests, redesigns and new prototypes. This development feedback loop ended in a final prototype ready to undergo a thorough laboratory assessment of its capabilities and limitations and a final test in a real world application, the field trial. The development process can be divided roughly into three parts.

First is the selection and manufacturing of all hardware components. The heart piece of the sensor system is the ADA sensor chip, developed and manufactured by Hierlemann et al [21].

The sensitive material deposition onto the µ-hotplates was performed by Krauss et al [22]. Next to the sensor chip is the supporting system platform, the sensor system prototype. Over the course of the development process, several system prototypes were designed, tested and redesigned, starting with the ADA toolbox and ending with the final ADA system prototype. This work was performed in close cooperation with A. Krauss and included the selection and evaluation of an appropriate hardware platform, gas flow architecture (pumps, valves, etc.), packaging and electronic board as well as the programming of a sophisticated system controller managing all functions.

The second part, conducted in parallel to the first, is the evaluation and selection of strategies and operation modes to ensure an optimal system performance in the targeted application. Semiconductor sensors are characterised by a problematic selectivity. The problem to be solved was therefore an analytical one: the qualitative and quantitative detection of two target pollutants in a mixture of two or more pollutants. The first strategies tried to improve the sensors selectivity were the selection of optimal sensitive materials and operation temperatures. As the ADA sensor chip allows operating all three µ-hotplates independently, it was possible to design a sensor system able to discriminate between two pollutants. However, the targeted applications, especially outdoors, are in uncontrolled environments where moderate background concentrations and/or short-term heights of unknown other pollutants are likely to be encountered. Therefore, additional strategies were added to ensure a high quality and reliability of the sensor data: a gas filter unit and sensor temperature modulations. The interfering pollutants are of unknown nature and strength. The most commonly encountered are, however, VOCs and inorganic gases such as ozone. A wide range of filter materials were therefore tested towards their ability to eliminate these gases. Among them, active charcoal was best suited to the task, completely eliminating ozone and moderate concentrations of ethanol and heptane, the representative polar and non-polar test VOCs. With the semiconductor sensors temperature dependent sensitivity and selectivity, modulating the sensor operation temperature effectively transforms each of the three µ-hotplates from one sensor to a multitude of "virtual sensors". Together with a sophisticated data evaluation based on pattern recognition techniques even complex gas mixtures can be analysed qualitatively and, to some extent, quantitatively.

The third and final part of the development process was the calibration of the sensor system. Several calibration algorithms have been analysed towards their accuracy and simplicity. A suitable algorithm with high correlation to experimental values and moderate simplicity was selected. To conclude, the necessary steps to produce a working gas sensor system are:

- Manufacturing of the sensor
- Manufacturing of the board
- Implementation of pump, filter and gas flow architecture
- Implementation of a firmware (microcontroller) to manage the sensor, pump, valve and data transmission
- Characterization of the sensor system: exposure to the pollutant gases under laboratory conditions
- Elaboration of individual calibration parameters for each sensor system
- Implementation of this calibration into the firmware for each sensor system
- Validation of the calibration
- Correction of the calibration in a feedback loop

Several sensor systems have been manufactured and calibrated. They were then examined thoroughly in laboratory and real world conditions, as discussed in the following section.

4 Laboratory Validation and Field Trials

4.1 ADA Sensor System

The final ADA sensor system was investigated thoroughly under laboratory and real world conditions. The ADA prototype system was used as sensor platform. For the laboratory validation and outdoor field trials the ADA sensor chip was installed; for the indoor field trials the AS sensors were installed. The final system uses all strategies discussed in *section 3* to ensure an optimal sensor performance under all conditions.

4.1.1 Sensor Operation Temperature

As discussed in *section 3.4.2*, the optimal operation temperatures for all gas-specific μ-hotplates were determined by establishing the sensor signal strength as a function of its operation temperature. The resulting values were

- 350°C for the detection of **methane CH$_4$**
- 275°C for the detection of **carbon monoxide CO**
- 275°C for the detection of **nitrogen dioxide NO$_2$**

Over the course of the laboratory characterisation of the ADA sensor chip, these initial temperatures had to be adjusted:

- 300°C for the detection of **methane**: the temperature control unit of the hotplate was starting to drift after continuous operation over several weeks at this high temperature (350°C). To avoid a continued sensor signal drift the operation temperature was reduced.
- 300°C for the detection of **nitrogen dioxide**: the sensor response time after exposure to the pollutant was too low. A higher operation temperature ensured a faster surface chemistry.

The new temperatures were retained for all consecutive measurements as well as the field trials.

4.2 Laboratory Validation

The final ADA sensor system was thoroughly examined to assess its ability to detect each target pollutant individually and in mixtures. A range of performance characteristics was investigated similar to commercial gas detection devices: calibration quality, Lower Detection Limit, sensitivity and analytical sensitivity, accuracy, long-term stability and humidity influence. All measurements were conducted at fixed temperature and humidity, except where noted otherwise. Each assessment is based on a substantial number of measurements, minimum three, to allow a statistical evaluation and ascertain reproducibility of results.

4.2.1 Carbon Monoxide (CO)

4.2.1.1 Calibration Quality

The measurement range of the carbon monoxide sensor is from 0 to 50ppm. A good calibration matches the experimental values perfectly over the whole concentration range. Ideally, it is a single, monotonous function, allowing to calculate the pollutant concentration directly from the sensor signal. For the ADA sensor chip the signal of interest is the change of conductance ΔG between exposure to clean air (G_0) and mixtures with pollutant (G). As discussed in *section 3.5.5*, the power law function

$$G = G_0 + a * \left(p_{Gas} \right)^b \tag{4.1}$$

proved to be most successful during the calibration investigation. Formula (1) resulted in a good calibration when applied to the sensor data. However, the calibration prediction was deteriorating towards the edges of the concentration range, for high and low values. The reason for this model deterioration is probably the large measurement range of 2 magnitudes (0.5-50ppm). Therefore it was decided to implement a separate calibration function for low (0.5-5ppm) and high (5-50ppm) concentrations. The increased effort in implementing the calibration into the sensor system is justified by the improved calibration quality. To test the calibration a set of measurements were performed under the same conditions as the calibration measurements. The resulting sensor signals were subjected to the calibration function to predict concentrations of carbon monoxide. Figure 4.1 and table 4.1 present the results of the prediction with the section-defined calibration curve for carbon monoxide. As can be seen, the correlation between experimental data and calibration function is very good.
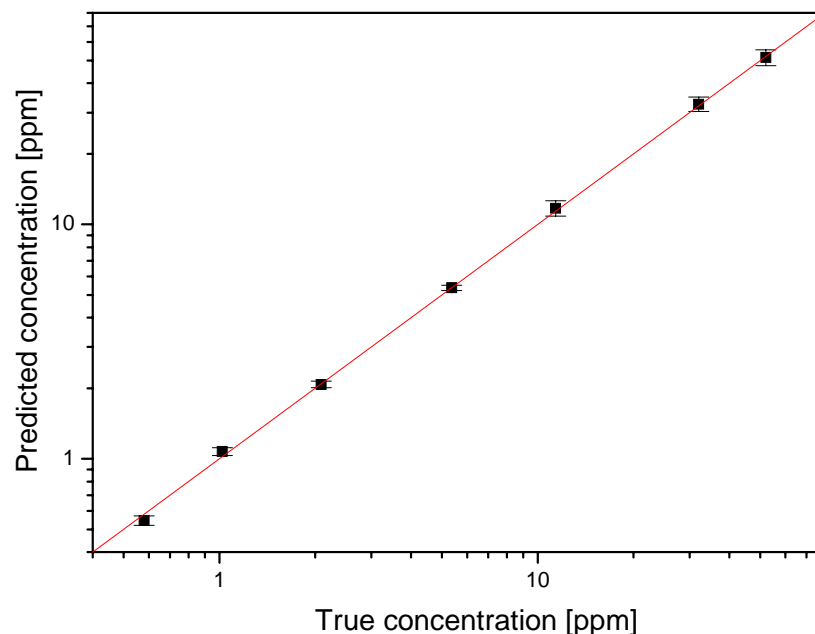

Figure 4.1: Calibration quality: true and predicted concentrations for 0 to 52ppm carbon monoxide. Based on several measurements with CO-sensor at 50% r.h. and RT.

The deviation of the measured signals from the ideal behaviour represented by the above formula leads to an inherent calibration error detailed in table 4.1. The prediction is very good

over the whole concentration range with very low absolute and relative errors. The remaining prediction error introduced here is calibration inherent.

Calibration quality - carbon monoxide				
True [ppm]	Predicted - M1 [ppm]	Predicted - M2 [ppm]	Predicted - M3 [ppm]	Average relative Error [%]
52.1	53.1	54.7	47.1	5.5
32.1	34.8	33.0	30.2	5.7
11.4	12.5	12.0	10.8	6.7
5.37	5.19	5.45	5.44	2.1
2.09	2.00	2.11	2.12	2.2
1.02	1.03	1.08	1.11	5.1
0.58	0.52	0.54	0.57	6.0

Table 4.1:   True and predicted concentrations of carbon monoxide. Calibration tested with several independent measurements.

4.2.1.2 Lower Detection Limit (LDL)

The LDL is the lowest concentration value at which a sensor signal can still be distinguished from the noise. The noise is defined as changes and fluctuations within the resistance of the sensor without changing conditions during a limited time specified for each measurement. It is calculated as detailed in *section 6.1.5*.

Table 4.2 presents the LDL for carbon monoxide. The value for dependent measurements is determined by evaluating several consecutive measurements. The value for independent measurements is determined by evaluating several measurements with a 10-day time difference. During that time the chip has been uninstalled and reinstalled several times and the sensor system switched on and off and been subject to different pollutants. It gives a measure of the LDL under unfavorable conditions and includes the sensor drift over time. Both values are well below those typically encountered in outdoor environmental monitoring (0.3-5ppm) [209] and prove the sensors ability to perform as a carbon monoxide monitor in outdoor and indoor applications.

Lower Detection Limit		
Gas	Dependent measurements	Independent measurements
Carbon monoxide	0.05ppm	0.2ppm

Table 4.2:   Lower Detection Limit of the CO-sensor at 50% r.h. and RT. Results for dependent and independent measurements.

4.2.1.3 Sensitivity and Analytical Sensitivity

The sensitivity *m* is a measure of the sensors ability to detect even smallest concentrations. It is defined as the slope of the calibration curve at the concentration of interest. The sensitivity is a good value to compare similar sensor types. However, it is not dimensionless and as such dependent on the measurement principle. Also, there is a need for including the accuracy in a comparison of sensors. This is provided by the analytical sensitivity *γ*, as defined in *section*

6.1.3. The analytical sensitivity γ is a measure for the sensors ability to discriminate or detect small changes in concentration at the examined concentration.
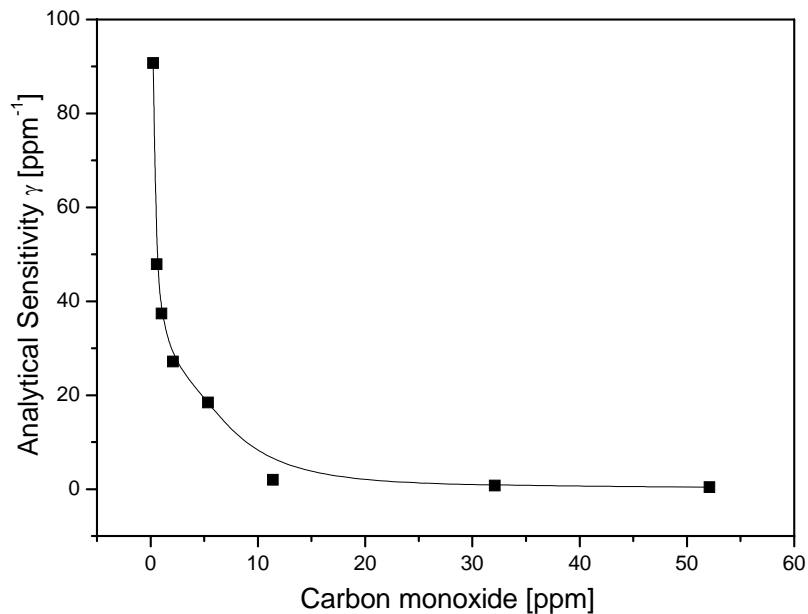
Figure 4.2:   Analytical sensitivity of the CO-sensor for 0 to 50ppm carbon monoxide. Several measurements at 50% r.h. and RT.

As demonstrated in figure 4.2, the sensor exhibits the highest sensitivity at low pollutant concentrations. At higher concentrations the sensitivity reaches saturation. The exponential behaviour is due to the non-linear change in conductance characteristic of semiconductor sensors. The sensor will perform best at the detection of small quantities of carbon monoxide or small changes at low concentrations. At higher concentrations the sensor accuracy will decrease fast.

4.2.1.4 Accuracy

The sensor accuracy is a measure of how closely the result of an experiment approximates the true value; it is a measure of the concentration uncertainty during a measurement. A sensor signal never corresponds to an exact concentration but a concentration span. It is defined as the standard deviation of the concentration at a certain concentration. As defined in *section 6.1.3*, it is the reciprocal of the analytical sensitivity. A good calibration and a stable sensor system will provide a low accuracy value and allow to measure concentrations with a narrow uncertainty span.

In accordance with International Standards [163][169] an accuracy of 10% of the measured concentration was set as target for the developed sensor system. As detailed in table 4.3, the sensor system stays well below the target margin for all measured concentrations. The relative accuracy is best for 0.5 to 5ppm carbon monoxide, worsening slightly for higher and very low concentrations. These accuracy values are very good for semiconductor sensors and indicate a high signal reproducibility and stability of the sensor system.

Sensor accuracy - carbon monoxide			
Concentr. [ppm]	Criterion [ppm]	Accuracy [ppm]	Accuracy [%]
52	5.0	2.3	4.3
32	3.2	1.3	4.1
11	1.1	0.51	4.5
5.4	0.54	0.054	1.0
2.1	2.1	0.037	1.8
1.0	1.0	0.027	2.6
0.58	0.058	0.021	3.6
0.23	0.023	0.011	4.8

Table 4.3:   Sensor accuracy for 0.2 to 52ppm carbon monoxide. Several measurements with CO-sensor at 50% r.h. and RT.

4.2.1.5 Stability

A common problem of semiconductor sensors is their drift. This effect slowly changes the sensor signal. Due to ageing of the sensitive layer its chemical properties change and therefore also the parameters of reactions at its surface. This effect decreases the quality of calibration with time and makes regular recalibration necessary. A long operation time before recalibration reduces the maintenance efforts and proves high reliability of the system. Ideally, a sensor system needs recalibration only after several months.

To evaluate the stability of the developed sensor system, a calibration curve has been established and tested with a set of measurements. These measurements were repeated under the same conditions after 10 days and after 6 weeks. During this time the system was reassembled several times and used to measure different pollutants. The sensor signals were subjected to the same calibration algorithm and the true and predicted concentrations compared. As demonstrated in figure 4.3 and table 4.4, the sensor signal remains relatively stable and reproducible for a period of at least 10 days. The prediction error is still very low, except for 0.23ppm carbon monoxide. After 6 weeks, a serious drift occurs. The change in sensor resistance is very strong, rendering the initial calibration completely ineffective. The sensor stability and signal drift is discussed in detail in *section 4.2.4*.
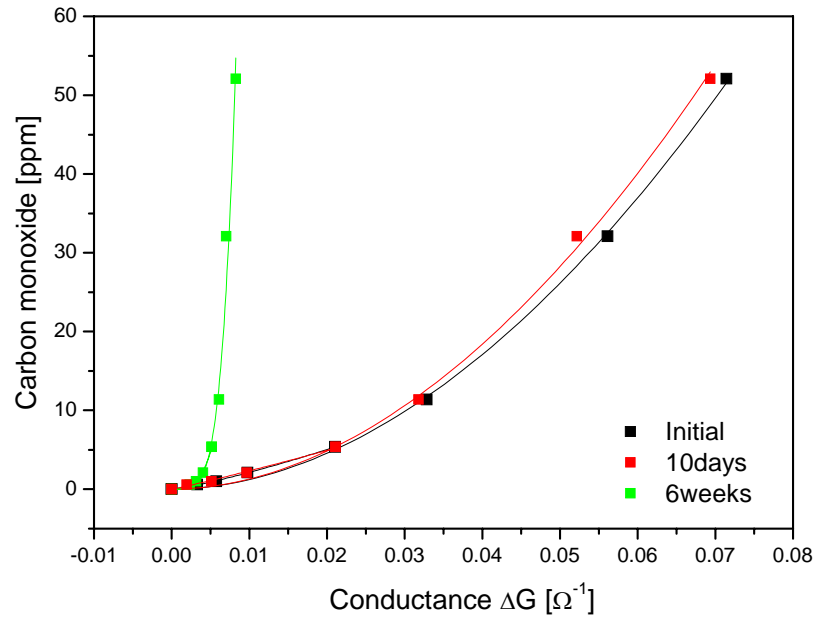
Figure 4.3:   Three different concentration predictions for carbon monoxide with the same original calibration. Measurements at RT and 50% r.h..

Sensor system stability - carbon monoxide				
True [ppm]	10 days - prediction [ppm]	Average relative Error [%]	6 weeks - prediction [ppm]	Average relative Error [%]
52.1	59.2	13	1.69	97.
32.1	34.5	7.3	1.38	96
11.4	12.6	10.3	1.15	90
5.37	5.65	5.1	0.94	82
2.09	2.06	1.4	0.70	67
1.02	0.93	9.1	0.51	50
0.58	0.27	54	0.35	39

Table 4.4:   Long-term stability of carbon monoxide prediction. Predicted concentrations with initial calibration after 10 days and after 6 weeks.

4.2.1.6   Humidity Influence

Semiconductor sensors are influenced in their signal to pollutants by the ambient humidity. Changes in relative humidity will decrease or increase the sensor signal, thereby producing wrong concentration readouts and false negative or false positive alarms. To compensate for the humidity influence, the ADA sensor system has a humidity sensor located directly next to the sensor chip. As demonstrated in figure 4.4, calibration curves can be established for every level of ambient humidity. This allows selecting the appropriate calibration for every level of humidity during data evaluation. Errors induced by changes in ambient humidity can thereby be avoided.
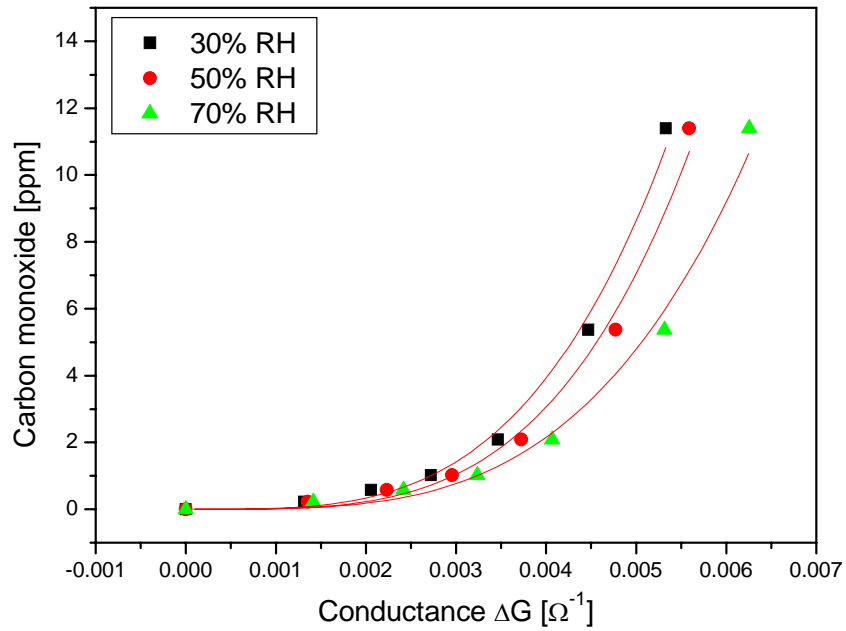
Figure 4.4: Calibration curves for 0.2 – 12ppm carbon monoxide for 30, 50 and 70% r.h.. Each curve based on 9 measurements at RT.

4.2.2 Methane (CH$_4$)

4.2.2.1 Calibration Curve

The main application of the methane sensor is as an alarm for the explosive concentration threshold (LEL 5-15% [210]). To be able to detect gas leaks at an early stage and to monitor the evolution of the explosive gas concentration, a calibration was also established for lower concentrations. As for carbon monoxide, a power law function (1) proved to be the most successful algorithm. A monotonous calibration curve with good correlation to the experimental data was established. To test the calibration, a set of measurements were performed under the same conditions as the calibration measurements and subjected to the calibration function. Figure 4.5 and table 4.5 present the results of the prediction.
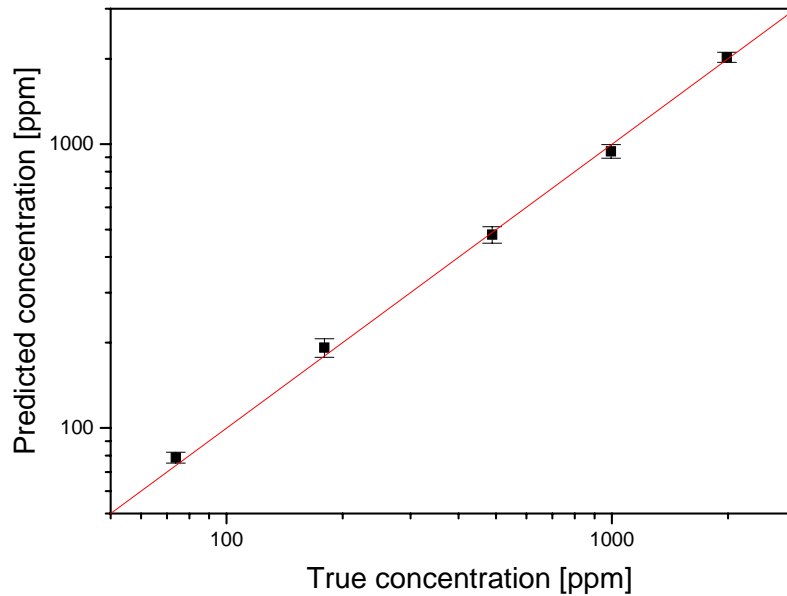
Figure 4.5: Calibration quality: true and predicted concentrations for 0 to 2000ppm methane. Based on several measurements with CH₄-sensor at 50% r.h. and RT.

The prediction error is very good over the whole concentration range with low absolute and relative errors. Unlike for carbon monoxide, there is no model deterioration towards high or low concentrations. The remaining prediction error introduced here is calibration inherent.

Calibration quality - methane				
True [ppm]	Predicted - M1 [ppm]	Predicted - M2 [ppm]	Predicted - M3 [ppm]	Average relative Error [%]
1987	2100	2033	1938	3.5
993	1004	915	913	5.7
488	509	485	446	4.5
179	209	184	183	7.0
73.8	82.1	78.9	75.1	6.7

Table 4.5: True and predicted concentrations of carbon monoxide. Calibration tested with several measurements.

4.2.2.2 Lower Detection Limit

Table 4.6 presents the LDL for methane. The values for dependent measurements and independent measurements are determined as discussed for carbon monoxide. The value for independent measurements gives a measure of the LDL under unfavorable conditions and includes the sensor drift over time. The very low value for dependent measurements proves the high reproducibility of the sensor signal under identical conditions. The much higher value for independent measurements illustrates the effect of varying ambient conditions on the sensor performance. However, both values are well below the measurement range and confirm the sensors systems ability to perform as a gas leakage early warning device.

Lower Detection Limit		
Gas	**Dependent measurements**	**Independent measurements**
Methane	0.01ppm	21.7ppm

Table 4.6:   Lower Detection Limit of the CH₄-sensor at 50% r.h. and RT. Results for dependent and independent measurements.

4.2.2.3 Sensitivity and Analytical Sensitivity

As discussed for carbon monoxide and defined in *section 6.1.3*, the sensitivity and analytical sensitivity are good values to compare the quality of different sensors and sensor types. The analytical sensitivity in particular is a measure for the sensors ability to discriminate or detect small changes in concentration at the examined concentration, and will be examined in more detail here.
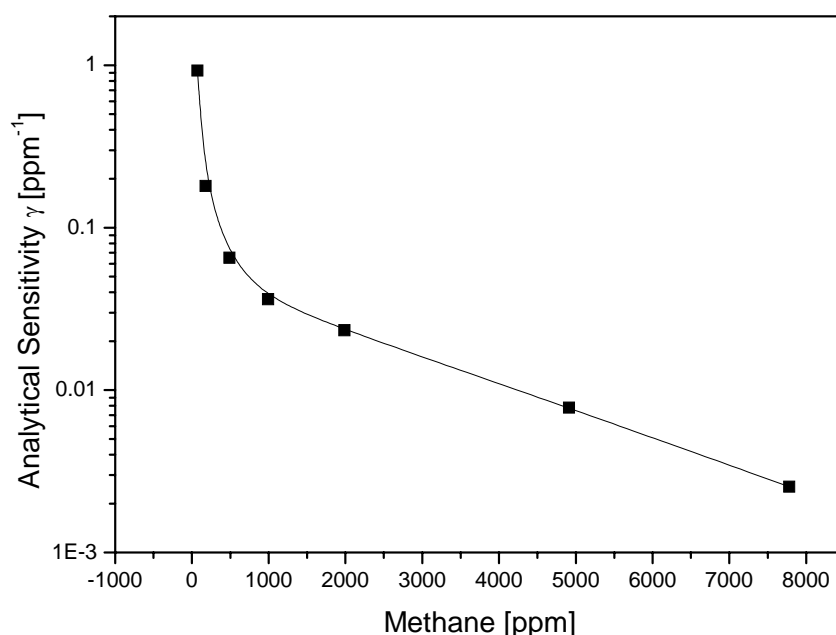
Figure 4.6:   Analytical sensitivity of the CH₄-sensor for 0 to 2000ppm methane. Several measurements at 50% r.h. and RT.

As demonstrated in figure 4.6, the sensor exhibits the highest sensitivity at low pollutant concentrations. At higher concentrations the sensitivity decreases continuously. The sensor will perform best at the detection of small quantities of methane or small changes at low concentrations. At higher concentrations the sensor accuracy will decrease continuously.

4.2.2.4 Accuracy

The accuracy is a measure of the concentration uncertainty during a measurement. It is calculated as discussed for carbon monoxide and defined in *section 6.1.3*. In accordance with International Standards [163][169] an accuracy of 10% of the measured concentration was set as target for the developed sensor system. As detailed in table 4.7, the sensor system stays well below the target margin for all measured concentrations. The relative accuracy is best for low concentrations, worsening for higher values. These accuracy values are very good for semiconductor sensors and indicate a high signal reproducibility and stability of the sensor system.

Sensor accuracy - methane			
Concentr. [ppm]	Criterion - 10%	Accuracy [ppm]	Accuracy [%]
7800	780	393	5.1
4900	490	128	2.6
2000	200	43	2.2
1000	100	28	2.8
490	49	15	3.1
180	18	5.5	3.1
74	7.4	1	1.5

Table 4.7:   Sensor accuracy for 74 to 7800ppm methane. Several measurements with CH4-sensor at 50% r.h. and RT.

4.2.2.5   Stability

To evaluate the stability of the developed sensor system, a calibration curve has been established and tested with a set of measurements. These measurements were repeated under the same conditions after 10 days and after 6 weeks. During this time the system was reassembled several times and used to measure different pollutants. The sensor signals were subjected to the same calibration algorithm and the true and predicted concentrations compared.
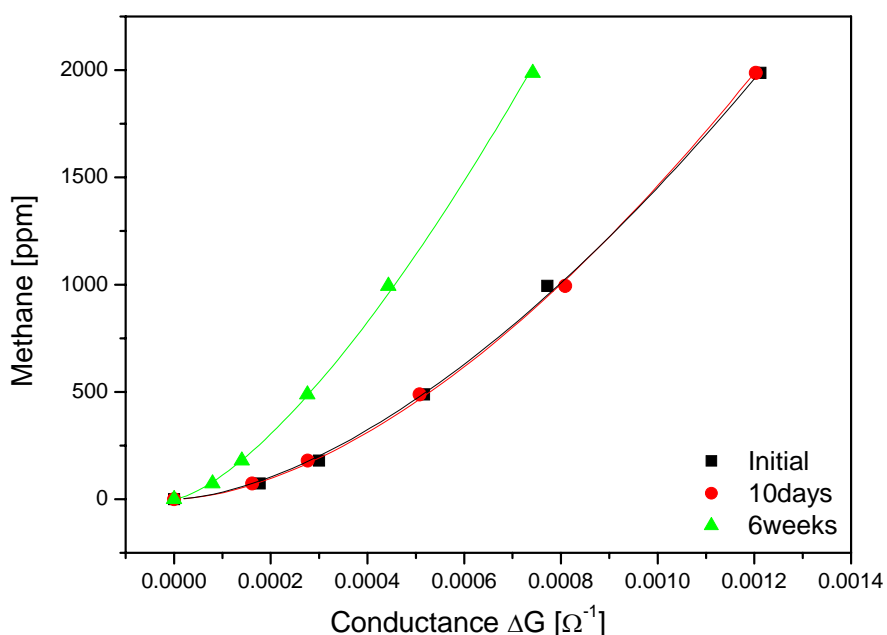
Figure 4.7:   Three different concentration predictions for methane with the same original calibration. Measurements at RT and 50% r.h..

As demonstrated in figure 4.7 and table 4.78, the sensor signal remains stable and reproducible for a period of at least 10 days. After 6 weeks, a signal deviation is detected. During all that time the sensor has been in use continuously. As mentioned in *section 4.1.1*, the operation temperature of the CH4 µ-hotplate had to be reduced from 350 to 300°C. This change in sensor operation temperature is the reason for the inaccurate concentration prediction after 6 weeks with the original calibration. Leaving this external influence on the sensor signal aside, the very good 10-day-prediction can be recognised as the normal sensor

stability. The issue of the sensors long-term stability and signal drift is discussed in further detail in *section 4.2.4*.

	Long-term stability - methane			
True [ppm]	**10 days - prediction [ppm]**	**Average relative Error [%]**	**6 weeks - prediction [ppm]**	**Average relative Error [%]**
1987	2141	7.8	883	56
993.6	1005	1.2	370	63
488.4	479	1.8	166	66
179.2	175	2.4	53.4	70
73.8	72.4	1.9	20.6	72

Table 4.7:   Long-term stability of methane prediction. Predicted concentrations with initial calibration after 10 days and after 6 weeks.

4.2.2.6   Humidity Influence

Humidity-dependent calibration curves allow compensating the sensors cross-sensitivity to changes in ambient humidity. The same procedure as detailed for carbon monoxide can be applied to the detection of methane to avoid humidity interference.

4.2.3   Nitrogen Dioxide (NO$_2$)

4.2.3.1   Calibration Quality

The main application of the nitrogen dioxide sensor is the outdoor monitoring where typical concentrations between 20 and 100ppb [209] of nitrogen dioxide are encountered. Therefore a concentration range of 10 to 2000ppb nitrogen dioxide was selected for the calibration function. As nitrogen dioxide is an oxidising gas (carbon monoxide and methane are reducing gases) the calibration algorithm was based on the sensor resistance instead of the conductance. The power law function resulting in the best match with the experimental data was

$$R = R_0 + a * \left(p_{Gas}\right)^b \qquad (4.2)$$

To test the calibration a set of measurements were performed under the same conditions as the calibration measurements and subjected to the calibration function. As detailed in figure 4.8 and table 4.8 the calibration offers a good concentration prediction over the whole concentration range of more than 2 magnitudes.
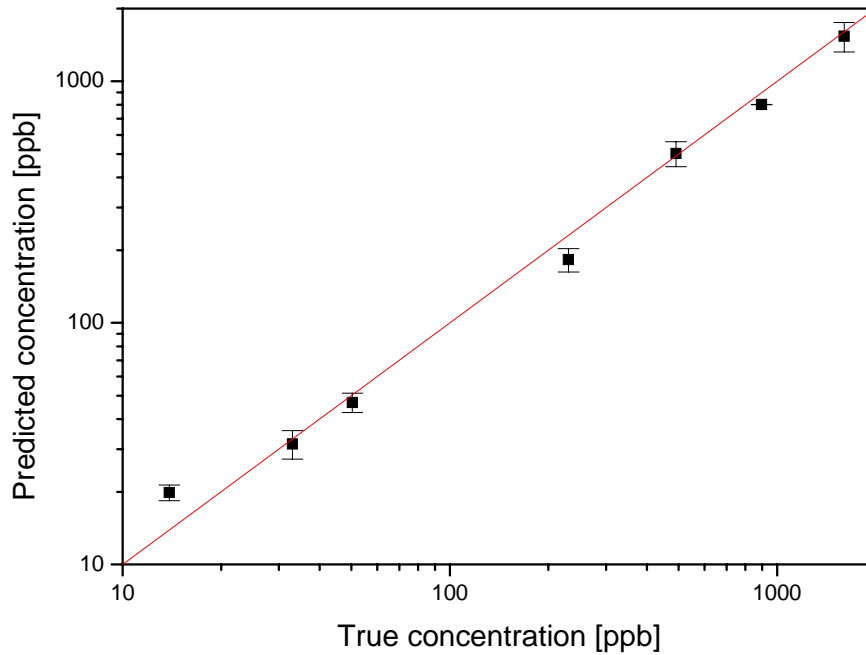
Figure 4.8: Calibration quality: true and predicted concentrations for 0 to 1.6ppm nitrogen dioxide. Based on several measurements with NO₂-sensor at 50% r.h. and RT.

The prediction error is equally good over the whole concentration range with sometimes strong variations in quality between the different measurements. The remaining prediction error introduced here is calibration inherent.

Calibration quality - nitrogen dioxide			
True [ppb]	**Predicted - M1 [ppb]**	**Predicted - M2 [ppb]**	**Average relative Error [%]**
1605	1384	1688	9.5
896.1	801.7	800.1	10.6
491.4	460.9	544.3	8.5
230.6	168.6	196.9	20.8
50.4	43.8	49.9	7.2
33.0	28.5	34.5	9.0
13.9	18.8	20.9	43.0

Table 4.8: True and predicted concentrations of nitrogen dioxide. Calibration tested with several measurements.

4.2.3.2 Lower Detection Limit

Table 4.9 presents the LDL for nitrogen dioxide. The values for dependent measurements and independent measurements are determined as discussed for carbon monoxide. The value for independent measurements is determined here by evaluating measurements with a 3-day time difference. It gives a measure of the LDL under unfavorable conditions and includes the sensor drift over time. The low value for dependent measurements proves the high reproducibility of the sensor signal under identical conditions. The higher value for

independent measurements illustrates the effect of varying ambient conditions on the sensor performance. However, both values are below the measurement range and confirm the sensors systems ability to perform as an outdoor pollutant monitoring device.

Lower Detection Limit		
Gas	Dependent measurements	Independent measurements
Nitrogen dioxide	0.31ppb	7.6ppb

Table 4.9:   Lower Detection Limit of the NO$_2$-sensor at 50% r.h. and RT. Results for dependent and independent measurements.

4.2.3.3   Analytical Sensitivity

As discussed for carbon monoxide and defined in *section 6.1.3*, the sensitivity and analytical sensitivity are good values to compare the quality of different sensors and sensor types. The analytical sensitivity in particular is a measure for the sensors ability to discriminate or detect small changes in concentration at the examined concentration, and will be examined in more detail here.
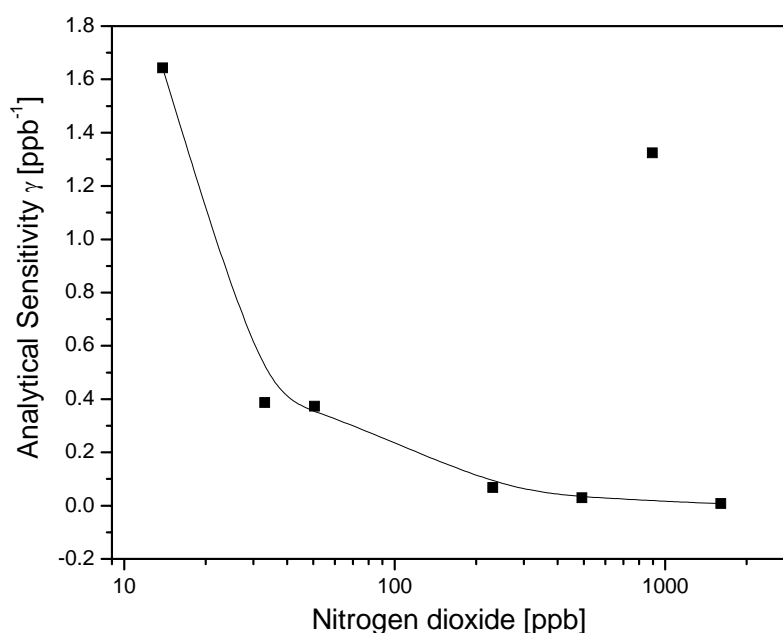
Figure 4.9:   Analytical sensitivity of the NO$_2$-sensor for 0 to 2ppm nitrogen dioxide. Several measurements at 50% r.h. and RT.

As demonstrated in figure 4.9, the sensor exhibits the highest sensitivity at low pollutant concentrations. At higher concentrations the sensitivity decreases continuously. The sensor will perform best at the detection of small quantities of nitrogen dioxide or small changes at low concentrations. At higher concentrations the sensor accuracy will decrease continuously. The high analytical sensitivity at 900ppb NO$_2$ can be considered as a measurement error.

4.2.3.4 Accuracy

The accuracy is a measure of the concentration uncertainty during a measurement. It is calculated as discussed for carbon monoxide and defined in *section 6.1.3*. In accordance with International Standards [163][169] an accuracy of 10% of the measured concentration was set as target for the developed sensor system. As detailed in table 4.10, the sensor system stays below the target margin for all measured concentrations. The relative accuracy is of similar quality for all concentrations. These accuracy values are good for semiconductor sensors and indicate a good signal reproducibility and stability of the sensor system.

Sensor accuracy - nitrogen dioxide			
Concentr. [ppb]	**Criterion - 10%**	**Accuracy [ppb]**	**Accuracy [%]**
13.9	1.39	0.61	4.4
33.0	3.30	2.58	7.8
50.4	5.04	2.68	5.3
231	23.1	14.8	6.4
491	49.1	33.7	6.9
896	89.6	0.76	0.1
1605	160.5	131.4	8.2

Table 4.10: Sensor accuracy for 14 to 1600ppb nitrogen dioxide. Several measurements with NO_2-sensor at 50% r.h. and RT.

4.2.3.5 Humidity Influence

Humidity-dependent calibration curves allow compensating the sensors cross-sensitivity to changes in ambient humidity. The same procedure as detailed for carbon monoxide can be applied to the detection of nitrogen dioxide to avoid humidity interference.

4.2.4 Sensor Stability

It has been discussed earlier (*see sections 4.2.1.5 and 4.2.2.5*) that a sensor signal drift occurs after 6 weeks of operation. To analyse this phenomenon the sensor baselines have been recorded during all measurements performed as presented in figure 4.10. The signal evolution over time shows a different behaviour for the three µ-hotplates.

The methane sensor is staying relatively stable over time. The variations are due to a systematic temperature error and variations of ambient conditions. The temperature error has already been mentioned in *section 4.1.1*. During the first weeks of measurements the sensor operation temperature continuously decreased due to a deterioration of the poly-Si heater. Finally, the temperature could be stabilised at 300°C. The difference to the original operation temperature (350°C) is responsible for the errors in the concentration prediction after 6 weeks. Variations of ambient conditions such as changing humidity and different measurement stations employed account for the singular small variations.
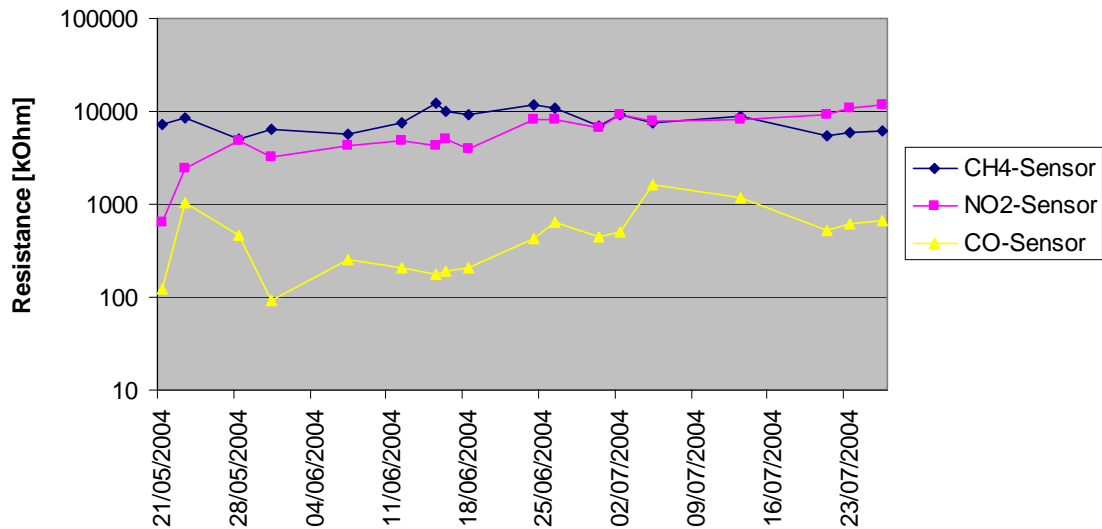
Figure 4.10: Baseline evolution of all 3 ADA sensor chip μ-hotplates during the laboratory examinations. Ambient conditions such as humidity and gas mixing station have been changed repeatedly. Recorded measurement period of two months.

The NO2-sensor is stabilising during the first week of operation. Afterwards, it exhibits a small drift over time, suggesting a stability of four weeks. Longer measurements are required to determine whether this drift is continuous or is only an extended stabilisation time of several weeks.

The CO-sensor is showing a very erratic behaviour. Apart from a short period of stability, huge signal leaps appear without clear connection to changes in laboratory conditions. The source of this serious instability is most probably the contact electrodes-sensitive layer, i.e. the layer is slowly peeling off. A deterioration of the sensitive layer itself is unlikely as the ratio signal to baseline stays stable and good calibration curves can be established during all stages. An examination of the layer by optical microscope shows no apparent defect, as demonstrated in figure 4.11.
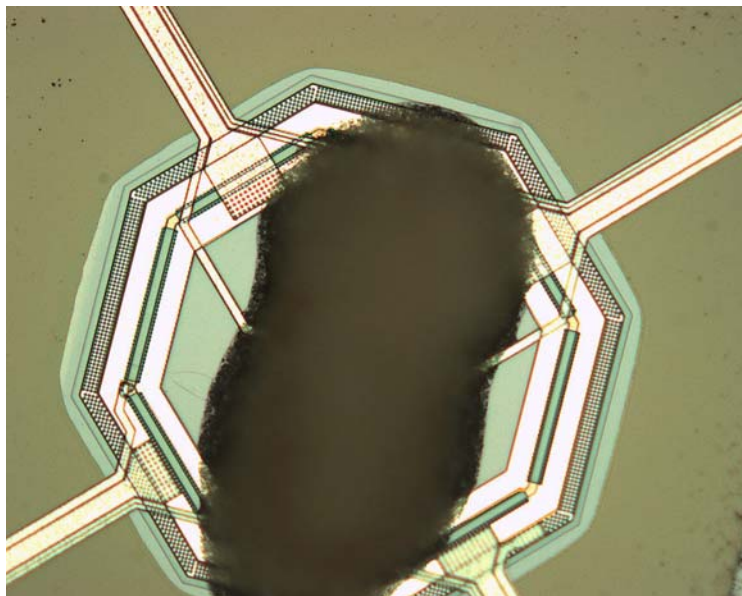
Figure 4.11: CO-sensitive μ-hotplate. 428 x 342 μm.

Previous work with this material (same sensitive material as used in the AS sensor) has shown no such problems. However, that sensor system was based on a classical transducer and not the ADA sensor chip. Therefore, the error has to lie in the sensor fabrication. The deposition and adhesion of the sensitive layer are some of the new manufacturing problems introduced with the sensor microchip. In the past, a peeling of the carbon monoxide-sensitive layer has caused several sensor chips to fail the final production tests. This adhesion problem could not be detected optically, similar to the present problem. This leads to the conclusion that the discussed resistance change is due to a slow peeling of the sensitive layer, increasing with time during the laboratory measurements.

4.2.5 Binary Mixtures

Apart from the detection of single gases the ADA sensor chip has to be able to qualitatively and quantitatively detect the target gases in binary mixtures. As demonstrated in figures 4.12 and 4.13, the three µ-sensors have a different sensitivity and selectivity to the gases of interest. The CH_4-µ-sensor is sensitive to all gases of interest, the CO-µ-sensor is sensitive to carbon monoxide and nitrogen dioxide and the NO_2-µ-sensor is sensitive to only nitrogen dioxide. With the use of appropriate data evaluation techniques the binary mixtures carbon monoxide and nitrogen dioxide as well as carbon monoxide and methane can be analysed qualitatively and quantitatively [211]. The sensors good selectivity even suggests the possibility of analysing ternary mixtures.

Figure 4.12: Sensor signals to 0.2-50ppm carbon monoxide and 100-8000ppm methane at RT and 50% r.h..

Figure 4.13: Sensor signals to 11-2000ppb nitrogen dioxide at RT and 50% r.h..

4.2.6 Carbon Monoxide and Methane
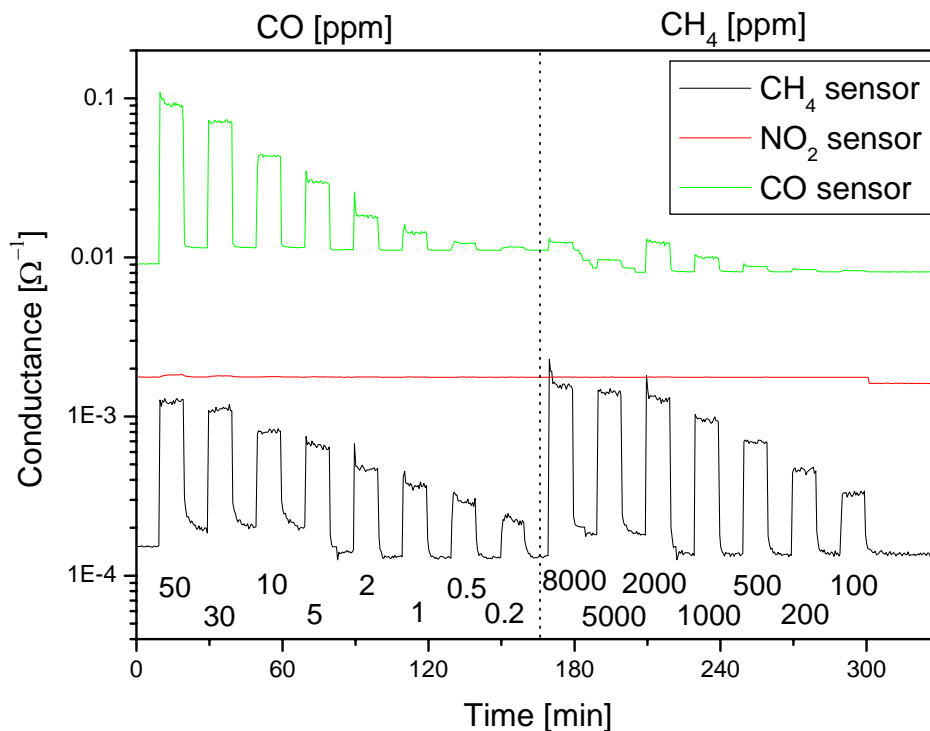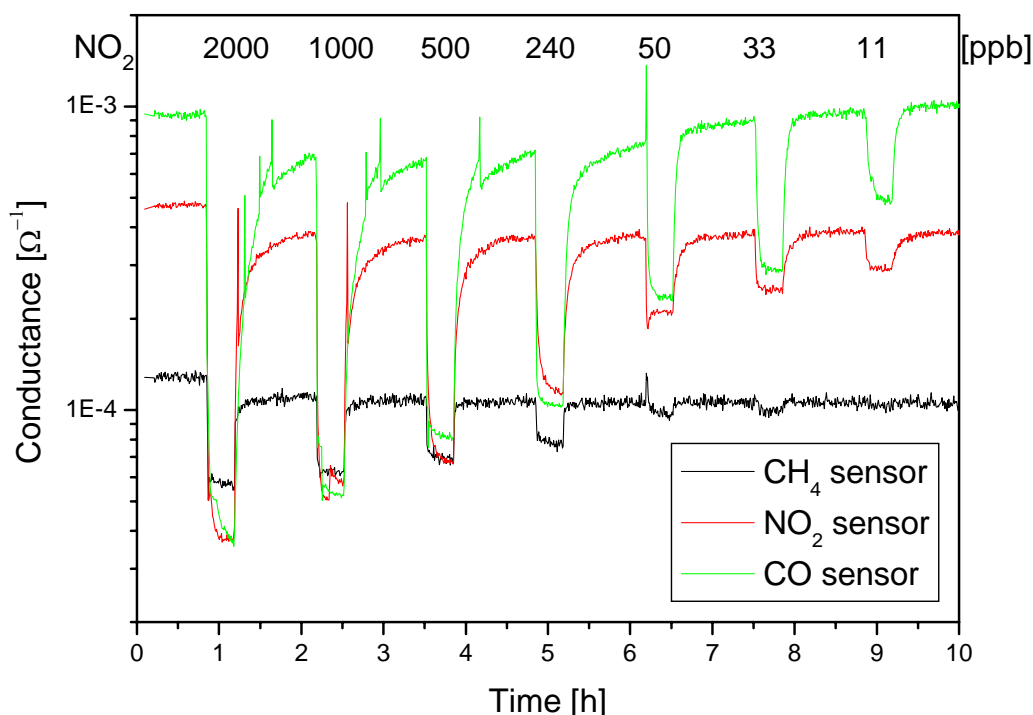
Single gas measurements of 0.5-50ppm carbon monoxide and 100-2000ppm methane and binary mixtures of both were submitted to pattern recognition methods (PCR, Unscrambler 7.6) to establish a valid calibration. An independent data set based upon measurements of binary mixtures (0.5-50ppm carbon monoxide with a background of 1000ppm methane and 100-2000ppm methane with a background of 5ppm carbon monoxide) were used for prediction. The results of the prediction are presented in the figures 4.14 and 4.15 as well as the tables 4.11 and 4.12.

The prediction quality for carbon monoxide is satisfactory for high concentrations, but decreases strongly towards lower concentrations. For methane the concentration predictions are problematic over the whole concentration range. In both situations a systematic prediction error is apparent, causing a shift of the slope to values < 1. However, the standard deviation σ (M1 – M2) of the sensors signals between the different prediction data sets is quite low, indicating a change in sensor behaviour between measurement of the calibration and of the prediction data sets. The source of the systematic prediction error is therefore most probably the same as discussed in *section 4.2.4* on sensor stability problems: layer peeling of the CO-sensor and heater drift of the CH_4-sensor. For carbon monoxide this reason suffices to explain the difficult prediction results in binary mixtures. Methane however, shows a decidedly worse performance in mixtures than carbon monoxide while having less baseline fluctuations over the measurement time (see figure 4.10). Even though the effect of temperature drift on the signal to methane could be stronger than on the sensor baseline discussed in figure 4.10, another factor has to be considered. As presented in figure 4.12 the CH_4-sensor exhibits a strong cross-sensitivity to carbon monoxide. This lack of selectivity may be too profound to be countered by the selected pattern recognition method employed (PCR).

89
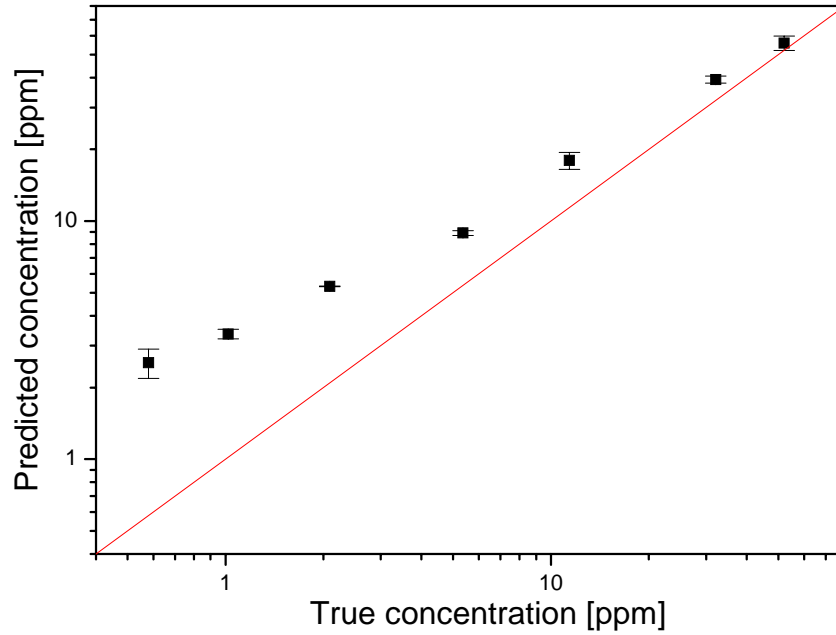
Figure 4.14: Prediction of carbon monoxide concentrations in binary mixtures with methane. Sensor exposure to 0.5-50ppm carbon monoxide with a background of 1000ppm methane. Two data sets with binary mixtures were used for prediction and five independent data sets with single gases were used to establish the calibration model. Measurements at RT and 30% r.h..

Carbon monoxide prediction in binary mixtures				
True [ppm]	Predicted - M1 [ppm]	Predicted - M2 [ppm]	σ (M1 - M2) [ppm]	Average relative Error [%]
0.58	2.79	2.29	0.35	338
1.02	3.24	3.46	0.16	228
2.09	5.33	5.31	0.01	155
5.37	9.06	8.77	0.21	66
11.4	19	16.9	1.48	57
32.1	40.2	38.3	1.3435	22
52.1	58.7	53.1	3.9598	7.3

Table 4.11: Prediction of carbon monoxide concentrations in binary mixtures with a background of 1000ppm methane.
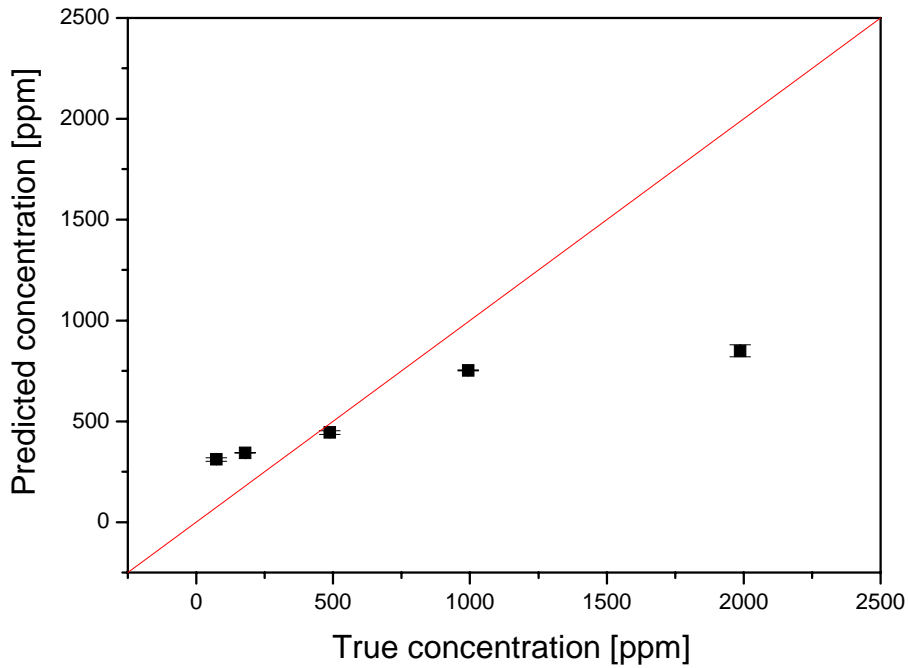
Figure 4.15: Prediction of methane concentrations in binary mixtures with carbon monoxide. Sensor exposure to 100-2000ppm methane with a background of 5ppm carbon monoxide. Two data sets with binary mixtures were used for prediction and five independent data sets with single gases were used to establish the calibration model. Measurements at RT and 30% r.h..

Methane prediction in binary mixtures				
True [ppm]	Predicted - M1 [ppm]	Predicted - M2 [ppm]	σ (M1 - M2) [ppm]	Average relative Error [%]
73.8	317	304	9.19	321
179	344	343	0.71	91
488	450	438	8.49	9.0
993	754	751	2.12	24
1987	828	870	29.7	57

Table 4.12: Prediction of methane concentrations in binary mixtures with a background of 5ppm carbon monoxide.

4.2.7 Carbon Monoxide and Nitrogen Dioxide

As demonstrated in figure 4.16 carbon monoxide can be detected in the presence of nitrogen dioxide without any change to the signal. The active charcoal gas filter completely adsorbs all nitrogen dioxide, allowing an accurate quantitative detection of carbon monoxide.
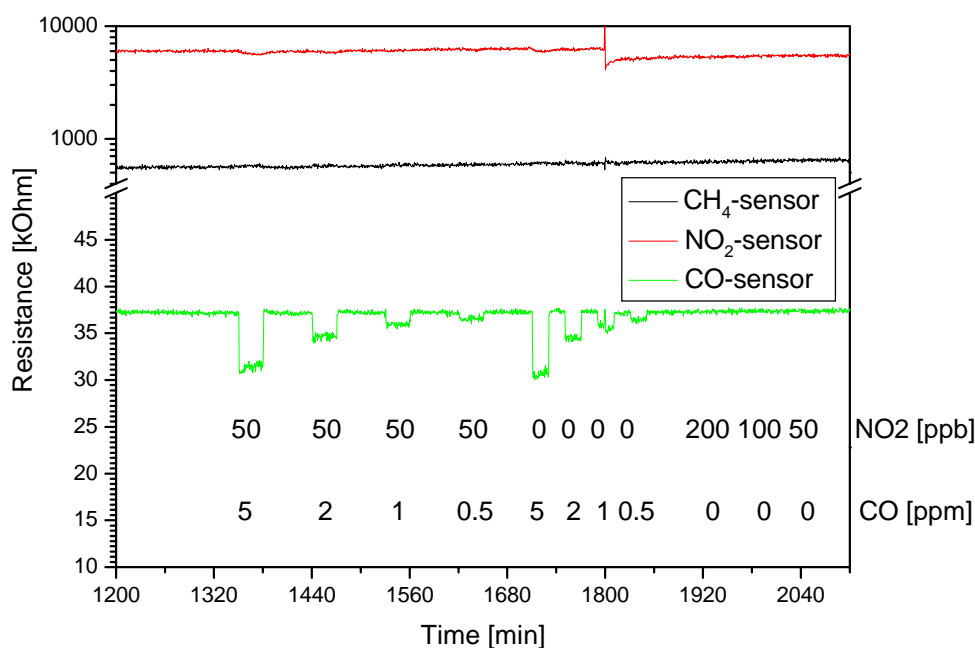
Figure 4.16: Binary mixture of carbon monoxide and nitrogen dioxide. Gas filter active.

The quantitative prediction of nitrogen dioxide in the presence of carbon monoxide is less good. The sensor system was exposed to 50-1000ppb nitrogen dioxide and a calibration established. Then the measurement was repeated with a constant background of 0.5ppm carbon monoxide. The sensor signals were evaluated with the previously established calibration based on single gas measurements. Although figure 4.12 suggests no direct interaction between carbon monoxide and the NO_2 μ-sensor, the prediction deteriorates, with a high relative error for medium concentrations. The observed error could be due to a sensitive layer peeling as experienced for the CO-sensitive μ-sensor.

Nitrogen dioxide: true and predicted concentrations		
True [ppb]	Predicted [ppb]	Relative error [%]
1000	895.65	10.44
500	300.15	39.97
200	116.04	41.98
100	73.44	26.56
50	44.18	11.65

Table 4.13: True and predicted concentrations of nitrogen dioxide upon exposure to 50-100ppb with a background of 0.5ppm carbon monoxide. Measurements at RT and fixed level of humidity. Calibration based on independent single gas measurements.

4.2.8 Volatile Organic Compounds (VOCs)

Preliminary investigations of the CO-sensors cross-sensitivity to ethanol and heptane were very encouraging. This led to an adaptation of the tests to lower concentrations of carbon monoxide. The results are demonstrated in figure 4.17 and table 4.14. To facilitate the comparison between the sensors response to the target pollutants and VOCs, the signals are

normalised: the sensor signals corresponding to 5ppm carbon monoxide and 1000ppm methane are the normalisation basis. The CO-sensor signal to 100ppm ethanol and 100ppm heptane is normalised to its signal to 5ppm carbon monoxide. The CH_4-sensor signal to 100ppm ethanol and 100ppm heptane is normalised to its signal to 1000ppm methane.
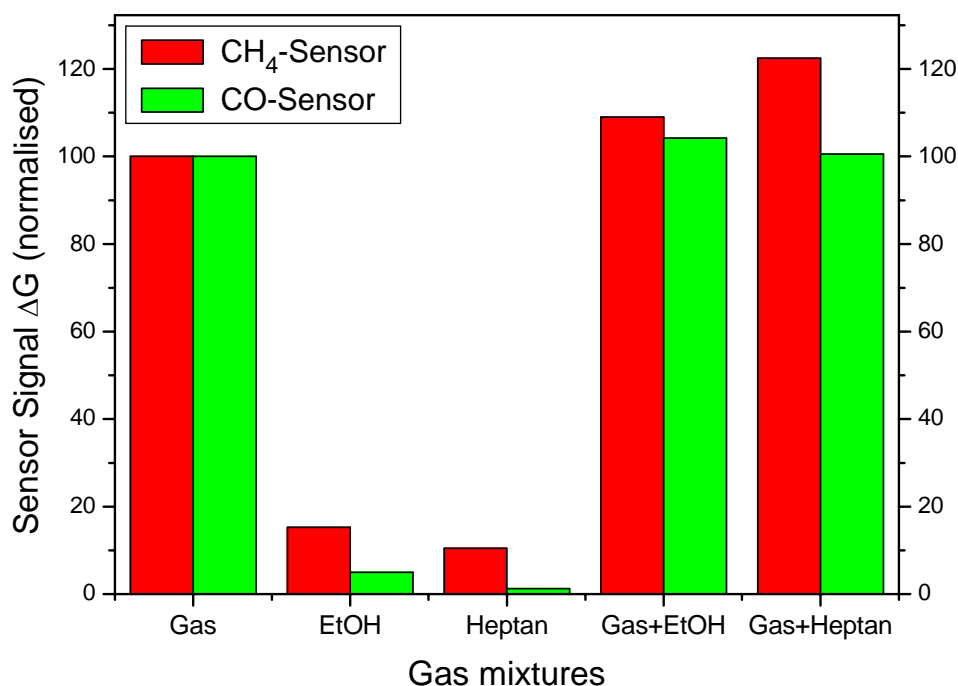
Figure 4.17: Signals normalised to target pollutant. Green - signal of CO-sensor to 5ppm carbon monoxide, 100ppm ethanol, 100ppm heptane and mixtures of 5ppm carbon monoxide and 100ppm VOC. Red - signal of CH4-sensor to 1000ppm methane, 100ppm ethanol, 100ppm heptane and mixtures of 1000ppm methane and 100ppm VOC. Measurements at RT and 50% r.h.. Filter active charcoal.

Sensor signal to CO, CH$_4$ and VOCs		
Gas	**CH$_4$-sensor signal [%]**	**CO-sensor signal [%]**
5ppm CO	**X**	100
1000ppm CH$_4$	100	**X**
100ppm Ethanol	15.3	4.93
100ppm Heptane	10.4	1.21
CH$_4$ + Ethanol	109.0	**X**
CH$_4$ + Heptane	122.5	**X**
CO+Ethanol	**X**	104.2
CO+Heptane	**X**	100.6

Table 4.14: CO-sensor signals to carbon monoxide, ethanol, heptane and mixtures of 5ppm pollutant and 100ppm interferent. CH$_4$-sensor signals to methane, ethanol, heptane and mixtures of 1000ppm pollutant and 100ppm interferent. Filter active charcoal.

The CO-sensor has a very low cross-sensitivity to ethanol and heptane. Even at 5ppm carbon monoxide, the signal ratio to the VOCs is higher than 10. In mixtures, a background

concentration of 100ppm ethanol results in an error of 4.2%, a background concentration of 100ppm heptane is not noticed by the sensor.

The CH_4 sensor has a higher cross-sensitivity. The signal to 100ppm heptane is around the target value of 10%, the signal to ethanol exceeds it. In mixtures, the results are reversed. A background concentration of 100ppm ethanol leads to an error < 10%. A background concentration of 100ppm heptane exceeds the target value.

Figure 4.18 and table 4.15 demonstrates the sensor systems ability to quantitatively detect nitrogen dioxide in the presence of interfering pollutants such as ethanol and heptane. As the gases of interest have a diametrically opposed effect on the sensor signal, unprocessed measurement data are presented to illustrate their effect. In this case the gas filter is inactive as it would also eliminate nitrogen dioxide. The NO_2-sensitive μ-sensor reacts strongly to ethanol, completely eliminating any signal to nitrogen dioxide in mixtures. For heptane the situation is better: even high concentrations of up to 100ppm result in only a small signal and mixtures with nitrogen dioxide are affected only weakly.

Figure 4.18: Resistance values of the NO_2-sensitive μ-hotplate during exposure to nitrogen dioxide, ethanol, heptane and a mixture of gases. No Filter active.

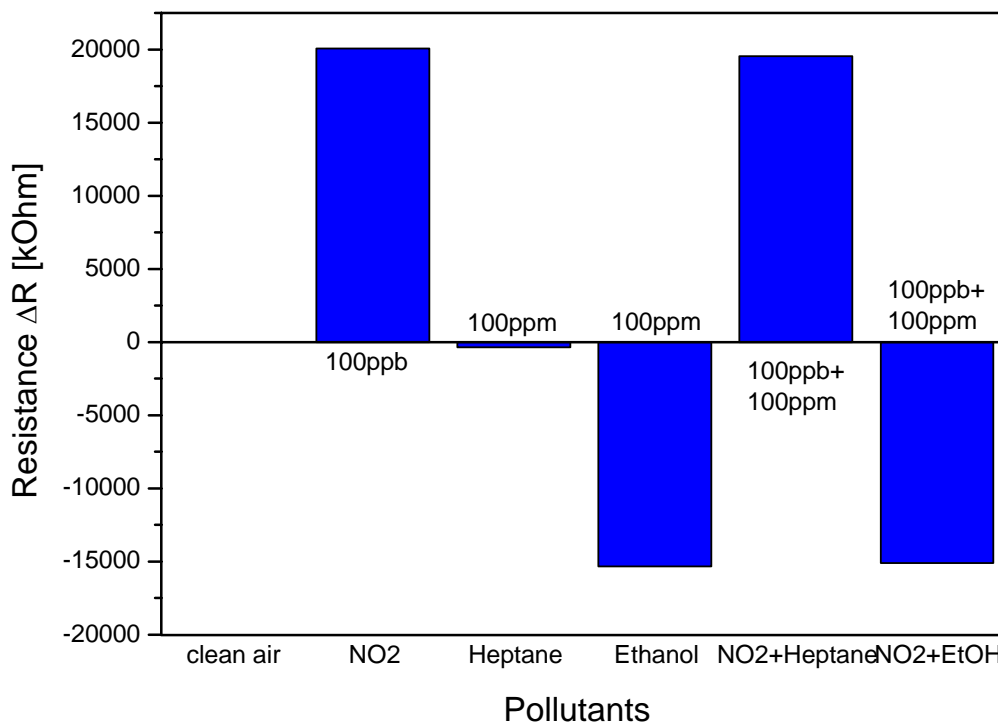| Sensor signal to NO_2 and VOCs	
Gas	**NO_2-sensor signal [%]**
100ppb NO_2	100
100ppm Heptane	-1.75
100ppm Ethanol	-76.4
NO_2 + Heptane	97.4
NO_2 + Ethanol	-75.3

Table 4.15: Resistance values of the NO_2-sensitive μ-hotplate during exposure to nitrogen dioxide, ethanol, heptane and a mixture of gases. No Filter active.

94

The detection of nitrogen dioxide is of interest only in outdoor applications where the concentration of VOCs can be assumed as stable compared to indoor applications. The influence of ethanol could therefore be seen as a systematic error and accordingly be compensated. This has been achieved with some success during the field trials (*see section 4.3*) where an in-field calibration has been used to predict the pollutants, thereby compensating background gases with constant concentrations.

4.2.9 Ozone

The sensor system has been exposed repeatedly to 50-500ppb ozone with and without gas filter active. No signal to ozone was detected with the gas filter active. Without the gas filter, even small concentrations of 50ppb ozone produce a strong signal and are recognised as about 10 times that high a concentration of nitrogen dioxide. The measurement of nitrogen dioxide requires the deactivation of the gas filter and is therefore always influenced by ambient ozone. Temperature modulation of the sensor μ-hotplates may offer a solution to this problem. Until then, the measured nitrogen concentration has to be recognised as an indicator of the total amount of oxidising gases, both nitrogen dioxide and ozone.

4.2.10 Summary

One ADA sensor chip has been intensively investigated under laboratory conditions to ascertain its functionalities and performance according to the project requirements. The parameters tested include sensitivity, selectivity, Lower Detection Limit, accuracy, signal stability, long-term stability, humidity influence, cross-sensitivity to polar and non-polar VOCs and to other pollutants (binary mixtures).

The results are very good for single gas measurements. All performance criteria discussed at the start of the system development are exceeded. The very good sensitivity, LDL, accuracy, reaction time and signal stability during exposure to pollutants prove the ADA sensor chip performs at least as well as conventional thick film semiconductor gas sensors. Here, the technology transfer to a smaller, less power consuming sensor platform with CMOS compatibility has succeeded.

An exception is the sensors long-term stability. After continuous operation for approximately one month, the carbon monoxide- and methane-sensitive μ-hotplates started to exhibit a drift. This drift increased in strength with time, rendering the original calibrations invalid (see *sections 4.2.1.5* and *4.2.2.5*). The drift of the methane-sensitive μ-hotplates can be traced to the instability of the on-chip poly-Si temperature control unit [212]. Its deterioration made it necessary to constantly adapt the operation temperature of the methane-sensitive μ-hotplate during the laboratory investigations. As a consequence, it is difficult to compare sensor results over extended periods of time. Especially the long-term stability measurements were affected. The drift of the carbon monoxide μ-hotplate is most probably due to a slow peeling of the sensitive layer [213].

The investigation of the sensors selectivity has produced ambivalent results. It was possible to compensate the cross-sensitivity to humidity and reduce the cross-sensitivity to VOCs to very low levels, even for complex mixtures. However, the following measurements of binary gas mixtures stayed below expectations. First measurements over a wide concentration range had shown very promising results (see figures 4.12 and 4.13). The good base selectivity of the system implicated that even ternary mixtures could be analysed with the right calibration or pattern recognition algorithm. The reason for the unexpected poor to satisfactory predictions for mixtures of carbon monoxide and methane is the sensor drift discussed above. As the measurements to establish the calibration data base and the test data base were performed

over the course of one month, the sensor drift introduces a considerable exogenous error. Consequently, these problems are not to be found for mixtures of nitrogen dioxide and carbon monoxide. Another problem is the sensors cross-sensitivity to ozone. Ozone is normally completely adsorbed by the gas filter inside the sensor system. However, for measurements of nitrogen dioxide, this filter is deactivated as it also eliminates this pollutant. As the sensor system exhibits a higher sensitivity to ozone than to nitrogen dioxide, quantitative and even qualitative predictions are severely restricted. The cross-sensitivity problems may be solved by modulating the operation temperatures of the sensor μ-hotplates, further discussed in *section 4.3*.

The laboratory investigations reported on were conducted on one ADA sensor chip. Two other chips were in use for several months in the field trials and system demonstrations at international fairs. They both performed as expected and were stable, requiring no maintenance during all their operation time. Also, no sensor signal drift appeared at either of them. This confirms the assumption of a technical problem, as discussed above and in *section 4.2.4*, as source of the drift instead of a systematic error.

To summarise, the sensors good performance qualifies them for qualitative detection, monitoring of concentration changes and alarm function for the pollutants carbon monoxide, methane and nitrogen dioxide. However, the sensitive layer manufacture and deposition has to be reworked to enable a reliable quantitative analysis of gas mixtures.

4.3 Field Trials

While the ADA sensor system has been successfully validated under controlled conditions it also has to function reliably in an uncontrolled environment. The selectivity strategies discussed earlier (e.g. gas filter, optimal operation temperature) are in part designed to ensure a good performance even during unforeseen problems such as unknown interfering pollutants or sudden atmospheric changes. Can the laboratory results and insights be transferred to real world situations? The field trials aim to answer this question.

4.3.1 Outdoor

4.3.1.1 System Configuration and Site Description

Two ADA sensor systems were installed for 3 months inside an Air Quality Monitoring Station (AQMS), measuring the same air samples as the standard analytical instruments used for air quality monitoring:

- One ADA sensor system equipped with AS sensors
- One ADA sensor system equipped with the ADA chip

The AQMS was located at a traffic hot spot, the Plaza del Marqués des Salamanca in Madrid, Spain, and is compliant with existing Spanish regulations [214]. The sensor system was installed with an open source configuration, sending raw data through the data transmission chain. As no calibration was implemented in the system it was possible to analyse the initial sensor data and adapt the calibration accordingly. All system operation modes were individually accessible. These allowed switching the filtering system on and off, run individual temperature modulation programs on the sensor μ-hotplates and fine-tune the duration of the measurement cycles. All measurements were cross-referenced with classical analytical instrumentation.

Figure 4.19: Air Quality Monitoring Station at the Plaza del Marqués des Salamanca in Madrid, Spain.

4.3.1.2 Air Quality Monitoring Station (AQMS)

The analytical instruments of the AQMS supply the concentrations of our pollutants of interest (carbon monoxide, methane, nitrogen dioxide) as well as other pollutants (ozone, nitrogen oxide, sulphur dioxide and total hydrocarbon concentration) and meteorological data (humidity, pressure, etc.). Typical results for one week are presented in figure 4.20. Even without further investigation of the ADA sensor system data, some important conclusions can be drawn from these results.
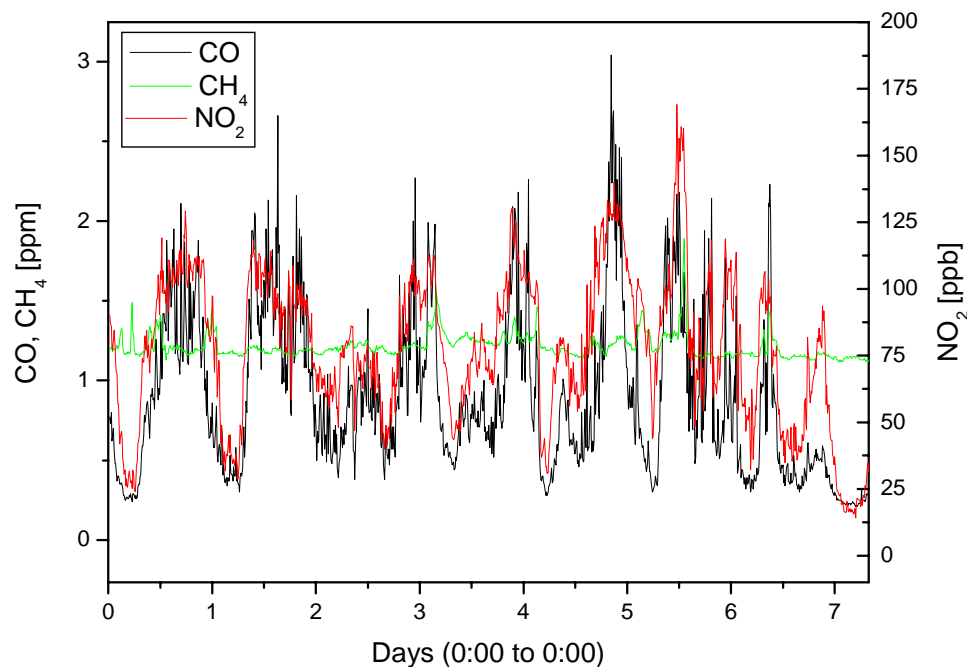

Figure 4.20: Signals recorded by Plaza de Salamanca AQMS during one week.

The concentrations of nitrogen dioxide and carbon monoxide follow a similar pattern. Both gases are clearly correlated with road traffic; daily cycles can be observed. The lowest

97

pollutant concentrations are recorded in the small hours of the night, from 03:00 to 07:00 o'clock. Peaks appear around morning to midday (people driving to work or lunch) and again late afternoon to night (people driving home from work or nightlife). The high pollutant concentrations are due to cold catalysts and/or increased traffic volume.

The methane concentrations observed (1-2ppm) are far below the targeted measurement range of the sensor systems (100-8.000ppm). Even though methane monitoring was only foreseen for the indoor application in the initial sensor system concept, the low LDL determined for methane *(see section 4.2.2.2)* seemed to allow including methane in the outdoor field trial. The very low methane concentration and lack of high alarm concentrations during the months of the field trial, led to a dismissal of that prospect.

The observed nitrogen dioxide concentrations range from 20 to 160ppb with singular maxima up to 300ppb, all well inside the operation and calibration range. The sensor system is therefore well suited to monitor and analyse the evolution of nitrogen dioxide.

The measured concentrations of carbon monoxide are very close to the LDL (0.2ppm), mostly between 0.3 and 1.5ppm and changing only slightly. Concentrations higher than 3ppm or an alarm were never observed. A low concentration by itself is not a serious problem as the sensor system can detect these values. However, the tight concentration span has a strong impact on the analytical situation. The sensor system was devised and optimised with a measurement range of 0.5-50ppm carbon monoxide as operational range. The small concentration span requires a very different calibration approach for optimal accuracy. If 99% of all measurements yield concentration values in the range of 1-5% of the maximum calibrated concentration then the calibration cannot be ideal, even if it provides good predictions.

The situation observed confirms the initial decision to install the ADA sensor system with an open source configuration. The access to the raw sensor data allowed adapting the calibration on-field to the changed situation.

4.3.1.3 Laboratory Calibration

The calibrations (without temperature modulation) established during the laboratory evaluation were tested with the sensor system data gathered at the AQMS. The laboratory calibrations were first tested with the ADA sensor system equipped with AS sensors, as it was available several weeks earlier than the sensors system with the ADA chip.

The ADA sensor system predicted reliably a methane concentration of 0ppm or below 1ppm CH_4 for the complete period; this corresponds to the actual very small and almost constant concentration of Hydrocarbons of between 0.9 and 1.3mg/m^3. Unfortunately not a single event of higher Methane concentration of at least a few ppm could be observed in the real-life test.

Figure 4.21 shows a direct comparison between real carbon monoxide concentrations (the measurement values from the AQMS) and the values predicted by the sensor system. The time interval between the laboratory calibration and field tests was 7 weeks. There was a significant systematic error between real and predicted carbon monoxide concentrations, due to the different conditions during the laboratory measurements and real-life tests. This systematic error appeared to be almost completely independent from time and allowed to introduce a correction function (see below).
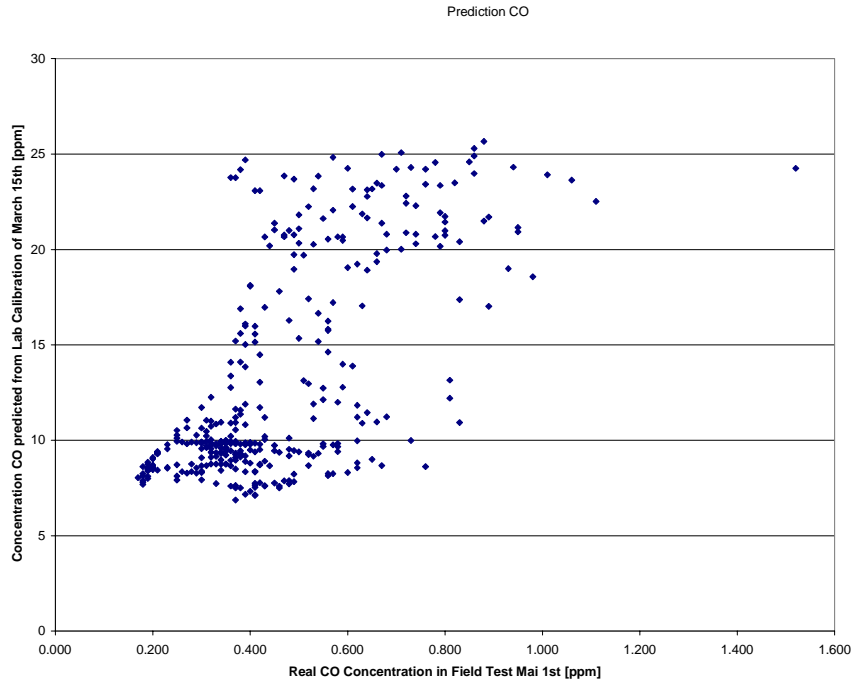
Figure 4.21: Real CO concentration and laboratory calibration prediction

Figure 4.22 shows the predicted carbon monoxide concentrations after application of a correction function. This linear function (parameter slope and offset) was introduced to correct the systematic error between lab calibration results and real-life results. The parameters of this correction function were calculated from an independent real-life measurement, the time interval between establishing the correction function and the measurement shown in the following figure is one week with continuous operation of the system in the field tests. The systematic prediction error with the laboratory calibration could be drastically reduced by the correction function (based purely on independent field test results.
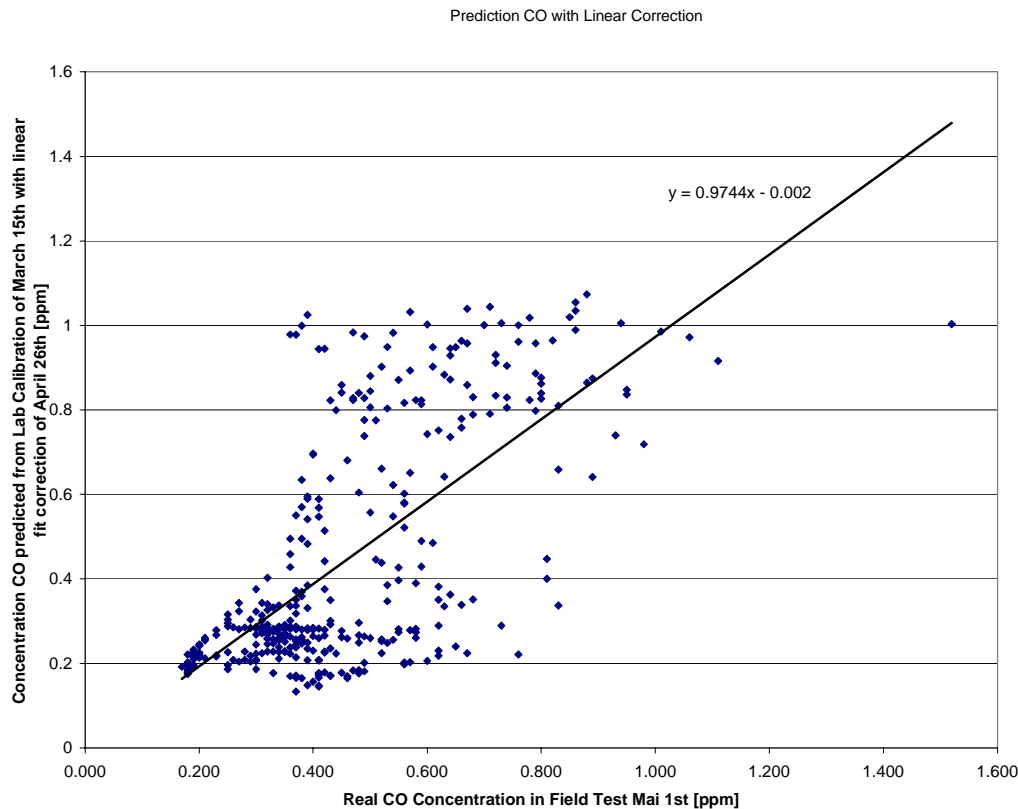
Figure 4.22: Real CO concentrations and corrected calibration prediction. Systematic error compensated by independent correction function.

Even though the correction function could be applied with some success to several field trail predictions, there still remains a high random error in the predictions based on laboratory calibrations.

For the sensor system equipped with the ADA chip the systematic error proved to be considerably lower. However, the random error was still considerable. These results for the two sensor systems discourage from using the laboratory calibration for the field trial. The further analysis of the field trial results was therefore conducted using an in-field calibration, which will be discussed in the following.

4.3.1.4   In-Field Calibration

The sensor system was installed with an open source configuration, allowing direct access to the raw sensor data. As the laboratory calibrations proved ineffective to predict the target pollutants in real world situations, new calibrations were established online with pattern recognition methods (PCR). In addition to the values from the three sensors, the actual humidity was taken into account. The sensor data was divided into two groups. One was referenced with the concentration values determined by the analytical instruments of the AQMS and used to establish a calibration system. This calibration was then applied to the second sensor data group to predict concentrations from raw sensor values. Several different system operation modes were investigated in the field as detailed in figures 3.28 and 3.29.:

- Slow temperature modulation: 250-350°C in 150s. Total cycle in 6min
- Fast temperature modulation: 250-350°C in 150s. Total cycle in 2min
- Constant temperature: each hotplate heated differently and constantly. Total cycle in 2min

The following discussion will focus on the results of the sensor system equipped with the ADA chip, as the early sensors system (equipped with AS sensors) does not allow temperature modulation and its predictions were constantly worse.

The temperature modulation allows increasing the number of sensors from three to 360, as the sensitive materials react differently to pollutants depending on their operation temperature. Temperature modulation seemed therefore the most promising strategy to cope with multidimensional analytical problems. Due to the open source configuration of the system, calibrations for all gases referenced by the AQMS could be established (carbon monoxide, nitrogen dioxide, nitrogen oxide, sulphur dioxide, ozone, methane and total hydrocarbon concentration).

The slow temperature modulation was tested first. Several calibrations based on different weeks and time spans of varying length were calculated and tested. However, the results always showed a high systematic and random error; no correlation could be established between signals from the sensor and reference instruments.

The fast temperature modulation proved to be more successful. Figure 4.23 shows a prediction of sensor data measured the same day as the calibration. The low random error is an improvement; the systematic error stays considerable with an offset in the range of the measured concentrations. Applying the calibrations to sensor data generated later reveal a rapid deterioration of the model after a few days. After several weeks all correlation between predicted sensor concentration and concentration changes measured by reference instruments are lost.
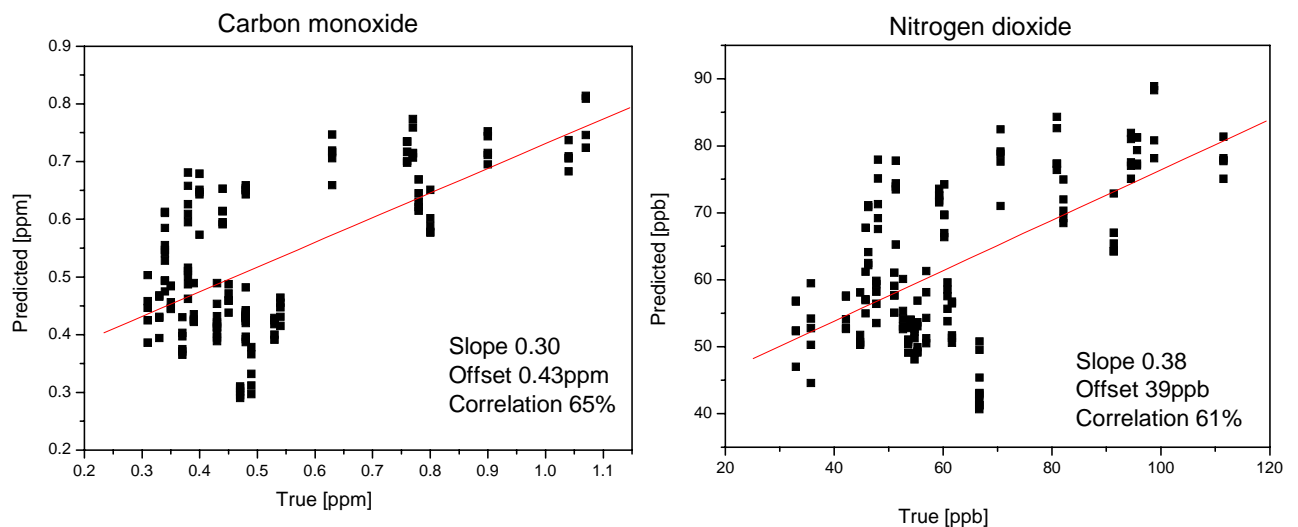
Figure 4.23: Same day prediction of carbon monoxide and nitrogen dioxide based on fast temperature modulation.

Operation of the sensors in constant temperature mode proved much more successful than the original favourites with temperature modulation. Initial calibration tests with same day predictions showed a low systematic error (offset of 0.2ppm for carbon monoxide) and a very low random error. Applying the established calibration model to sensor data up to several weeks older resulted in unchanging good predictions. Figure 4.24 shows results for a prediction of carbon monoxide and nitrogen dioxide with a calibration model two weeks old.

The prediction quality starts to deteriorate after four weeks, resulting again in a loss of correlation between sensor and reference instruments.
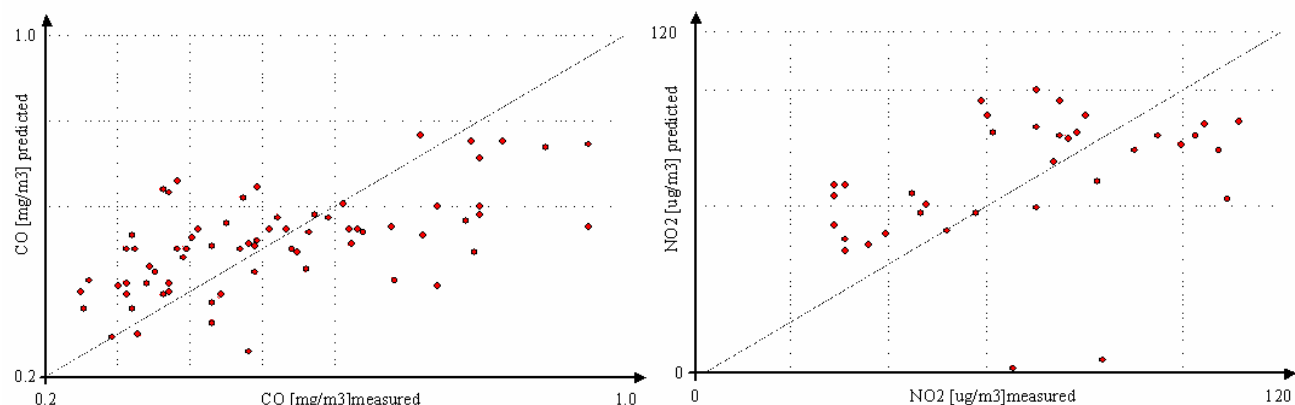
Figure 4.24: Prediction after two weeks of carbon monoxide and nitrogen dioxide with sensors at constant temperature.

The open source configuration of the sensor system allowed to try to establish calibrations for other pollutants than those originally targeted. Surprisingly this resulted in good prediction results especially for ozone and sulphur dioxide. During temperature modulation the prediction quality was of a similar quality as the predictions of carbon monoxide and nitrogen dioxide. With the sensors operated at constant temperature the predictions were slightly less good than those for carbon monoxide and nitrogen dioxide.

4.3.2 Indoor

4.3.2.1 System Configuration and Site Description

One complete ADA system equipped with AS sensors, pump and filtering system was tested for a period of two months. The system was calibrated in laboratory one week before the field trail started. The monitoring station was installed in the parking garage of *Telecom Italia Laboratory* (TILAB) office buildings in Turin, via Reiss Romoli, 274 (see figure 4.25). The Indoor car parking is placed on the ground floor and can accommodate a maximum of 250 cars with an area of 100 x 80m. Most of TILAB staff enter this car parking during the morning and leave at mid afternoon, so there are at least two periods during the day in which gas concentrations (related to car emissions) can have peaks. No ventilation is present except for the main gate which opens from 7:00am to 7:00pm.

The aim was to monitor the daily changes of the carbon monoxide concentration and to compare the ADA sensor system results with commercial sensors. The reference instrument was the portable TSI multi-gas monitor 8570. It was chosen on purpose as it is based on electrochemical cells and is in the same price category as a projected commercial ADA sensor system. It therefore allows to compare the ADA sensor system results with a commercial sensor system, contrary to the outdoor field trials discussed earlier which are referenced with analytical instruments of higher accuracy, reliability and price.
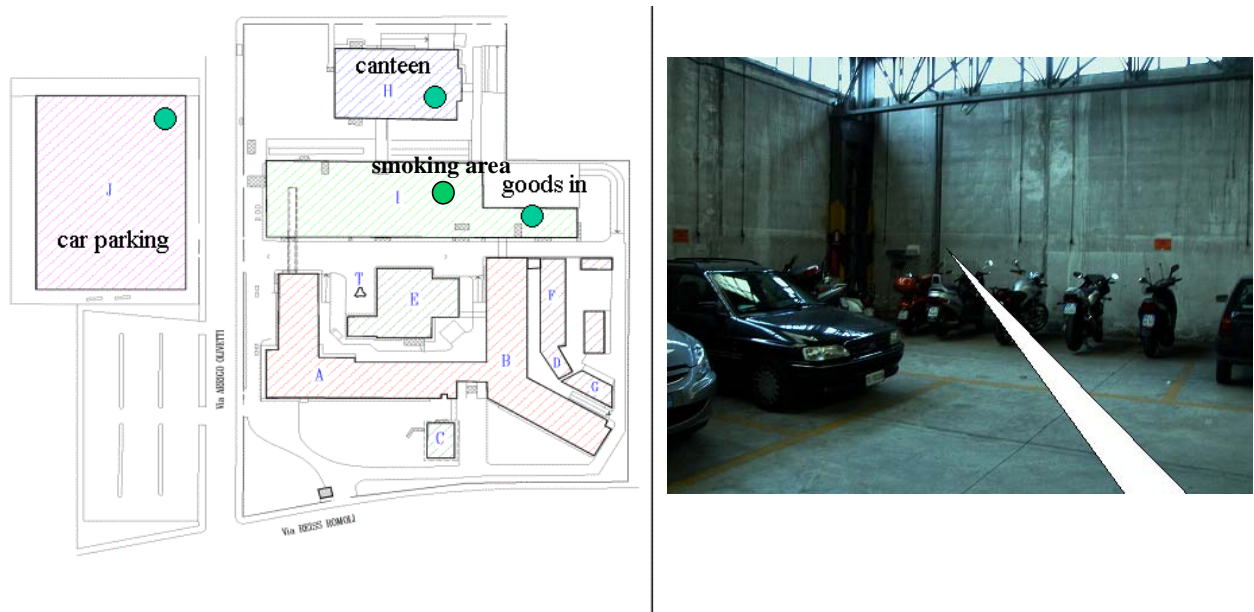
Figure 4.25: Field test site Italy. Location inside the parking garage.

4.3.2.2 Results

Figure 4.26 details the daily evolution of the carbon monoxide concentration during an exemplary week. No significant drift of the prediction was recorded over the measurement time of 2 months. The general evolution of the pollutant concentration follows the expected daily cycle. During the night the background level of 1-2ppm is reached, the concentration increases in the morning and reaches a maximum of approximately 10ppm every afternoon from 4 to 8pm, due to cars leaving the parking area with cold engines. This effect is less strong in the mornings as the car engines are already hot when they reach the parking garage. Singular strong peak of 20-30ppm appear sometimes in the afternoon and are probably due to motorcycles parked directly beneath sensors. As expected, on Saturdays and Sundays these effects are not present.
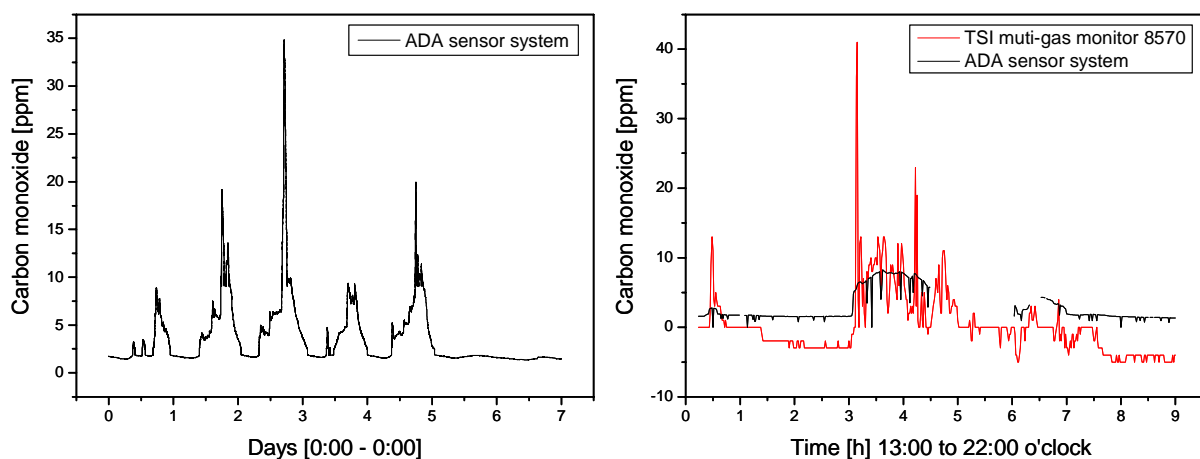
Figure 4.26: Evolution of carbon monoxide concentration as measured by ADA sensor system and TSI 8570. Results for one week and one afternoon.

Figure 4.26 also allows to compare the results of the ADA sensor system with the commercial sensor system TSI 8570. As can be seen, both sensor systems register a concentration increase, maximum and decrease at the same time. The absolute concentration values are very

similar, with the electrochemical cell showing more extreme read-outs (values below zero and short-term highs) while the ADA sensor system is prone to data loss. This failing of the system electronics was corrected after the field trials. After end of the exposition to pollutants from car exhausts, the ADA sensor system returns fast to concentration read-outs at the initial background level. The measurement values are less resolved than for the TSI, omitting the short peaks and fine structure. This is probably due to the much thinner filter of the TSI which allows a faster response to concentration changes. The high filter volume of the ADA sensor system results in a more moderate sensor reaction to concentration changes, possibly preventing false alarms due to very short concentration peaks.

4.3.3 Summary

The field trials illustrated the abilities and failings of laboratory calibrations in real world situations. Despite a filtering system able to eliminate a wide range of pollutants, the gas composition in the field was complex enough to produce a defined systematic error and occasional random errors. During the indoor field trials the correlation between ADA sensor system and commercial sensor system was still quite good. Apart from a constant concentration difference of factor two, both systems detected the same trends and concentration changes. A simple correction to the calibration function would eliminate this discrepancy. However, the ADA sensor system is compared to another (commercial) sensor system in this case, not a standard analytical instrument. There may be further systematic and/or random errors included in the measurements of both systems that are not revealed by the test configuration employed. During the outdoor field trials in Madrid the situation is different. Here, standard analytical instruments were used to reference the sensor read-outs. As a result, the correlation between sensor system and reference instruments was worse than during the indoor trials. A strong systematic and random error prevented the use of the laboratory calibration, even though the deviations were less intensive for the sensor system once equipped with the ADA chip. The field trials could be continued by directly evaluating the raw sensor data and establishing appropriate calibrations in field. Here, the individual temperature modulation of the chips sensor hotplates proved problematic. The high expectations of solving the analytical problem of multi-dimensional gas mixtures, based on previous investigations under laboratory conditions and literature [160], [184], could not be sustained. The classical approach with sensors heated at constant temperatures yielded results with a higher correlation to the reference instrument read-outs. However, the analytical instruments used as reference provided averaged pollutant concentrations for periods of 10min. While during the indoor field trials both tested system and reference system measured pollutants within similar time intervals (30s to 1min), the difference was much higher at the outdoor field trial: 1s for the tested sensor system to 10min for the reference instruments. This high difference in time resolution resulted in difficulties during the in-field calibrations: correlating concentration values with fine structures and peaks to averaged values. This effect is even amplified for the temperature modulation configuration, as the oscillating temperature prevents the sensitive layers from reaching a chemical equilibrium; effectively forcing an operation in a non-steady-state mode. These two factors are responsible for decreasing the quality and life-time of the sensor calibrations established in field. Regretfully, it was not possible to convince the involved local authorities to change the time interval of the reference instruments from 10min to 1min or lower; a feat technically possible. However, it was possible to create sensor calibrations with a lifetime of two weeks and good prediction qualities both for carbon monoxide and nitrogen dioxide. The range of monitored gases could even be extended to other pollutants such as sulphur dioxide and ozone (based on measurement cycles with deactivated filtering system).

5 Summary

The main achievement of this work was the development of a chemical gas sensor system for two relevant environmental applications: indoor (carbon monoxide and methane) and outdoor (carbon monoxide and nitrogen dioxide) monitoring of pollutants. Towards this end, three subsequent tasks were accomplished: Firstly, the planning, design and testing of the sensor system supporting the sensing element. Secondly, the laboratory evaluation of the system performance and limitations. Thirdly, the transfer to real world applications.

The development process started with a concept and went to a series of prototypes, tests and redesigns. As sensing element a monolithic micro-machined metal oxide sensor was chosen, the ADA sensor chip. It consists of a sensor array: three independent micro-hotplates with different sensing layers based on tin dioxide (SnO_2). Around this heart-piece, the supporting sensor system was constructed. To achieve mobility and low power consumption, the components were reduced to the necessary basics - small tubings, pump, gas filter, battery and system control electronics - and combined with a robust packaging. The targeted applications, i.e. qualitative and quantitative detection of binary gas mixtures in the presence of intereferents required a high sensor selectivity. Metal oxide sensors, such as utilised in this work, are known for their high sensitivity and low selectivity. Therefore a range of strategies towards improving the selectivity were investigated. The most effective were optimisation of sensor materials, sensor operation temperature and gas filters. The chemical properties of metal oxides such as grain size, annealing temperature and doping define their sensitivity and selectivity to gases. The same holds true for the sensor operation temperature, as the chemical reactions resulting in a sensor signal are temperature-dependent. Gas filters, on the other hand, are very effective at adsorbing whole substance categories depending on their chemical properties; here they were used to eliminate VOCs in the gas sample. The development process concluded in the ADA sensor system prototype, which was then characterised in the laboratory.

The laboratory investigations resulted in an extensive assessment of the sensor system functionalities. The parameters tested include sensitivity, selectivity, LDL, accuracy, long-term stability, humidity influence and cross-sensitivity to polar and non-polar VOCS. The results are very good for the detection of single gas mixtures and acceptable to good for binary mixtures. However, the sensitive layers on the chip deteriorate after several weeks due to layer peeling and heater degeneration, resulting in a strong drift over time. The problem has been analysed and remedial actions have been formulated.

As a final system evaluation, several ADA sensor systems were submitted to a 3-month field trial, where they were investigated in both outdoor (traffic hot-spot in Madrid, Spain) and indoor (offices and car parking in Turin, Italy) applications. The field trials illustrated the abilities and failings of laboratory calibrations in real world situations. For the indoor field trials the correlation between ADA sensor system and a commercial sensor system was quite good. Apart from a systematic concentration offset, both systems detected the same trends and concentration changes. During the outdoor field trial the appearance of both systematic and random errors prevented an effective use of the laboratory calibration. The situation could be resolved to some extent by directly evaluating the raw sensor data and establishing appropriate calibrations in the field: it was possible to create sensor calibrations with a lifetime of two weeks and good prediction qualities both for carbon monoxide and nitrogen dioxide. The range of monitored gases could even be extended to other pollutants such as sulphur dioxide and ozone.

To conclude, the developed sensor system constitutes a successful transfer of metal oxide sensor technology to micro system technology with all advantages a monolithic micromachined sensor system offers: reduced size, packaging and power consumption, integration of electronics, sensor array and on-chip data-evaluation. The integration of metal oxide sensor technology into CMOS-compatible structures allows for a sensor mass production with established microelectronic and microtechnological processes and facilitates cost-effective commercialisation. The ADA chip is currently the most advanced mircomachined gas sensor. As ADA sensor system, together with the supporting sensor system, it equals or exceeds conventional metal oxide sensor technology in all performance criteria relevant for environmental monitoring.

Sensor systems are often seen as cheap alternative to analytical instruments by their supporters and as inaccurate low-reliability-devices by their opponents. However, the author sees their potential as a supplement of classical analytical instruments. Owing to the potential high mobility and their increased temporal and spatial resolution gas sensor systems can complement classical analytical instruments and improve their effectiveness.

6 Annex

6.1 Definitions

The performance of sensors can be discussed and compared through features which allow a quantitative comparison of sensing properties. However, no generally accepted, uniform set of definitions exists. In the following, typically used definitions are detailed which are helpful to quantify a given sensors performance.

6.1.1 Sensor Signal

The sensor signal is used to create a relation between the sensors response and the zero response (baseline) in the absence of stimulus. In most applications the sensor resistance R or conductance G is measured. Literature suggests definitions as in equations $(6.1) - (6.3)$.

$$S_{red} = \frac{R_0}{R_{red}} \quad \text{and} \quad S_{ox} = \frac{R_{ox}}{R_0} \tag{6.1}$$

$$S_{red} = \Delta R_{red} = R_0 - R_{red} \quad \text{and} \quad S_{ox} = \Delta R_{ox} = R_{ox} - R_0 \tag{6.2}$$

$$S_{red} = \frac{R_0}{\Delta R_{red}} = \frac{R_0}{R_0 - R_{red}} \quad \text{and} \quad S_{ox} = \frac{\Delta R_{ox}}{R_0} = \frac{R_{ox} - R_0}{R_0} \tag{6.3}$$

6.1.2 Sensitivity

The sensitivity of a sensor, m_i, to detect a certain gas species i is defined as the slope of the calibration curve, which is the best interpolation of the experimental results at the gas concentration of interest.

$$m_i = \left. \frac{\partial S}{\partial p_i} \right|_X \tag{6.4}$$

S is the sensor signal as defined above or any other sensor response parameter, p_i, is the partial pressure of the gas species i and X denotes the parameters kept constant during the experiment, such as the humidity, temperature and partial pressure of O_2. In the case of linear sensors, i.e. sensors with a linear dependency of the signal upon the partial pressure of a gas, the sensitivity m is constant. In the case of non-linear sensors, such as the metal oxide sensors used in this work, the sensitivity depends on the absolute value of the partial pressure of a gas.

6.1.3 Analytical Sensitivity and Accuracy

The response sensor signal of a sensor cannot be measured with absolute accuracy and therefore the derived value of the partial pressure (and thereby concentration) is to some extent inaccurate. The origin of the inaccuracy might be e.g. the noise of the measurement or the limited reproducibility of the measurement due to insufficient stability of the sensors. Consequently, high sensor sensitivity does not imply per se a good sensor performance. To rate the quality of the of the sensor performance not only the sensitivity but also the accuracy with which the sensor signal can be measured plays a large role. A meaningful way to include

the accuracy in the definition of the sensitivity is to divide the sensor sensitivity by the standard deviation of the sensor signal σ_s, resulting in the analytical sensitivity γ [215]:

$$\gamma = \frac{m}{\sigma_s} \qquad (6.5)$$

Taking into account the total differential of the sensor response x

$$dx = \left(\frac{\partial x}{\partial p}\right) dp \qquad (6.6)$$

one can derive

$$\sigma = \left(\frac{\partial x}{\partial p}\right) \sigma_p \qquad (6.7)$$

with σ_p the standard deviation of the concentration, i.e. the accuracy with which a concentration can be determined. Consequently, the analytical sensitivity can be written as the reciprocal of the standard deviation of the determined concentration.

$$\gamma = \frac{1}{\sigma_p} \qquad (6.8)$$

This formula helps to interpret the analytical sensitivity. The analytical sensitivity is the reciprocal of the standard deviation of the concentration, i.e. the accuracy with which the concentration of a gas can be determined. It gives a measure of the ability of the sensor to discriminate or detect small changes in concentration at the concentration of interest. According to equation (6.8), 10ppm^{-1} equals a standard deviation of the concentration of 0.1ppm.
In contrast to e.g. the sensitivity of a sensor, the analytical sensitivity of a sensor is independent of the concentration. Therefore it is possible to compare quantitatively the performance of sensors with sensor response which are different in nature by means of analytical sensitivity.

6.1.4 Selectivity

Sensors are normally sensitive to more than one gas and usually show cross-sensitivities. The selectivity is a measurand for evaluating the specificy of a sensor by comparing the effects of different gases on a sensor. The selectivity m_{ij} of a sensor compares sensor signal or the sensitivity to be monitored to the sensor signal (sensitivity) of the interfering gas. One possibility for comparison is to build the ratio of signals (sensitivities) according to

$$m_{ij}(p_i, p_j) = \frac{S_i}{S_j} \qquad \text{or} \qquad m_{ij}(p_i, p_j) = \frac{m_i}{m_j} \qquad (6.9)$$

Another possibility is to calculate the corresponding concentration, i.e. the concentration of gas *a* for which the sensor supplies a signal of the same strength as for a fixed concentration of gas *b*.

6.1.5 Lower Detection Limit (LDL)

The Lower Detection Limit is the minimum concentration which can be detected by a given sensor. It relates the sensors response to the statistical fluctuations in the zero response R_0 (baseline). The minimum sensor response which is certainly detected is usually chosen as three times the standard deviation of the zero response σ_0, which is considered to be the noise of the measurement.

$$R_{min} = \overline{R}_0 + 3 \cdot \sigma_0$$

with the average zero response $\overline{R}_0$.

6.1.6 Response and Recovery Time

Two measurands are usually used to measure the speed of a sensor. The first is the so-called response time t_{res}, which refers to the time needed to reach a stable sensor response after stepwise increase in the concentration. Hence it measures the minimum time needed to measure a concentration. Usually the response time is defined as t_{90}, i.e. the time it takes for 90% of the sensor response change after an increase in the concentration is accomplished. The second is the recovery time t_{rec}. It refers to the time the sensor needs to recover from a concentration exposure. The recovery time is defined similar to the response time. It is the time needed for 90% of the sensor response change after concentration exposure removal is accomplished.

6.2 Airborne Pollutants

6.2.1 Carbon monoxide CO

Molecular weight: 48 g/mol
Melting point: -205°C
Boiling point: -192°C
Relative density in air: 1
Solubility in water: 30mg/l
Auto ignition temperature: 620°C
Flammability range 12.5 - 74vol% in air
Hazards: F+, T
R12, R23, R48, R61

CO is a lethal poison that is produced when fuels such as gasoline are burned. It is one of many chemicals found in engine exhaust and can rapidly accumulate even in areas that might appear to be well ventilated. Because CO is colourless, tasteless, odourless, and non-irritating, it can overcome the exposed person without warning. It produces weakness and confusion, depriving the person of the ability to seek safety.
CO poisons primarily by tightly binding to haemoglobin in the blood (forming carboxyhaemoglobin), replacing oxygen, and reducing the oxygen-carrying capacity of the blood. CO may also poison by binding to tissues and cells of the human body and interfering with their normal function. Recognizing early warning signs of CO poisoning is sometimes

difficult because early symptoms of CO exposure (headache, dizziness, and nausea) are non-specific and may be mistaken for symptoms of other illnesses such as colds, flu, or food poisoning. Confusion and weakness can inhibit a person's ability to escape the hazardous environment.

6.2.2 Methane CH_4

Molecular weigth: 16.043 g/mol
Melting point: -182.5C
Boiling point: -161.6°C
Relative density, gas (in air): 0.6
Solubility in water: 26 mg/l
Auto ignition temperature: 595°C
LEL: 5-15vol%
Hazards: F+
R12

Methane is a natural gas widely used for domestic heating and cooking. The main danger for the populace is not, contrarily to NO_2 and CO, its toxicity. CH_4 is a highly explosive gas. It is colourless, has no odour and is therefore difficult to detect without an appropriate sensing device. In the case of a gas leak, the extremely flammable methane will accumulate and ignite at the smallest spark.
As methane is lighter than air, even underground leaks from pipelines pose a threat to human health as the gas will rise up through the ground and accumulate in buildings. The threat of methane is therefore a well known problem at mining sites.

6.2.3 Nitrogen dioxide NO_2

Molecular weight: 46.05 g/mol
Melting point: -11.2°C
Bp: 21.1°C
Relative density in air: 2.8
Hazards: T+, C
R26, R34

Nitrogen dioxide is a typical air pollutant released into the atmosphere from very localised sources, primarily by combustion in factories and automobiles. It is known to cause global environmental problems such as acid rain, photochemical smog and corrosion of metals. Acute exposure to NO_2 concentrations of less than 1 ppm rarely produces observable effects in normal healthy humans. At NO_2 levels around 2.5 ppm over 2 hours the first effects are experienced by exposed subjects, meaning decreases in pulmonary function. Asthmatics and more generally people with pulmonary dysfunctions may react to concentrations as low as 0.3ppm. In the case of long-term exposure over several weeks, concentrations as low as 0.5ppm produce an increased susceptibility to lung diseases and dysfunctions. Nevertheless, the conducted studies on the health effects of NO_2 exposure have found no evidence for a clearly defined concentration-response relationship. The health guidelines given by different organisations are therefore chosen with the lowest possible risk for the general populace in mind.

6.2.4 Environmental monitoring

Area Type	Station Type		Pollutants of greater interest
Urban	Traffic		NO_2, PM_{10}, $PM_{2.5}$, CO and VOCs
	Industrial		NO_2, PM_{10}, $PM_{2.5}$, SO_2 and VOCs, heavy metals and specific pollutants of the emissions of the said industries.
	Background		NO_2, PM_{10}, $PM_{2.5}$, SO_2, CO, VOCs and O_3
Suburban	Traffic		NO_2, PM_{10}, $PM_{2.5}$, CO and VOCs
	Industrial		NO_2, PM_{10}, $PM_{2.5}$, SO_2 and VOCs, heavy metals and specific pollutants of the emissions of the said industries.
	Background		NO_2, VOCs, O_3 and also PM_{10} and $PM_{2.5}$
Rural	Traffic		NO_2, NOx and VOCs
	Industrial		NO_2, PM_{10}, $PM_{2.5}$, SO_2 and VOCs, heavy metals and specific pollutants of the emissions of the said industries.
	Background	Next to cities	Not specified
		Regional	NO_2, SO_2, O_3, NH_3, acid deposition, SO_4, NO_3 and $PM_{2.5}$
		Remote	O_3, CFCs and also S and N compounds related to acid deposition, and also background levels of PM and VOCs

Table 6.1:   Pollutants of interest according to the type of fixed measuring station [2].

Main pollutants	Main pollutant sources due to human activity
SO2	Installations de combustion (soufre de combustible)
(NO, NO2)	Vehicles – Heating systems
Particulate Matter (PM)	Combustion - Vehicles – incineration
Volatile organic compounds (VOCs)	Chemist and Oil Industry, solvents, Cars
CO	Incomplete combustions – Vehicles
HCI	Waste incineration
Metallic compounds (Pb, Mn, Cd, Hg, Ni,...)	Heavy industry- Combustion – waste incineration
Aromatic compounds (HAM, HAP)	Incineration- Combustion - Vehicles

Table 6.2:   Main pollutants and their sources due to human activity [2].

NO2-Guideline (Outdoor)	Averaging Period	Limit Value
Directive 99/30/EC (2010)	1 hour	105 ppb
	24 hours	20 ppb
	Vegetation	15 ppb
	Alert threshold	209 ppb
DEFR (UK)	1 hour	150 ppb
OSHA (USA)	15-min-TWA	1000 ppb
NIOSH (USA)	Immediately dangerous	20 ppm
WHO	1 hour	100 ppb
CO-Guidelines (Outdoor)	**Averaging Period**	**Limit Value**
Commisions Proposal COM (1998) 591 Final	8-hour-TWA	8 ppm
DEFR (UK)	8-hour-TWA	10 ppm
EPA (USA)	8-hour-TWA	9 ppm
	Short-term-exposure	25 ppm
CO-Guidelines (Indoor/Workplace/Residential):	**Averaging Period**	**Limit Value**
OSHA (USA)	8-hour-TWA	50 ppm
NIOSH (USA)	8-hour-TWA	35 ppm
	Ceiling limit	200 ppm
	Immediately dangerous	1,200 ppm
ACGIH (USA)		25 ppm
WHO	8-hour-TWA	50 ppm
	15-min-TWA	86 ppm
CPSC (USA)	8-hour-TWA	15 ppm
	Short-term-exposure	25 ppm
CH4-Guidelines	**LEL**	**Auto ignition Temperature**
ILO	5-15 vol% in air	537°C

Table 6.3:   International Air Quality Guidelines [216].

7 References

[1]   K. Cammann, *Instrumentelle Analytische Chemie*, Spektrum, Akad. Verl. **(2001)**

[2]   C. Ramirez, *personal communication*, SICE, Spain **(2004)**

[3]   ANALYTICA 2002, *personal communications*, Germany **(2002)**

[4]   Electrical Transducer Nomenclature and Terminology, *ANSI Standard MC6.1-1975 (ISA S37.1)*, Research Triangle park, NC: Instrument Society of America

[5]   *Terms and Definitions in Industrial-Process Measurement and Control*, IEC draft 65/84, International Electrotechnical Committee **(1982)**

[6]   R.G. Seippel, *Transducers, Sensors and Detectors*, Reston: Reston Publishing **(1983)**

[7]   W. Göpel, J. Hesse, J.N. Zemel (1992), *Sensors – a comprehensive study*, vol. 1-3, Wiley-VCH, Weinheim, Germany **(1989-1991)**

[8]   S. Strathmann, Sample conditioning for Multi-Sensor Systems, *PhD thesis*, University of Tuebingen **(2001)**

[9]   M.S. Nieuwenhuizen and A. Venema, Mass-sensitive Devices, in: W. Göpel, J.Hesse, J.N. Zemel (eds.), *Sensors: a comprehensive survey*, vol. 2, Wiley-VCH, Weinheim, Germany **(1991)** 647

[10]   G. Sauerbrey, *Z. Phys.* 155 **(1959)** 206

[11]   J.W. Grate, S.J. Martin, R.M. White, *Anal. Chem.* 65 **(1993)** 940A and 987A

[12]   J. Mitrovics, H. Ulmer, U. Weimar, W. Göpel, Modular sensor systems for gas sensing and odour monitoring: the MOSES concept, *Acc. Chem. Res.,* 31 **(1998)** 307

[13]   J. Bardeen, W.H. Brattin, Surface properties of germanium, *Bell. Syst. Techn. J.* 32 **(1952)** 1

[14]   T. Seiyama, A. Kato, K. Fujushi, M. Nagatani, A new detector for gaseous components using semiconductive thin films, *Anal. Chem.* 34 **(1962)** 1502

[15]   N. Taguchi, Japanese Patent 45-38200

[16]   N. Taguchi, Japanese Patent 47-38840

[17]   N. Taguchi, US Patent 3 644 795

[18]   Figaro Products Catalogue, *Figaro gas sensors 2000-series*, Figaro Engineering Inc., European Office, Germany

[19]   FIS, Product list (specifications: Sb/sp series), FIS incorporated **(1999)**

[20]   UST, *Product information*, Umweltsensortechnik GmbH, Geschwenda, Germany **(1999)**

[21]   U. Frey, M. Graf, S. Taschini, and A. Hierlemann, Physical Electronics Laboratory (PEL), ETH Zürich, Zürich, Switzerland

[22]   A. Krauss, AppliedSensor GmbH, Reutlingen, Germany

[23]   J. Kappler, "Characterisation of high-performance SnO_2 gas sensors by a combination of in-situ techniques", *Ph.D. Thesis*, University of Tübingen, Shaker Verlag, Germany **(2001)**

[24]   A.Gurlo, N. Bârsan, U. Weimar, *Metal Oxides: Chemistry and Applications*, Mercal Decker, New York **(2004)**

[25]   G. Heiland, Homogeneous semiconducting gas sensors, *Sens Act*, 2 **(1982)** 343

[26]   N. Yamazoe, Y. Kurokawa, Proceedings of the International Meeting on Chemical Sensors, Fukuoka, Japan **(1983)** 35

[27]   R.S. Niranjan, S.R. Sainkar, K. Vijayamohanan, I.S. Mulla, Ruthenium: tin oxide thin film as a highly selective hydrocarbon sensor, *Sens. Actuators B*, 82 **(2002)** 82

[28]   U. Schönauer, *Technisches Messen*, 56 **(1989)** 260

[29]   A.N. Willis, N. Silarajs, *U.S. Patent 4,197,089* **(1980)**

[30] M. Ando, S. Suto, T. Suzuki, T. Tsuchida, C. Nakamaya, N. Miura, N. Yamazoe, *Chemistry Letters*, **(1994)** 335

[31] G. Sberveglieri, S. Groppelli, P. Nelli, WO_3 sputtered thin films for NO_x monitoring, *Eurosensors VIII Conference*, Toulouse **(1994)** 129

[32] B. Fruhberger, N. Stirling, F.G. Grillo, S. Ma, D. Ruthven, R.J. Lad, B.G. Frederick, Detection and quantification of nitric oxide in human breath using a semiconducting oxide based chemiresistive microsensor, *Sens. Actuators B*, 76 **(2001)** 226

[33] N. Koshizaki, T. Oyama, Sensing characteristics of ZnO-based NO_x sensor, *Sens. Actuators B*, 66 **(2000)** 119

[34] G. Heiland, *A.Phys*. 148 **(1957)** 15

[35] G. Heiland, *A.Phys*. 138 **(1954)** 459

[36] R. Sanjines, F. Levy, K. Prasad, H. Tang, TiO_2 anatase films as gas sensors, *Eurosensors VIII conference*, Toulouse **(1994)** 125

[37] Y. Takao, K. Miyazaki, Y. Shimizu, M. Egashira, *J. Electrochem. Soc.,* 141 **(1994)** 1028

[38] T. Takada, Ozone detection by In_2O_3 thin film gas sensor, in T.Seiyama (ed.): *Chemical Sensor Technology*, Vol.2, Elsevier, Amsterdam/Kodansha, Tokyo **(1989)** 59

[39] G. Neri, A. Bonavita, S. Galvagno, P. Siciliano, S. Capone, CO and NO_2 sensing properties of doped-Fe_2O_3 thin films prepared by LPD, *Sens. Actuators B*, 82 **(2002)** 40

[40] M. Fleischer, H. Meixner, *Sens Act B*, 6 **(1992)** 277

[41] M. Fleischer, H. Meixner, Comparison of AC and DC *measurement techniques using semiconducting Ga_2O_3 sensors,* Eurosensors VIII Conference, Toulouse, **(1994)** 307

[42] M. Fleischer, H. Meixner, *Sens Act B*, 5 **(1992)** 115

[43] W. Göpel and G. Reinhardt, Metal oxide sensors: new devices through trailoring interfaces on the atomic scale, in H. Baltes, W. Göpel, J. Hesse (eds.): *Sensors update*, vol.1, VCH, Weinheim, Germany **(1996)** 105

[44] R.S. Katiyar, Dynamics of the Rutil Structure: I. Space Group representations and the normal mode analysis, *J Phys C*, **1970**, 3, 1087

[45] E. Lax, C. Synowietz, *Taschenbuch für Chemiker und Physiker*, **1967**, 1.Band, 3.Auflage

[46] J. Robertson, Electronic structures of SnO_2, GeO_2, PdO_2, TeO_2 and MgF_2, *J. Phys.,* C12 **(1979)** 4767

[47] C.G. Fonstad, R.H. Rediker, Electrical properties of High-Quality stannicoxide crystals, J. *Appl. Phys.*, 42 **(1971)** 2911

[48] S. Samson, C.G. Fonstad, Defect structures and electronic donor levels in stannic oxide crystals, *J. Appl. Phys.*, 44 **(1973)** 4618

[49] Z.M. Jarzebski, Physical properties of SnO_2 Materials II, *J. Electrochem. Soc.*, 123 N.9 **(1976)** 300C

[50] J.S. Blackmose, *Semiconductor statistics*, Pergammon Press, UK **(1962)**

[51] Ph. Barbarat, S.F. Matar, G. Le Blevennec, First principles investigations of the electronic, optical and chemical bonding properties of SnO_2, *J. Mater. Chem.,* 7 (12) **(1997)** 2547

[52] J.M. Themlin, M. Chtaïb, L. Henrard, Ph. Lambin, J. Darville, J.M. Gilles, Characterisation of tin oxides by x-ray-photoemission spectroscopy, *Phys.Rev. B,* 46 (4) **(1992)** 2460

[53] P. Depadova, M. Fanfoni, R. Larciprete, M. Mangianti, S. Priori, P. Perfetti, A synchrotron radiation photoemission study of the oxidation of tin, *Surf. Sci.,* 313 **(1994)** 379

[54] L. Kövér, G. Moretti, Zs. Kovács, R. Sanjinés, I. Cserny, G. Margaritondo, J. Pálinkás, H.Dachi, High resolution photoemission and Auger parameter studies of electronc structure of tin oxides, *J. Vac. Sci. Technol. A,* 13 (3) **(1995)** 1382

[55] B. Stjerna, C.G. Granqvist, A. Seidel, L. Häggström, Characterisation of rf-sputtered SnO_x thin films by electron microscopy, Hall effect measurement and mössbauer spectrometry, *J. Appl. Phys.,* 68 **(1990)** 6241

[56] M. Mizuhashi, *Thin Solid Films,* 70 **(1980)** 91

[57] W. Fliegel, Korngefüge, elektrische und gassensitive Eigenschaften von dotiertem Zinndioxid, *PhD Thesis,* University of Dresden, Germany **(1995)**

[58] W.M.H. Sachtler and P. van der Plank, *Surf. Sci.,* 18 **(1969)** 62

[59] O. Johnson, *J.Catal.* 28 **(1973)** 503

[60] Z. Knor, *Adv.Catal.* 22 **(1972)** 51

[61] F.F. Volkenshtein, The electronic theory of catalysis on semiconductors, MacMillan, New York **(1963)**

[62] S.G. Davidson and J.P. Levine, in vol. 25 of *Solid State Physics*, ed. F. Seitz and D. Turnbull, Academic Press, New York **(1970)**

[63] S.R. Morrison, *The chemical physics of surfaces*, 2nd ed., Plenum press, New York **(1990)**

[64] M. Henzler and W. Göpel in: *Oberflächenphysik des Festkörpers*, Teubner, Stuttgart **(1994)**

[65] A. Hierlemann, Fundamental principles and thermodynamics of chemical sensing, *1st NOSE II short course*, Bressanone, Italy **(2002)** 11

[66] P.W. Atkins, *Physikalische Chemie*, VCH, Weinheim **(1990)** 799

[67] E. Iglesia, D.G. Barton, J.A. Biscardi, M.J.L. Gines, S.L. Soled, Bifunctional pathways in catalysis by solid acids and bases, *Catalysis Today,* 38 **(1997)** 339

[68] K. Tanabe, M. Misono, Y. Ono, H. Hattori, New solid acids and bases: catalytic properties, *Studies in Surface Science and Catalysis*, 52 Elsevier **(1989)**

[69] M.V. Lebedev, Surface modification of III-V semiconductors: chemical processes and electronic properties, *Progress in Surface Science,* 70 **(2002)** 153

[70] H.H. Kung, Transition metal oxides: surface chemistry and catalysis, *Studies in Surface Science and Catalysis,* 45 Elsevier **(1989)** 80

[71] A.A. Davydov, Infrared spectroscopy of adsorbed species on the surface of transition metal oxides, ed. C.H.Rochester, John Wiley & Sons, Chichester, England **(1990)**

[72] J. March, *Advanced Organic Chemistry*, Wiley, New York **(1985)** 218

[73] J.N. Brønsted, *Recl. Trav. Chim*., Netherlands, 42 **(1923)** 718

[74] G.N. Lewis, Valence and the Structure of Atoms and Molecules, *Chemical Catalogue*, New York **(1923)**

[75] M.A. Barteau, *J. Vac. Sci. Technol. A,* 11 **(1993)** 2162

[76] P.C. Stair, *J. Am. Chem. Soc*., 104 **(1982)** 4044

[77] S. Matsushima, T. Maekawa, J. Tamaki, N. Miura, N. Yamazoe, *Chem.Lett.,* **(1989)** 845

[78] J. Tamaki, T. Maekawa, S. Matsushima, N. Miura, N. Yamazoe, *Chem.Lett.,* **(1990)** 477

[79] G. Centi, G. Golonelli, G. Busca, *J. Phys. Chem.,* 94 **(1990)** 6813

[80] P. Conception, A. Galli, J.M. Lopez Nieto, A. Dejoz, M.I. Vazquez, *Topics Catal.,* 3 **(1996)** 451

[81] J.C. Vedrine, J.M.M. Millet, J.-C. Volta, Molecular description of active sites in oxidation reactions: acid-base and redox properties, and role of water, *Catalysis Today,* 32 **(1996)** 115

[82] S.R. Morrison, *The chemical physics of surfaces*, 2nd ed., Plenum press, New York **(1990)** 30

[83] H.K. Henisch, Semiconductor Contacts: an approach to ideas and models, *International series of monographs on physics*, vol. 70, Clarendon Press, Oxford, UK **(1984)** 43

[84] N. Bârsan and U. Weimar, Conduction model of metal oxide gas sensors, *Journal of Electroceramics,* 7 (**2001**)143

[85] P.T. Moseley, D.E. Williams, Oxygen surface species on semiconducting oxides, in: P.T. Moseley, J.O.W. Norris, D.E. Williams (Eds.), *Techniques and Mechanisms in Gas Sensing*, Adam Hilger, Bristol **(1991)** 46

[86] S. Lenaerts, J. Roggen, and G. Maes, FTIR characterization of tin dioxide gas sensor materials under working conditions, *Spectrochimica Acta Part A-Molecular Spectroscopy,* 51 **(1995)** 883

[87] J.P. Joly, L. Gonszalez-Cruz, Y. Arnaud, désorption à la temperature programmée de l'oxygène labile de SnO₂, *Bulletin de la Societé Chimique de France* **(1986)** 11

[88] B. Gillot,C. Fey, D. Delafosse, Surface properties of tin (IV) oxide depending upon the mode of preparation, *Journal of Chemical Physics,* 73 **(1976)** 19

[89] N. Yamazoe, J. Fuchigami, M. Kishikawa, T. Seiyama, Interactions of tin oxide surfaces with O₂, H₂O and H₂, *Surf. Sci,* 86 **(1979)** 335

[90] A.M. Volodin and A.E. Cherkasin, Surface bonds on zinc oxide and tehir role in photoadsorption and oxidative photolysis, *React. Kinet. Catal. Lett.*, 17 **(1981)** 329

[91] S.C. Chang, Oxygen cehmisorption on tin oxide: Correlation between electrical conductivity and EPR measurements, *J. Vac. Sci. Technol.*, 17 **(1980)** 366

[92] M. Schweizer-Berberich, Gas sensors based on stannic oxide, *PhD Thesis*, University of Tübingen, Shaker Verlag, Germany **(1998)**

[93] C.D. Kohl, Oxidic semiconductor gas sensors, in G.Sberveglieri (ed.), *Gas Sensors*, Kluwer, Dordrecht **(1992)** 43

[94] M. Egashira, M. Nakashima, S. Kawasumi, Change of thermal desorption behaviour of adsorbed oxygen with water coadsorption on Ag⁺-doped Tin(4) oxide, *J. Chem Soc Chem Comm* **(1981)** 1047

[95] K. Morishige, S. Kittaka, T. Morimoto, The thermal desorption of surface hydroxide on tin (IV) oxide, *Bull. Chem. Soc. Japan*, 53 **(1980)** 2128

[96] A. Guest, *PhD Thesis*, University of Nottingham, UK **(1985)**

[97] E.W. Thornton and P.G. Harrison, Tin oxide surfaces, Part 1: Surface hydroxyl groups and the chemisorption of carbon dioxide and carbon monoxide on tin (IV) oxide, *J. Chem. Soc. Faraday Trans.,* 71 **(1975)** 461

[98] F. Berger, E. Beche, R. Berjoan, D. Klein, and A. Chambaudet, An XPS and FTIR study of SO₂ adsorption on SnO₂ surfaces, *Appl. Surf. Sci.,* 93 **(1996)** 9

[99] M.A. Barteau, *J. Vac. Sci. Technol.,* 11 **(1993)** 2161

[100] G. Heiland and D. Kohl in T. Seiyama (ed.), *Chemical Sensor Technology*, vol.1, Kodansha, Tokyo **(1988)** 15

[101] N. Yamazoe, J. Fuchigami, M. Kishikawa, T. Seiyama, Ineractions of tin oxide surfaces with O₂, H₂O and H₂, *Surf Sci*, 86 **(1976)** 19

[102] Y. Matsuura, K. Takahata, K. Ihokura, Mechnism of gas sensitivity change with time of SnO₂ gas sensors, *Sens Actuators*, 14 **(1988)** 223

[103] K.D. Schierbaum, U. Weimar, W. Göpel, Conductance, work function and catalytic activity of SnO₂ based gas sensors, *Sens Actuators B*, 3 **(1991)** 205

[104] V.A. Henrich, P.A. Cox, *The Surface Science of Metal Oxides*, University press, Cambridge **(1994)** 312

[105] D. Koziej, N. Bârsan, V. Hoffmann, J. Szuber, U. Weimar, Complementary phenemenological and spectroscopic studies of propane sensing with tin oxide based sensors, *Chemical Sensors* **(2004)** submitted

[106] M. Caldararu, D. Sprinceana, V.T. Popa, N.I. Ionescu, Surface dynamics in tin dioxide-containing catalysts II, *Sens Act B*, 30 **(1996)** 35

[107] D.S. Vlachos, P.D. Skafidas, J.N. Avaritsiotis, Transient effects of tin oxide CO sensors in the presence of water vapour, *Appl. Phys. Lett.,* 63 (13) **(1993)**

[108] R. Ionescu, A. Vancu.C. Moise, A. Tomescu, Role of water vapour in the interaction of SnO_2 with CO and CH_4, *Sens Act B*, 61 **(1999)** 39

[109] P.K. Clifford and D.T. Tuma, Characteristics of semiconductor gas sensors I: steady state gas response, *Sens Actuators*, 3 **(1982/83)** 233

[110] J.F. Boyle and K.A. Jones, The effects of carbon monoxide, water vapour and surface temperature on the conductivity of a tin (IV) oxide gas sensor, *Electron. Mater.,* 6 **(1977)** 717

[111] S.J. Gentry and T.A. Jones, The Role of Catalysis in solid-state gas sensors, *Sensors and Actuators,* 10 **(1986)** 1

[112] H. Windischmann and P. Mark, A model for the operation of a thin-film SnO_x conductance-modulation carbon monoxide sensor, *J. Electrochem. Soc.: Solid-State Sci Technol,* 126 **(1979)** 672

[113] M.J. Willett, Spectroscopy of Surface Reactions, in P.T. Moseley, J.O.W. Norris, D.E. Williams*, Techniques and Mechanisms in Gas Sensing*, Vol. 3, Adam Hilger, Bristol, UK **(1991)** 61

[114] S. Harbeck, A. Satvanyi, N. Bârsan, U.Weimar, V. Hoffmann, DRIFT studies of thick-film un-doped and Pd-doped SnO_2 sensor: temperature changes effect and CO detection mechanism in the presence of water vapour, *Thin Solid Films*, 436, **(2003)** 76

[115] M. Egashira, M. Nakashima, S. Kawasumi, Influence of coadsorbed water on the reactivity of oxygen adsorbates on noble metal-doped tin(IV) oxides, *Conf. Proc. IMCS Fukuoka*, Japan **(1983)**

[116] R. Ionescu, A. Vancu, Time-dependence of the conductance of SnO_2:PtSb in atmospheres containing oxygen, carbon monoxide and water vapour I, *Appl. Surf. Science* 74 **(1994)** 207

[117] D. Koziej, *personal communication*, University of Tübingen **(2005)**

[118] S. Strässler, A. Reis, Simple models for n-type metal oxide semiconductor gas sensors, *Sens Actuators B*, 5 **(1991)** 7

[119] N. c R. Ionescu, The mechanism of interaction between CO and an SnO_2 surface: the role of water vapour, *Sens Actuators B,* 12 **(1993)** 71

[120] J.F. McAleer, P.T. Mosley, J.O. Norris, D.E. Williams, Tin oxide gas sensors Part 1, *J. Chem. Soc., Faraday Trans.1*, 83 **(1987)** 1323

[121] R. Burch, D.J. Crittle, M.J. Hayes, C-H bond activation in hydrocarbon oxidation on heterogeneous catalysts, *Catal. Today,* 47 **(1999)** 229

[122] R. Burch, M.J. Hayes, *J.Mol.Catal.,* 100 **(1995)** 13

[123] C.A. Cooper, C.R. Hammond, G.J. Hutchings, S.H. Taylor, D.J. Willock, K. Tabata, A combined experimental and theoretical approach to the study of methane activation over oxide catalysts, *Catalysis Today*, 71 **(2001)** 3

[124] V. Sokolovskii, *Catal. Today,* 24 **(1995)** 377

[125] M. Ai, *Proceedings of the 7th International Congress on Catalysis*, eds. T. Seiyama and K. Tanabe, Tokyo **(1980)** 1060, Elsevier, Amsterdam/New York **(1981)**

[126] K. Otsuka and M. Hanato, *J.Catal.,* 108 **(1987)** 252

[127] V.R. Choudhary, V.H. Rane, *J.Catal.,* 130 **(1991)** 411

[128] P.B. Weisz, Effects of electronic charge transfer between adsorbate and solid on chemisorption and catalysis, *Journal of Chemical Physics*, 21 **(1953)** 1531

[129] G. Tournier, C. Pijolat, Influence of oxygen concentration in the carrier gas on the response of tin dioxide sensor under hydrogen and methane, *Sens Actuators B*, 61 **(1999)** 43

[130] L. Savary, J. Saussy, G. Costentin, M.M. Bettahar, M. Gubelmann-Bonneau, J.C. Lavalley, Propane oxydehydrogenation reaction on a VPO/TiO$_2$ catalyst. Roel of the nature of acid sites determined by dynamic in-situ IR studies, *Catalysis Today,* 32 **(1996)** 57

[131] Römpp, CD Römpp Chemie Lexikon – Version 1.0, Thieme Verlag, Stuttgart, Germany **(1995)**

[132] D. Kohl, Surface processes in the detection of reducing gases with SnO$_2$-based devices, *Sens. Actuators*, 18 **(1989)** 71

[133] I. Sayago, J. Gutiérrez, L. Arés, J.I. Robla, M.C. Horillo, J. Getino, J.A. Agapito, The interaction of different oxidising agents on doped tin oxide, *Sens. Actuators B*, 24-25 **(1995)** 512

[134] E. Leblanc, L. Perier-Camby, G. Thomas, R. Gibert, M. Primet, P. Gelin, NO$_x$ adsorption onto dehydroxylated or hydroxylated tin oxide surface. Application to SnO$_2$-based sensors, *Sens. Actuators B*, 62 **(2000)** 67

[135] B. Ruhland, T. Becker, G. Müller, Gas-kinetic interactions of nitrous oxides with SnO$_2$ surfaces, *Sens. Actuators B*, 50 **(1998)** 85

[136] R. Rella, P. Siciliano, S. Capone, M. Epifani, L. Vasanelli, A. Lieciulli, Air quality monitoring by means of sol-gel integrated tin oxide thin films, *Sens. Actuators B*, 58 **(1999)** 283

[137] C. Pijolat, C. Pupier, M. Sauvan, G. Tournier, R. Lalauze, Gas detection for automotive pollution control, *Sens. Actuators B*, 59 **(1999)** 195

[138] A. Chiba, Development of the TGS gas sensor, in S.Yamauchi (ed.), *Chemical gas sensor technology*, vol. 4, Elsevier **(1992)** 1

[139] N. Bârsan, M. Schweizer-Berberich, W. Göpel, Fundamental and practical aspects in the design of nanoscaled SnO$_2$ gas sensors: a status report, *Fresenius J Anal Chem*, 365 **(1999)** 287

[140] U. Weimar, Gas sensing with tin oxide: elementary steps and signal transduction, *Habilitation Thesis*, University of Tübingen, Germany **(2001)**

[141] N. Yamazoe, New approaches for improving semiconductor gas sensors, *Sens Act B* **5** **(1991)** 7

[142] A. Cabot, J. Arbiol, J.R. Morante, U. Weimar, N. Bârsan, W. Göpel, Analysis of the noble metal catalytic additives introduced by impregnation of as obtained SnO$_2$ sol-gel nanocrystals for gas sensors, *Sens. Actuators B*, 70 **(2000)** 87

[143] D.-D. Lee, B.-K. Sohn, Se*ns Act,* 12 **(1987)** 441

[144] C. Xu, J. Tamaki, N. Miura, N. Yamazoe, Promotion of tin dioxide gas sensor by aluminium doping, *Talanta,* 38 **(1991)** 1169

[145] W. Fliegel, G. Behr, J. Werner, G. Krabbes, Preparation, development of microstructure, electrical and gassensitive properties of pure and doped SnO$_2$ powders, *Sen Act B,* 18-19 **(1994)** 474

[146] V. Ambrazeviciene, A. Galdikas, S. Grbinskij, A. Mironas, H. Tvardauskas, Gas-sensing properties of chemically deposited SnO$_x$ films doped with Pt and Sb, *Sensors and Act B,* 17 **(1993)** 27

[147] S.R.Morrison, Selectivity in semiconductor sensors, *Sens Act,* 12 **(1987)** 425

[148] I. Simon, N. Bârsan, M. Bauer, U. Weimar, Micromachined metal oxide gas sensors: opportunities to improve sensor performance, *Sens Act B,* 73 **(2001)** 1

[149] D. Briand, B. van der Schoot, N.F. de Rooij, A. Krauss, U. Weimar, N. Bârsan, W. Göpel, High temperature micro-hotplates for drop coated gas sensors, *Conf. Proc. of Eurosensors XIII*, The Hague, The Netherlands **(1999)** 109

[150] I. Simon, Thermal conductivity and metal oxide gas sensors: micromachining as an opportunity to improve sensor performance, *PhD thesis*, University of Tuebingen, Shaker Verlag **(2003)**

[151] S. Fung, Z. Tang, P. Chan, J. Sin, P. Cheung, Thermal analysis and design of a micro-hotplate for integrated gas-sensor applications, *Sens Act A,* 54 **(1996)** 482

[152] A. Götz, I. Gràcia, C. Cané, E. Lora-Taniayo, M. Horrillo, G. Getino, C. Gràcia, J. Gutiérez, A micromachined solid state integrated gas sensor for the detection of aromatic hydrocarbons, *Sens Act B,* 44 **(1997)** 483

[153] G. Sberveglieri, W. Hellmich, G. Müller, Silicon hotplates for metal oxide gas sensor elements, *Microsyst. Technol.,* 3 **(1997)** 183

[154] M. Hauser, J. Zacheja, J. Binder, Multi-electrode substrate for selectivity enchancement in air monitoring, *Sens Act B,* 43 **(1997)** 11

[155] R. Cavicchi, J. Suehle, P. Chaparala, K. Kreider, M. Gaitan, S. Semancik, Micro-hotplate gas sensor, in: *Proceedings of the 1994 Solid State Sensor and Actuator Workshop*, Hilton Head, SC, USA **(1994)** 53

[156] M. Graf, U. Frey, P. Reichel S. Taschini, N. Bârsan, U. Weimar, A. Hierlemann, Monitoring of environmentally relevant gases by a digital monolithic metal-oxide microsensor array, IEEE Sensor, Vienna, Austria **(2004)**

[157] A. Hierlemann and H. Baltes,CMOS-based chemical microsensors, *Analyst,*128 **(2003)** 15

[158] A. Hierlemann, O. Brand, C. Hagleitner, H. Baltes, Microfabrication techniques for chemical/biosensors, *Proceedings of the IEEE*, vol. 91, 6 **(2003)** 839

[159] N. Bârsan, S. Raible, U. Weimar, Auftragevorrichtung zum lokalen Auftragen viskoser oder flüssiger Materialien in definierter Menge, *Patentanmeldung P10239DE*

[160] A. Heilig, N. Barsan, U. Weimar, M. Schweizer-Berberich, W. Göpel and J.W. Gardner, Gas identification by modulating temperatures of SnO_2-based thick film sensors, *Sens Act B,* 43 **(1997)** 45

[161] www.oecd.org

[162] P. Reichel, N. Barsan, U. Weimar, *"International Air Quality Guidelines for CO, NO_2 and CH_4"*, 1st NOSE II Short Course, Bressanone, Italy **(2002)**

[163] Electrical apparatus for the detection of carbon monoxide in domestic premises – Guide on the selection, installation, use and maintenance, *CENELEC standard prEN50292/1999*

[164] Ventilation for Acceptable Indoor Air Quality, *ASHRAE standard 62-2001*, American Society of Heating, Refrigirating and Air-conditioning Engineers

[165] Carbon monoxide detectors (electrical) for domestic use, *BS 7860,* Bristish Standard

[166] Evaluation of explosives vapor detectors, *ASTM F 2069-00*, American Society for Testing and Materials

[167] Testing systems for measuring dynamic responses for carbon monoxide detectors to gases and vapors, *ASTM D 6332-99*, American Society for Testing and Materials

[168] Residential Gas Detectors, *UL 1484*, Underwriters Laboratories **(2001)**

[169] Single and multiple station carbon monoxide alarms,UL 2034, Underwriters Laboratories **(2001)**

[170] LabView 7.1, National Instruments Corporation, Austin, Texas, USA, http://www.ni.com/labview

[171] M. Graf, D. Barrettino, P. Käser, J. Cerda, A. Hierlemann, Switzerland, and H. Baltes, Smart single-chip CMOS microhotplate array for metal-oxide-based gas sensors, *Proc. IEEE Transducers*, Boston, MA, USA **(2003)** 123

[172] M. Graf, D. Barrettino, S. Taschini, C. Hagleitner, A. Hierlemann, and H. Baltes, "Monolithic metal-oxide microsensor system in industrial CMOS technology", *Tech. Digest MEMS*, Kyoto, Japan **(2003)** 303

[173] D. Barrettino, M. Graf, M. Zimmermann, C. Hagleitner, A. Hierlemann, H. Baltes, "A micro-hotplate-based monolithic CMOS gas sensor array", *Proc. ISCAS IV* **(2003)** 852

[174] M.Y. Afridi, J.S Suehle, M.E. Zaghloul, D.W. Berning, A.R. Hefner, R.E. Cavicchi, S. Semancik, C.B. Montgomery, and C.J. Taylor, A monolithic CMOS microhotplate-based gas sensor system, *IEEE Sensors Journal 2* **(2002)** 644

[175] J.A. Covington, F. Udrea, and J.W. Gardner, Resistive gas sensor with integrated MOSFET micro hot-plate based on an analogue SOI CMOS process, *Proc. IEEE Sensors,* Florida, USA **(2003)**

[176] M. Graf, D. Barrettino, S. Taschini, A. Hierlemann, H. Baltes, S. Hahn, N. Bârsan, and U. Weimar, CMOS microhotplate with MOS transistor heater for integrated metal-oxide microsensors, *Proc. Eurosensors XVI,* Prague, Czech Republic **(2002)** 456

[177] Standard for a Smart Transducer Interface for Sensors and Actuators - Transducer to Microprocessor Communication protocols and Transducer Electronic Data Sheet (TEDS) Formats, *IEEE standard 1451.2-1997*

[178] W. Göpel, J. Hesse, J.N. Zemel, *Sensors: A Comprehensive Survey*, vol. 2.1, VCH, Weinheim, Germany **(1991)** 430

[179] J. Kappler, N. Bârsan, U. Weimar, A. Dieguez, J.L. Alay, A. Romano-Rodriguez, J.R.Morante and W. Göpel, "Correlation between XPS, Raman and TEM measurements and the gas sensitivity of Pt and Pd doped SnO2 based gas sensors", *Fres. J. Anal. Chem*., 361 **(1998)** 110

[180] N. Yamazoe, N. Miura, Some basic aspects of semiconductor gas sensors, in: S.Yamazuchi (Ed.), *Chemical Sensor Technology*, vol.4, Kodanasha, Tokyo **(1992)** 19

[181] A.P. Lee, B.J. Reedy, Temperature modulation in semiconductor gas sensing, *Sens Act B,* 60 **(1999)** 35

[182] G.Wedler, *Lehrbuch der physikalischen Chemie*, 4th ed., Wiley-VCH, Weinheim **(1997)**

[183] A. Heilig, Selektivitätssteigerung von SnO$_2$-Gassensoren, *PhD-thesis*, University of Tübingen, Germany **(1999)**

[184] Y. Kato, K. Yoshikawa, M. Kitora, Temperature-dependent dynamic response enables the qualification and quantification of gases by a single sensor, *Sens Act B,* 40 **(1997)** 33

[185] W.M. Sears, K. Colbow, F. Consandori, General characteristics of thermally cycled tin oxide gas sensors, *Semicond. Sci. Technol.,* 4 **(1989)** 351

[186] W.M. Sears, K. Colbow, F. Consandori, Algorithms to improve the selectivity of thermally cycled tin oxide gas sensors, *Sens. Act.,* 19 **(1989)** 333

[187] S. Nakata, M. Nakasuji, N. Ojima, M. Kitora, Characteristic nonlinear responses for gas species on the surface of different semiconductor gas sensors, *Appl. Surf. Sci*., 135 **(1998)** 285

[188] G. Kraus, U. Weimar, G. Gauglitz, W. Göpel, Mustererkennung und Multikomponentenanalyse bei chemischen Sensoren, *Technisches Messen*, 62 **(1995)** 6

[189] S. Capone, P. Siciliano, N. Barsan, U. Weimar, L. Vsanelli, Analysis of CO and CH$_4$ gas mixtures by using a micromachined sensor array, *Sens Act B,* 78 **(2001)** 40

[190] I.T. Jolliffe, *Principal Component Analysis*, Springer-Verlag **(1986)**

[191] http://www.cis.hut.fi/aapo/papers/NCS99web/node5.html

[192] http://www.vias.org/tmdatanaleng/cc_pcr.html

[193] R. Henrion, G. Genrion, *Multivariate Datenanalyse*, Springer-Verlag **(1994)**

[194] http://www.neurosolutions.com/products/ns/whatisNN.html

[195] J. Zupan, J. Gasteiger, *Neural Networks in Chemistry and Drug Design*, 2nd ed., Wiley-VCH **(1999)**

[196] M. Schweizer-Berberich, S. Strathmann, U. Weimar, R. Sharma, A. Seube, A. Peyre-Lavigne, W. Göpel, Strategies to avboid VOC cross-sensitivity of SnO2-based CO sesnors, *Sens Act B,* 58 **(1999)** 318

[197] M. Fleischer, S. Kornely, T. Weh, J. Frank, H. Meixner, Selective gas detection with high-temperature operated metal oxides using catalytic filters, *Sens Act B,* 69 **(2000)** 205

[198] C.H. Kwon, D.H. Yun, H.-K. Hong, S.-R. Kim, K. Lee, H.Y. Lim, K.H. Yoon, Multi-layered thick-film gas sensor array for selective sensing by catalytic filtering technology, *Sens Act B,* 65 **(2000)** 327

[199] S. Strathmann, *Diploma thesis*, University of Tübingen, Germany **(1997)**

[200] www.sigmaaldrich.com

[201] www.purafil.com

[202] S. Kitsukawa, H. Nakagawa, K. Fukuda, S. Asakura, S. Takahashi, T. Shigemori, The interference elimination for gas sensor by catalyst filters, *Sens Act B,* 65 **(2000)** 120

[203] W.M. Meier, D.H. Olson , *Atlas of Zeolite Structure Types*, 3rd ed., Butterworth **(1992)**

[204] G. Maier, Polymermembranen zur Gastrennung, *Angew. Chemie*, 110 **(1998)** 3128

[205] *Römpp Kompakt Basislexikon Chemie*, Thieme Verlag Stuttgart **(1998)**

[206] C.O. Muller, W.G. England, *Achieving your indoor air quality goals: which filtration system works best?,* PURAFIL, http://dollarmaker.com/afslasvegas/assets/pdf/pur/achieve.pdf

[207] O. Hugon, M. Sauvan, P. Benech, C. Pijolat, F. Lefebvre, Gas separation with a zeolite filter: application to the selectivity enhancement of chemical sensors, *Sens Act B,* 67 **(2000)** 235

[208] D.A. Skoog, F.J. Holler, T.A.Nieman*, Principles of Instrumental Analysis*, 5th ed., Saunders College Publishing, Philadelphia, USA **(1998)**

[209] Evaluation of long-term measurements of environmental monitoring stations in Madrid, Spain

[210] www.ilo.org

[211] S. Hahn, N. Bârsan, U. Weimar, Investigation of CO/CH_4 mixture measured with differently doped SnO_2 sensors, *Sens. Actuators B*, 78 **(2001)** 64

[212] M. Graf, *personal communication*, PEL, ETH Zurich, Switzerland

[213] A. Krauss, *personal communication*, AppliedSensor GmbH, Germany

[214] http://www.mambiente.munimadrid.es/

[215] N. Bârsan, J.R. Stetter, M. Findlay, W. Göpel, Hugh performance gas sensing of CO, *Anal Chem*, 71 **(1999)** 2515

[216] P. Reichel, N. Bârsan, U. Weimar, International Air Quality Guidelines for CO, NO2 and CH4, *1st NOSE II Short Course*, Bressanone, Italy **(2002)**

List of Abbreviations

Symbol	Description
ADA	Advanced Distributed Architecture for telemonitoring services; EU- project IST-2000-28452
ANN	artificial neural networks
AQMS	air quality monitoring station
BAW	bulk acoustic wave
e.g.	exempli gratia
RT	room temperature
RIFS	Reflectometric Interference Spectroscopy
FET	Field effect transistor
CH_4	methane
CMOS	Complementary Metal Oxide Semiconductor
CO	carbon monoxide
CO_2	carbon dioxide
CVD	chemical vapour deposition
EPR	electron programmed resonance
EtOH	Ethanol
FTIR	Fourier transform infrared analysis
GCMS	Gas chromatography - mass spectrometry
HC	hydrocarbons
H_2O	water
HP 1, 2, 3	sensor hotplate 1, 2, 3
IAQ	international air quality
i.e.	id est
IR	infrared spectrometry
LDL	Lower Detection Limit
LEL	Lower Explosion Limit
MFC	mass flow controller
MLR	Multiple linear regression
MOS	metal oxide semiconductor
MOX	metal oxide sensor
NO_2	nitrogen dioxide
O_2	oxygen
PCA	principal component analysis
PCR	principal component regression
PM	particulate matter
ppb	parts per billion
ppm	parts per million
PVD	physical vapour deposition
QMB	quartz crystal microbalance
r.h. [%]	relative humidity
SAW	surface acoustic wave
SnO_2	tin dioxide
TPD	temperature programmed desoption
TSM	thickness-shear mode resonator
VOC(s)	volatile organic compound(s)

List of Variables

Symbol	Description
γ	analytical sensitivity
ε_R	dielectric constant
θ	surface coverage
μ	(electron) mobility
μ	electron affinity
σ	conductivity
σ	standard deviation
Φ	work function
χ	electron affinity
A	cross-section
a, b, c	lattice parameters
E_a	activation energy
E_{des}	desorption energy
E_{diss}	dissociation energy
E_{phys}	physisorption energy
E_{chem}	chemisorption energy
E_{vac}	vacuum energy
E_b	bulk band energy
E_c, E_v	conduction (valence) band energy
E_F	Fermi-level
$D(E)$	density of states
$f(E)$	Fermi-Dirac distribution
G	conductance
I	current
k (k_{ads}, k_{des})	rate constant (adsorption, desorption)
l	length
L_D	Debye-Length
m	sensitivity
N_C, N_V	effective density of states of the conduction (valence) band
$N_{(V)}$	concentration of free charge carriers (valence band)
$N_{e(V)}$	concentration of free electrons (valence band)
n (n_b, n_s)	density of free electrons (in the bulk, at the surface)
n, p	charge carrier concentration
p_i	pressure of gas *i*
Q_{SS}	surface state
qV_S	surface potential barrier
R	resistance
r	distance
r	grain radius
S	sensor signal
t_{90}	time to accomplish 90% of sensor response change
U	voltage
z_0	depletion region

List of Constants

Symbol	Description
ε_0	permittivity
π	pi
e	elementary charge
k	Boltzmann constant
m_e	mass of electron
m_p	mass of proton

List of Academic Teachers:

K. Albert, H.P.T. Ammon, E. Bayer, D. Christen, G. Drews, H. Eckstein, G. Gauglitz, W. Göpel, P. Grathwohl,G. Häfelinger, M. Hanack, D. Hoffmann, V. Hoffmann, W. Jäger, G. Jung, S. Kemmler-Sack, D. Krug, N. Kuhn, M. E. Maier, H.A. Mayer, H.J. Meyer, E. Lindner, U. Nagel, W. Nakel, H. Oberhammer, D. Oelkrug, H. Pommer, G. Reinhardt, W. Sarrazin, V. Schurig, M. Schwarz, E. Schweda,, F.F. Seelig, W. Voelter, J. Strähle, U. Weimar, K-P. Zeller, C. Ziegler.

Acknowledgements

CURRICULUM VITAE

Name	Patrick Caspar Maarten Sebastian
Geburtstag	08.04.1977
Geburtsort	Wien, Österreich
Familienstand	Ledig
Staatsangehörigkeit	Österreicher

AUSBILDUNG

09/1983 – 07/1995	**École Européenne in Luxemburg** (Gymnasium), „Europäisches Abitur", zertifiziert nach ZVS (1995) als deutsches Abitur
10/1995 – 09/2001	**Studienfach Chemie - Diplom** an der Eberhardt-Karls-Universität Tübingen Wahlpflichtfach Pharmakologie / Toxikologie
08/1997	**Vordiplomsprüfungen**
08/2001	**Diplomprüfungen** Diplomarbeit im Institut für Physikalische und Theoretische Chemie bei Prof. Günter Gauglitz „Auswirkung der Luftfeuchtigkeit auf die Leistung von SnO_2-Sensoren und elektrochemischen Zellen bei der CO-Analytik"
04/2001 – 02/2004	Kollegiat im **Graduiertenkolleg der DFG** „Quantitative Analyse und Charakterisierung pharmazeutisch und biochemisch relevanter Substanzen"
Ab 10/2001	**Promotion** am Institut für Physikalische und Theoretische Chemie bei Dr. habil Udo Weimar Dissertation „Development of a chemical gas sensor system" Abschluss Dezember 2004